AD-A153 691 LFMR DEFINITION STUDY(U) HUGHES AIRCRAFT CO EL SEGUNDO 1
CALIF SPACE AND COMMUNICATIONS GROUP APR 85
N00014-84-C-2290

UNCLASSIFIED F/G 5/1 NL

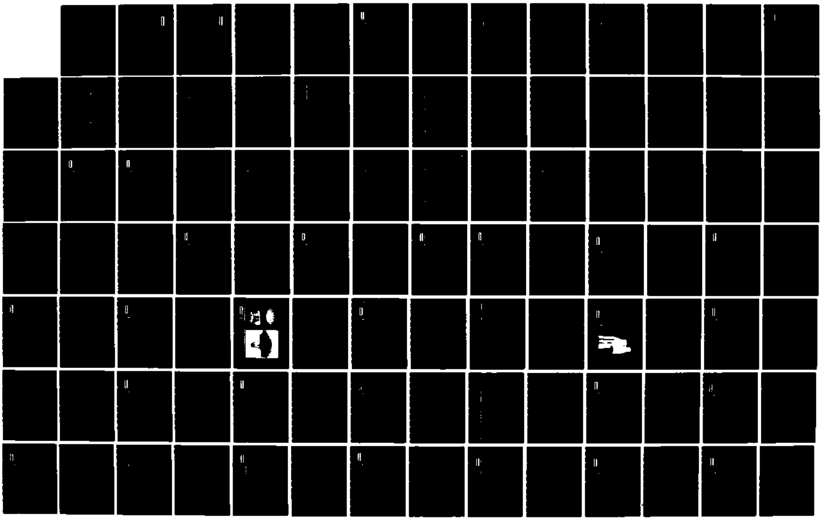

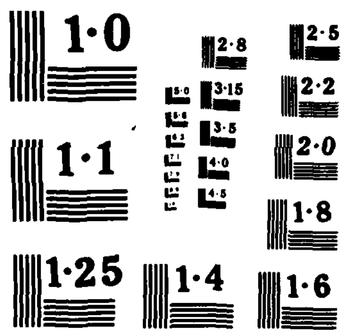
1·0
2·8
2·5
3·15
2·2
3·5
2·0
1·1
4·0
4·5
1·8
1·25
1·4
1·6

(12)

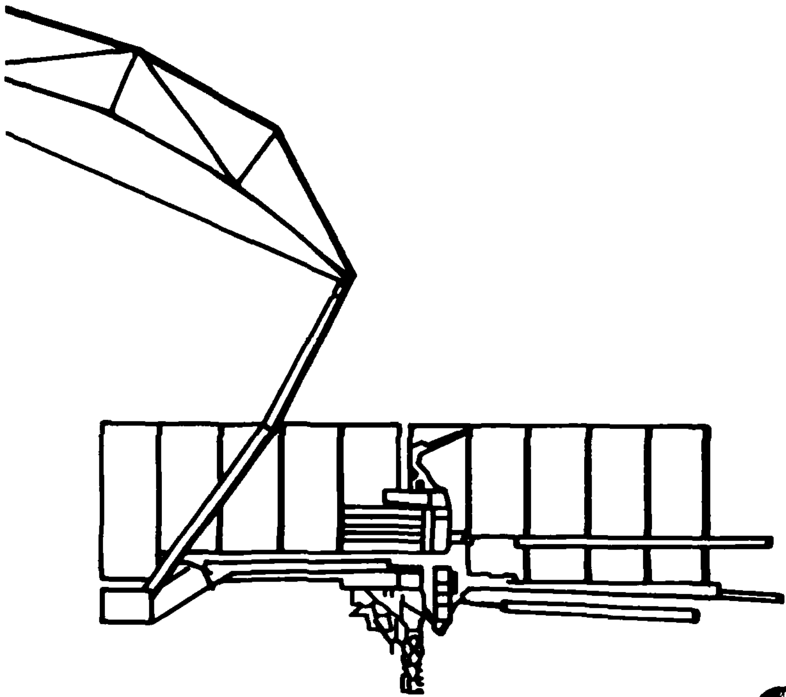

Final Report

LFMR Definition Study

April 1985

Hughes Aircraft Company

Space and Communications Group

Contract N0014-84-C-2290

HUGHES
A[illegible]CRAFT COMPANY

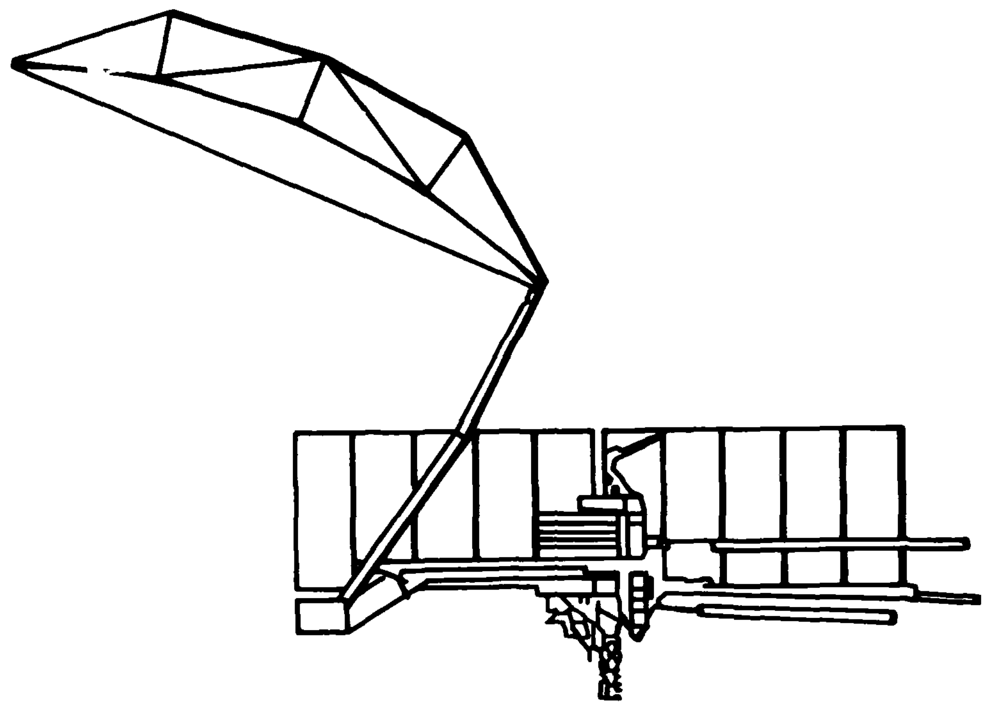

Final Report
LFMR Definition Study
April 1985

Hughes Aircraft Company
Space and Communications Group
Contract N0014-84-C-2290

HUGHES
A HUGHES AIRCRAFT COMPANY

LFMR DEFINITION STUDY

This is the final report of the LFMR definition study contract number N0014-84-C-2290 which satisfies the contract data requirements list (CDRL) A003.

The study was commissioned to evaluate the risks associated with fabrication of a flight qualified LFMR for the NROSS mission. Trade-off studies were performed to determine the impact of the LFMR on the S/C subsystem and the other instruments. The study identified no technological risks in the fabrication and testing of the LFMR. However, dynamic balancing, flexible body interaction, and antenna pointing are areas of concern that need to be closely monitored during the design, fabrication, and test of the sensor.

The report is divided into four major areas: System Engineering, Antenna Subsystem, Dynamics, and Balancing.

The topics covered in the System Engineering section are configuration studies, radiometric performance pointing accuracy, weight, RFI, and sampling. The sampling is covered in more detail in Appendix A.

Antenna configuration, feeds, cold load design, and overall antenna performance are covered in the antenna section. The details of periodic reflector analysis, both gore and facet surfaces, are covered in Appendix B.

The dynamics section includes LFMR structural modeling, f/D and spin rate studies, and dynamic balancing techniques.

Ground and on-orbit balancing techniques are covered in the balancing section.

The final section summarizes the results of the study and the recommendations for the hardware procurements phase of the LFMR contract.

TABLE OF CONTENTS

INTRODUCTION

STUDY LOGIC FLOW

This flow diagram indicates the study logic used to arrive at the LFMR preferred approach. The baseline requirements were analyzed and various options were studied before arriving at the preferred approach. The two options carried through the study were:

1. A side mounted LFMR, which was selected as the baseline and,
2. A back mounted LFMR studied as an alternate configuration.

STUDY LOGIC FLOW

HUGHES

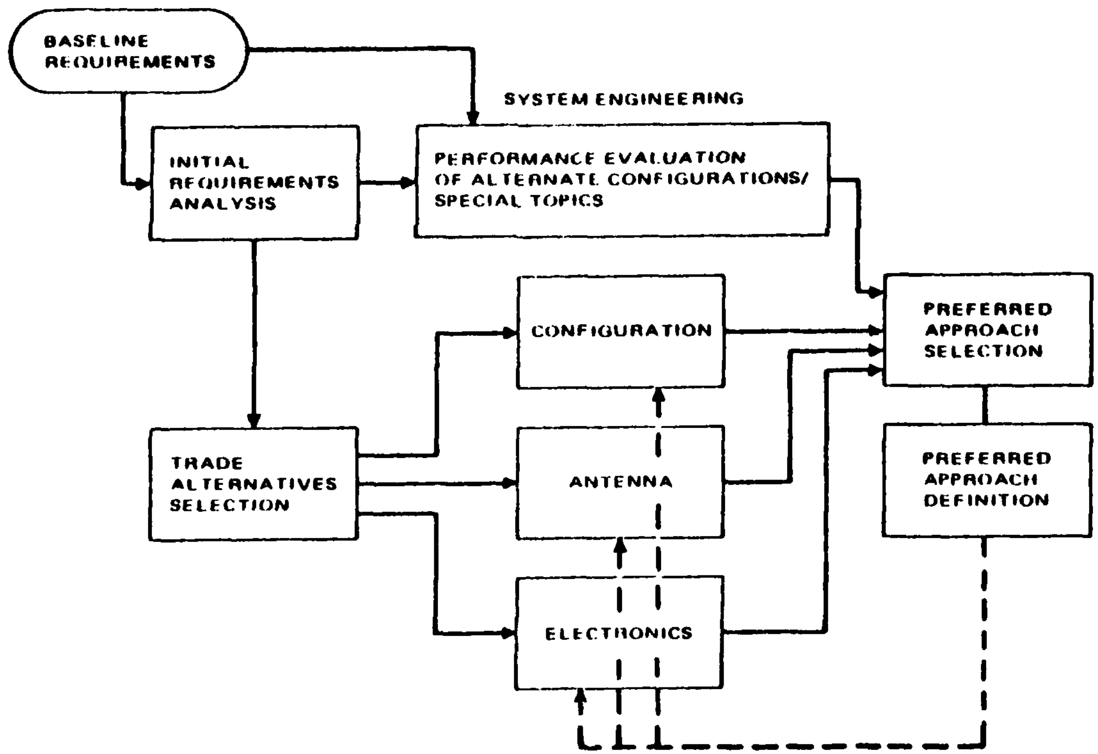

TASK STATEMENT CROSS REFERENCE

Each task statement in the contract has been covered in the Study. The location of the coverage is shown here.

TASK STATEMENT CROSS REFERENCE

HUGHES

	TITLE	WHERE COVERED
1.	INSTRUMENT POINTING ACCURACY	SYS ENG, ANTENNA, DYNAMICS
2.	CALIBRATION	SYS ENG, ANTENNA
3.	FEEDS	ANTENNA
4.	THERMAL EFFECTS	SYS ENG
5.	REFLECTED RADIATION	SYS ENG
6.	ELECTRONICS	SYS ENG
7.	ANTENNA MESH	SYS ENG, ANTENNA
8.	ANTENNA DEFORMATION	DYNAMICS
9.	ANTENNA wT AND POWER	SYS ENG, ANTENNA
10.	ANTENNA DIAMETER	ANTENNA
11.	RFI	SYS ENG
12.	ANTENNA F/D	ANTENNA
13.	ANTENNA TYPE	ANTENNA
14.	RADIOMETER LOCATION	SYS ENG, DYNAMICS
15.	SAMPLING	SYS ENG

NRL LFMR BASELINE

The NRL baseline requirements of the LFMR is shown here.

HUGHES

NRL LFMR BASELINE

ANTENNA - SIZE	5.9 METERS
- TYPE	OFFSET PARABOLA
CONE ANGLE	45°
SCAN ANGLE	102.4°
POINTING ACCURACY - RANDOM	.05°
- BIAS	.15°
BEAM EFFICIENCY	> 90%
FREQUENCY	5.2 AND 10.4 GHZ, DUAL POLARIZED
RESOLUTION, 3DB	15 x 25 RPM (5.2 GHZ)
ΔT	< .5°K
POWER	45 WATTS (INCLUDING MWA)
WEIGHT	150 LBS. (EXCLUDING S/C BOOM & MWA)
LAUNCH VEHICLE	TITAN II, 10 FT. FAIRING

HUGHES

SYSTEM ENGINEERING

HUGHES

POINTING ACCURACY BUDGET, DEGREES

	ALONG TRACK		CROSS TRACK	
A. INSTRUMENT SPIN AXIS	BIAS	UNCERTAINTY	BIAS	UNCERTAINTY
1. SPACECRAFT	.11*	.04*	.12*	.04*
2. BAPTA ALIGNMENT	.02	-	.02	-
3. BAPTA STIFFNESS	-	.001	-	.001
4. SCAN ACCURACY	-	-	.04	.02
B. ANTENNA BORESIGHT				
1. REFLECTOR HUB TO BAPTA	.08	.03**	.06	.03**
2. REFLECTOR RF AXIS	.04	.01	.03	.01
3. 0 G SIMULATION	.05	-	.04	-
RSS	.15	.05	.15	.05
REQUIREMENT	.15	.05	.15	.05

* ALLOWABLE FROM LFMR ALLOCATIONS

** LFMR RESPONSE TO 3 $\frac{IN}{SEC^2}$ (.03G) S/C INPUT

POINTING ACCURACY BUDGET

The pointing accuracy budget consists of two major parts, the instrument spin axis error and the antenna boresight error. Of the two types of errors discussed here, the uncertainty will be the only error covered in detail, since the bias error can be removed by ground processing. The allocation for the S/C was arrived at when the LFMR errors were accounted for.

INSTRUMENT SPIN AXIS

The BAPTA stiffness and spin axis uncertainties are values which were used in the SSM/I program. The design will remain the same for the LFMR, thus the errors will remain the same.

ANTENNA BORESIGHT

The reflector hub to BAPTA error is the flexible response to the LFMR servo system and a S/C excitation of 3 in/sec^2 acceleration. The response is detailed in the dynamics section of the report, but the S/C input is estimated. The reflector RF axis error is the flexible mesh responding to the dynamics input and it is also estimated.

HUGHES

PREDICTED SYSTEM CALIBRATION ACCURACY, °K

(6 FEEDS, T_B = 250°K)

CONTRIBUTOR	FREQUENCY (GHZ) 5.2 RANDOM	5.2 BIAS	10.4 RANDOM	10.4 BIAS
NONLINEARITY	.2		.2	
NOISE/DRIFT	.32		.41	
ERROR, HOT LOAD	.15		.15	
ERROR, COLD REFERENCE	.20		.20	
REFLECTOR/FEED TRANSFER FUNCTION		.5		.5
MESH REFLECTOR CONTRIBUTIONS	.13	1.0	.17	1.4
TOTAL, RSS °K	.47		.55	

PREDICTED SYSTEM CALIBRATION ACCURACY

This allocation table is for a 6 feed case with a brightness temperature of 250°K. The various contributions to the calibration accuracy are listed below.

1. NONLINEARITY - This is the deviation from a linear response between the calibration points. No physical mechanism predicts this effect and tests at Hughes show this number to be an upper bound.
2. NOISE/DRIFT - The noise of the radiometer (ΔT) and the drift are combined here. Again the drift number is supported by test data.
3. ERROR HOT LOAD - Lateral gradients and temperature sensor calibration are the largest contributors for this error.
4. ERROR COLD REFERENCE - Although the cold sky background is well known the contribution of the side lobes and other effects is expected to produce a .2°K error.
5. REFLECTOR/FEED TRANSFER FUNCTION - This error is invariant with time is thus able to be removed by ground processing. Feed spillover and inaccuracy in range measurements account for this error.
6. MESH REFLECTOR CONTRIBUTIONS - These errors were explained on previous pages.

MESH REFLECTOR CONTRIBUTED ERRORS (CON'T)

HUGHES

- MESH TRANSMISSION CONTRIBUTION TO SYSTEM RANDOM ERROR

$$= [\Delta \text{Trans} \times \text{Area} \times \text{Temp}] + [\text{Trans} \times \Delta \text{Area} \times \text{Temp}] + [\text{Trans} \times \text{Area} \times \Delta \text{Temp}]$$

$$= [.0002 \times .1 \times 300] + [.002 \times .02 \times 300] + [.002 \times .1 \times 50]$$

$$.006 + .012 + .01 = .016 \text{ RSS } (5.2 \text{ GHZ})$$

$$.058 \text{ RSS } (10.4 \text{ GHZ})$$

- MESH TRANSMISSION CONTRIBUTION TO SYSTEM CALIBRATION BIAS

$$= \text{TRANSMISSIVITY} \times \text{AREA FRACTION} \times \text{TEMPERATURE}$$

$$= .002 \times .1 \times 300 = .06°K \ (5.2 \text{ GHZ})$$

$$.21°K \ (10.4 \text{ GHZ})$$

MESH REFLECTOR CONTRIBUTED ERRORS (CONT)

Mesh Transmission

The energy leakage through the mesh causes both random and bias errors.

The transmissivity (Trans) of the mesh is taken from the mesh modelling reported elsewhere in this report to be .002 and a 10% error is assumed to compute Δ Trans. The Area (Area) occupied by other than the 3°K cold sky background is estimated to be .1, and a 10% error is also assumed to get the Δ Area. The structure temperature (Temp) is assumed to be 300°K with the uncertainty (Δ Temp) estimated at 50°K.

The random error for the 5 GHZ channel is an order of magnitude, .016°K, lower than the random mesh loss error, while the 10 GHZ channel is a factor of 3 lower at .058°K. The bias error is also smaller but again it can be removed during the ground processing.

This error is non-existent in a solid reflector.

HUGHES

MESH REFLECTOR CONTRIBUTED ERRORS

- MESH LOSS CONTRIBUTION TO SYSTEM RANDOM ERROR

  $= \Delta \epsilon \times T + \epsilon \times \Delta T$

  $= .00025 \times 400 + .0025 \times 30 = .13°K$ (5.2 GHZ)

  $.16°K$ (10.4 GHZ)

- MESH LOSS CONTRIBUTION TO SYSTEM CALIBRATION BIAS

  $= \epsilon \times T_{ANT}$

  $= .0025 \times 400 = 1.0°K$

MESH REFLECTOR CONTRIBUTED ERRORS

Mesh Loss

The mesh reflector causes two types of errors to the antenna temperature that are not found in solid reflectors. The mesh loss error is computed on this chart while the mesh transmission error is presented on the following chart.

$\Delta\varepsilon$ is the amount of error in the emissivity (ε). A 10% error was chosen as a representative value to a emissivity value of .0025 which was estimated by NRL to be the upper bound. The physical temperature of the mesh (T) is estimated to be 400°K. Temperature sensors installed on the mesh would give a uncertainty in the temperature of ± 30°K. Finally the ε is higher at 10.4 GHZ than 5.2 GHZ which gives a random error of .16°K versus an error of .13°K at 5.2 GHZ

The bias error is estimated to be 1.0°K, but this can be removed during the ground processing.

Solid reflectors have metalized surfaces (usually aluminum) which have much lower emissivities.

HUGHES

MESH ENERGY DIAGRAM

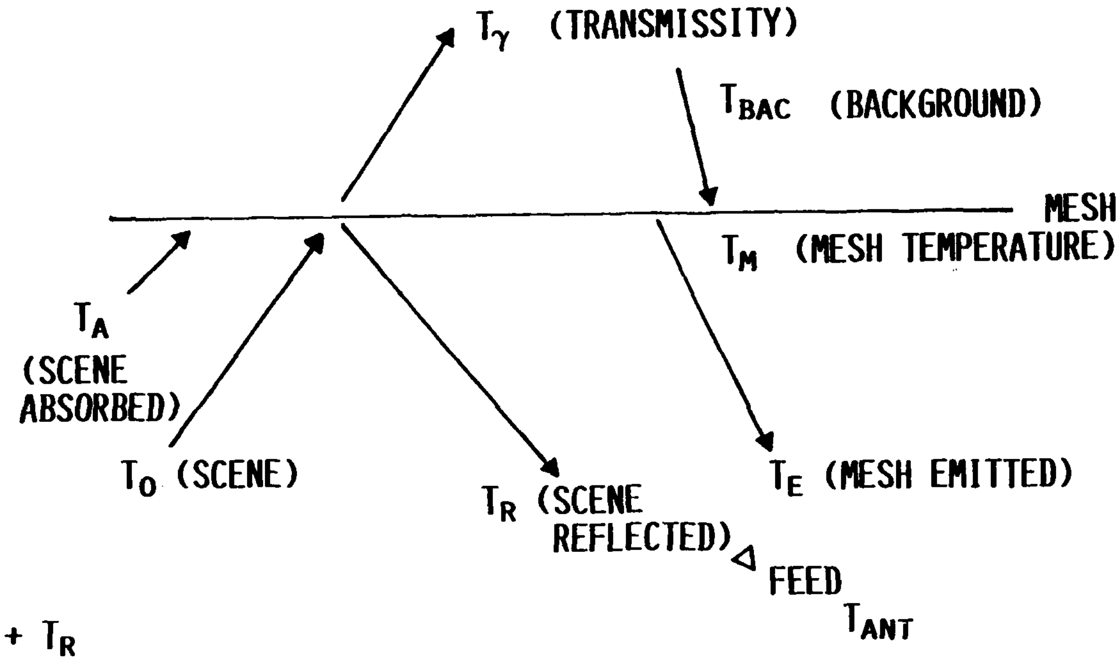

$$T_O = T_A + T_\gamma + T_R$$

$$T_A = \epsilon T_O \qquad T_E = \epsilon T_M$$

$$T_R = \ell T_O$$

$$1 = \ell + \epsilon + \gamma$$

$$T_{ANT} = \underbrace{T_O\,(1-(\epsilon+\gamma))}_{T_R} + \epsilon T_M + \gamma T_{BAC}$$

MESH ENERGY DIAGRAM

This diagram shows the various contributions to the antenna temperature. The scene energy is divided into three parts. T_A is absorbed, T_γ passes through the mesh and T_R is reflected toward the feed. The two other contributions to the antenna temperature are the energy passing through the mesh (T_{BAC}) at the background temperature and the mesh emitter temperature (T_E). The formulas for the various components are shown on the chart.

RADIOMETER PERFORMANCE SUMMARY

HUGHES

	3 FEEDS		6 FEEDS	
	5.2 GHz	10.4 GHz	5.2 GHz	10.4 GHz
INSERTION LOSS, dB (dual mode horn + OMT)	.3	.35	.3	.35
INPUT FILTER LOSS, dB	.1	.1	.1	.1
ISOLATOR LOSS, dB	.2	.2	.2	.2
TRANSITION LOSS, dB	.1	.1	.1	.1
AMPLIFIER NOISE FIGURE, dB	.7	1.2	.7	1.2
HARDWARE NOISE FIGURE, dB	1.4	1.95	1.4	1.95
RECEIVER NOISE TEMPERATURE, K	110	164	110	164
SYSTEM NOISE TEMPERATURE, K	360	414	360	414
PREDETECTION BANDWIDTH, MHz	300	500	300	500
INTEGRATION TIME, ms	2.54	1.27	5.08	2.54
RECEIVER ΔT, K	.41	.52	.29	.37
VIDEO NOISE CONTRIBUTION, K	.02	.03	.02	.03
A/D CONVERTER ΔT, K	.04	.04	.04	.04
TOTAL ΔT, K	.41	.52	.29	.37

RADIOMETER PERFORMANCE SUMMARY

The losses contributed by the feed horn, filter, isolator, and wave guide transition loss are based on current technology on Hughes communication satellites. The amplifier noise figure is based on the state of the art in 5 and 10 GHZ FET devices. Summing the losses and noise figure results in a 110°K and 164°K noise temperature for the 5 GHZ and 10 GHZ receiver portions of the radiometer. A standard scene temperature of 250°K and bandwidths of 300 and 500 MHZ for the 5 and 10 GHZ channels were used for the ΔT calculations. Using a 5 GHZ beamwidth of .68 degrees and sampling at twice the bandwidth along track results in a integration time of 2.54 ms at 5 GHZ for a 3 feed configuration (31.6 RPM).

$$\left(\frac{.68\ \text{deg}}{3\ \text{dB Beamwidth}} \times \frac{3\ \text{dB Beamwidth}}{2\ \text{samples}} \times \frac{22\ \text{Km}}{\text{Deg (At)}} \times \left(\frac{\text{sec}}{2980\ \text{Km}}\right)\right)$$

At 15.6 RPM the number of feeds are doubled to six and the integration time is doubled to 5.08 ms at 5 GHZ. The video noise contribution and analog to digital converter contributions are RSS'ed with the receiver ΔT resulting in a total ΔT of .29°K for 5.2 GHZ and .37°K for 10.4 GHZ with 6 feeds.

LFMR CONFIGURATIONS

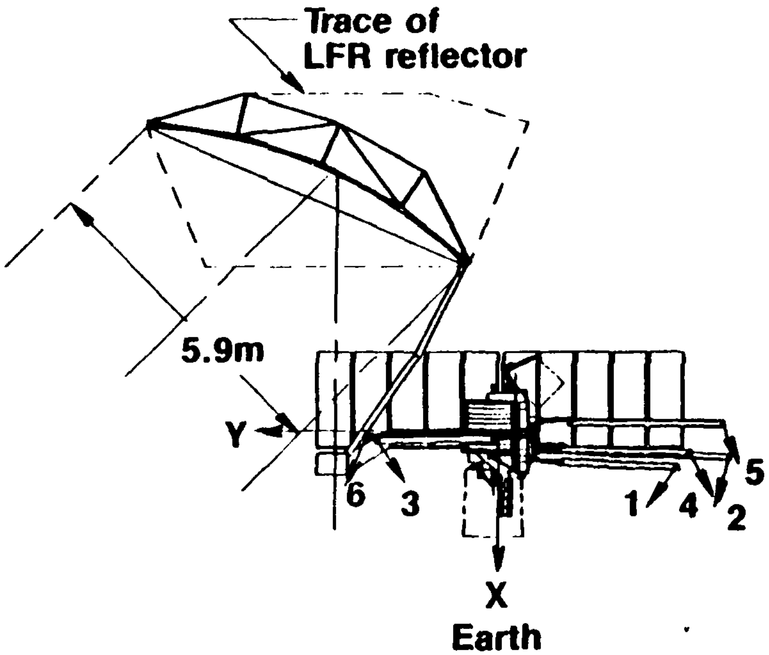

BASELINE

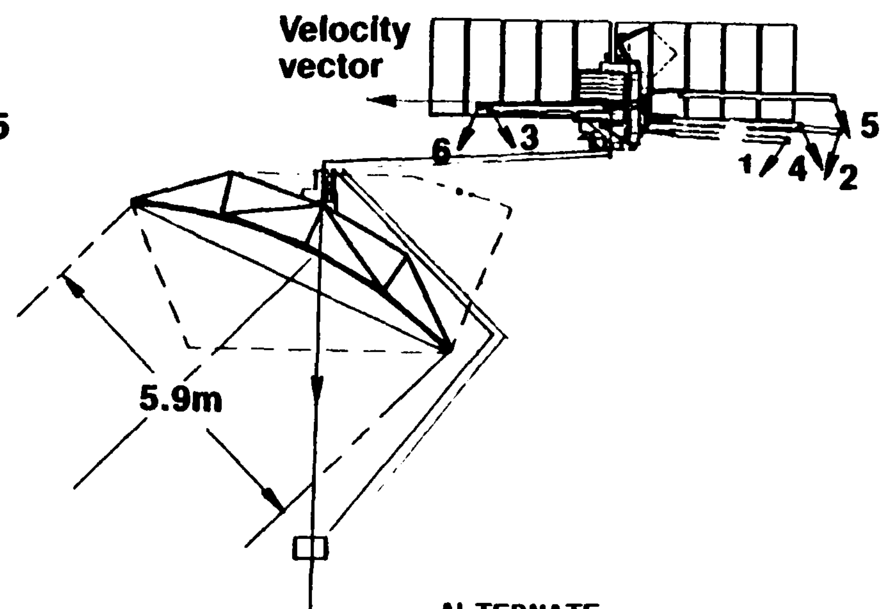

ALTERNATE

LFMR CONFIGURATION

Two configurations were analyzed. The baseline configuration consists of the LFMR deployed to the side of the S/C. This side mounted configuration allows a clear field of view for the LFMR as well as the other 3 instruments.

The alternate configuration requires a long boom mounted to the rear of the reflector to allow clear fields of view for the altimeter, tranet beacon, S/C antennas, and scatterometer. This configuration is a outgrowth of the bottom mounted option directed for study in the task statements. The original bottom mounted LFMR obscured the S/C antenna as well as the other instruments fields of view.

WEIGHT COMPARISON CHART

The weight budget for four cases consisting of two different configurations for each spin rate is shown here. The 15.8 RPM case has 5 lbs more receiver electronics, but the alternative has 2 lbs of the electronics moved from the spinning to non-spin section. If the minimum dynamic frequency of 1.0 Hz can be tolerated in ground test, the baseline configuration at 15.8 RPM has the lowest system weight.

WEIGHT COMPARISON CHART, LBS

5.9M ANTENNA

HUGHES

ITEM DESIGN		*15.8 RPM BASELINE		*15.8 RPM ALTERNATIVE		**31.6 RPM BASELINE		**31.6 RPM ALTERNATIVE
ANTENNA		71.6		87.1		89.0		87.1
REFLECTOR	37		37		37		37	
BOOM	34.6		50.1		52		50.1	
ELECTRONICS BOX		36		33		31		28
BAPTA (SPUN)		6		6		6		6
LOAD DESPIN MOTOR				10				10
BAPTA ENCLOSURE				3				3
BALANCE WEIGHT		15		5		15		5
BALANCE MECHANISM		12		12		12		12
HINGES		5.5		5.5		5.5		5.5
LAUNCH LOCKS		6.0		6.0		6.0		6.0
ACTUATORS		5.5		5.5		5.5		5.5
• TOTAL SPINNING		157.6		173.1		170.0		168.1

* DESIGNED FOR MINIMUM FREQUENCY = 1.0 Hz

** DESIGNED FOR MINIMUM FREQUENCY = 1.6 Hz

WEIGHT COMPARISON CHART, LBS (CONTINUED)

5.9M ANTENNA

HUGHES

	*15.8 RPM		**31.6 RPM	
ITEM DESIGN	BASELINE	ALTERNATIVE	BASELINE	ALTERNATIVE
BAPTA	14	14	14	14
ELECTRONICS BOX		6		6
HOT/COLD LOAD	4	4	4	4
• TOTAL DESPUN	18	24	18	24
• TOTAL LFMR	175.6	197.1	188.0	192.1
DEPLOYMENT BOOM	28.4	37.2	41.5	83.7
MOMENTUM WHEEL	45	45	75	75
• TOTAL	249.0	279.3	304.5	350.8
SPIN INERTIA (SLUG FT^2)	74.4	73.3	82.2	73.3

* DESIGNED FOR MINIMUM FREQUENCY = 1.0 Hz

** DESIGNED FOR MINIMUM FREQUENCY = 1.6 Hz

LFMR POWER BUDGET

The power budget for 15.8 RPM is 35.2 watts while the 31.6 RPM case is 43.1 watts. The principle difference is the momentum wheel power. The increase of 2.1 watts in the 15.8 RPM case is due to the three additional receivers and analog electronics.

LFMR POWER BUDGET, WATTS

HUGHES

	31.6 RPM		15.8 RPM	
	3 FEEDS, 6 RECEIVERS		6 FEEDS, 12 RECEIVERS	
ELECTRONICS		5.1		7.2
RF	.6		1.2	
ANALOG	1.5		3.0	
DIGITAL	3.0		3.0	
SPIN SUBSYSTEM		8.0		8.0
MOMENTUM WHEEL:		30.0		20.0
TOTAL POWER		43.1 WATTS		35.2 WATTS

FREQUENCY ALLOCATIONS

The next two charts are the frequency allocations as given in the International Frequency Registration Board (IFRB) for the 5 and 10 GHZ frequency bands.

FREQUENCY ALLOCATIONS, 5-6 GHZ

HUGHES

FREQUENCY, MHZ	SERVICE	RFI POTENTIAL
5000-5250	AERONAUTICAL RADIONAVIGATION	SMALL
5250-5350	RADIOLOCATION	SMALL
5350-5460	AERONAUTICAL RADIONAVIGATION	SMALL
5460-5470	RADIONAVIGATION	SMALL
5470-5650	MARITIME RADIONAVIGATION	SMALL
5650-5725	RADIOLOCATION	SMALL
5725-7075	FIXED-SATELLITE (EARTH TO SPACE)	HIGH

FREQUENCY ALLOCATIONS, 10-11 GHZ

FREQUENCY, MHZ	SERVICE	RFI POTENTIAL
10 - 10.45	FIXED, MOBILE RADIOLOCATION	MEDIUM
10.45 - 10.5	RADIOLOCATION	SMALL
10.5 - 10.7	FIXED, MOBILE RADIOLOCATION	MEDIUM
10.7 - 11.7	FIXED, MOBILE FIXED-SATELLITE (BOTH DIRECTIONS)	HIGH

POSSIBLE RFI - EMITTERS

This chart shows two possible sources of emitters and the effect on the LFMR for different configuration.

GROUND COMMUNICATION SERVICE

This case is a 1 foot reflector with a 1 watt transmitter. When the LFMR is looking at a sidelobe of the ground transmitter, the interference is 29 dB above an acceptable level. This is the most likely case and if an emitter is operating with the above parameters interference will be seen at that location as the LFMR scans. The ground antennas are fixed point to point microwave service.

GROUND TO SATELLITE SERVICE

As can be seen in the chart all cases, except when both antennas are off axis, cause interference. The IFRB does not allow this service in the 5 or 10 GHZ band so this case should be no problem.

POSSIBLE RFI - EMITTERS

- GROUND COMMUNICATION SERVICE

POWER - 1 WATT

ANTENNA - 1 FOOT

RFI INTERFERENCE

LFMR

		ON AXIS	OFF AXIS
GROUND	ON AXIS	+ 60 dB	0
	OFF AXIS	+ 29	-28

- GROUND TO SATELLITE SERVICE

POWER - 1000 WATT

ANTENNA - 40 FOOT

RFI INTERFACE

LFMR

		ON AXIS	OFF AXIS
GROUND	ON AXIS	+123	+65
ANTENNA	OFF AXIS	+55	0

RFI - SMMR

The chart shows some of the problems that the Scanning Multifrequency Microwave Radiometer (SMMR) observed during the NIMBUS-7 mission.

R F I - SMMR

HUGHES

RADIO FREQUENCY INTERFERENCE (RFI) WAS LOOKED FOR IN THE DATA FROM THE NIMBUS-7 SMMR.

NO EVIDENCE OF RFI WAS FOUND OVER OCEAN AREAS.

SOME LAND AREAS (E.G., WEST GERMANY) HAD BRIGHTNESS TEMPERATURES WELL IN EXCESS OF 300 K, INDICATING SOME SOURCE OF MAN-MADE RADIO EMISSION.

THERE WERE ISOLATED INSTANCES OF INDIVIDUAL RECORDS OVER THE OCEAN HAVING BRIGHTNESS TEMPERATURES THAT WERE TOO HIGH FOR NATURAL EMISSION, BUT THOSE WERE PROBABLY DUE TO MALFUNCTIONS IN THE INSTRUMENT OR DATA ERRORS.

LFMR DATA RATE

To achieve 2 samples per beamwidth (Nyquist rate) a 13.4 KBPS data rate is necessary. If 6 feeds are used at 31.6 RPM to lower the ΔT, the data rate is doubled to 26.9 KBPS.

HUGHES

LFMR DATA RATE

	31.6 RPM 3 FEEDS		15.8 RPM 6 FEEDS		31.6 RPM 6 FEEDS	
	5 GHZ	10 GHZ	5 GHZ	10 GHZ	5 GHZ	10 GHZ
NUMBER OF SCENE STATIONS PER SCAN	213	426	213	426	213	426
NUMBER OF BEAMS	1	2	2	4	2	4
POLARIZATIONS	2	2	2	2	2	2
BITS PER SAMPLE	12	12	12	12	12	12
	5112	20448	10224	40896	10224	40896
TOTAL	25560		51120		51120	
SCAN TIME, SEC	1.9		3.8		1.9	
DATA RATE, K BITS/SEC	13.452		13.452		26.905	

OFFSET DESIGN CONFIGURATIONS

Two offset reflector configurations were also considered; one is the single offset reflector. The other one is the two reflector (offset Cassegrain) system. These two configurations both feature no aperture blockage and the beam efficiency can be maximized by the high feed taper.

AXIS SYMMETRY DESIGN CONFIGURATIONS

HUGHES

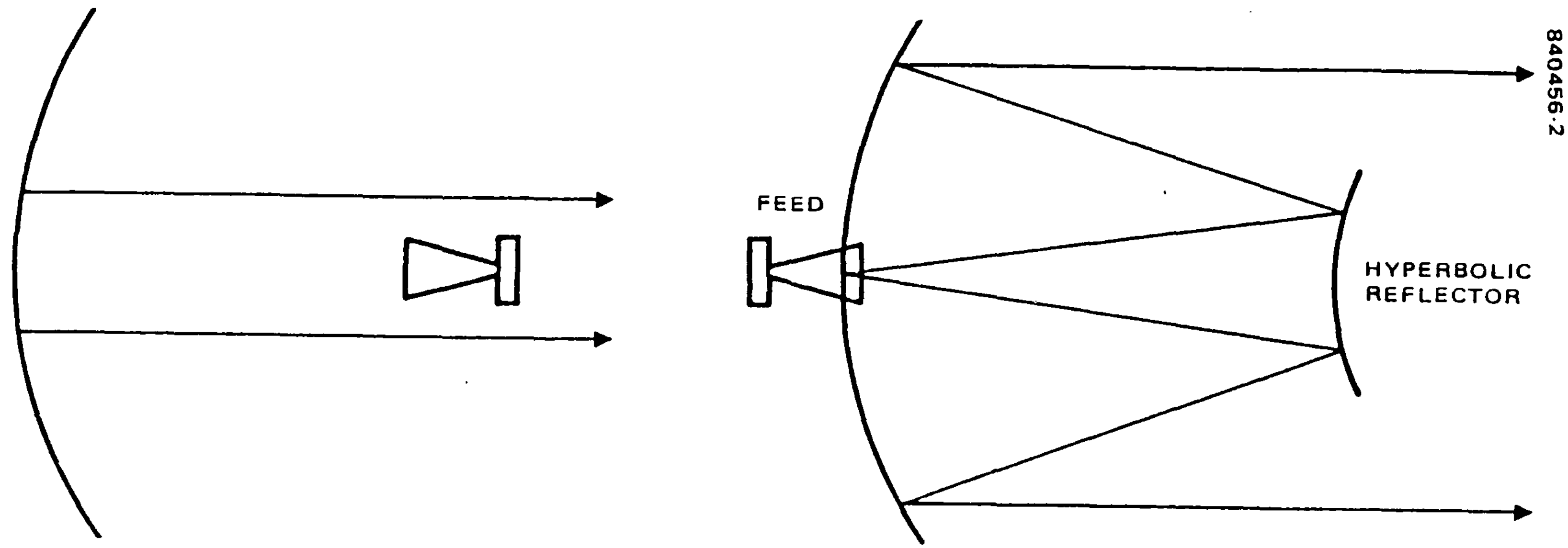

a) PRIME FOCUS

b) CASSEGRAIN

AXIS SYMMETRY DESIGN CONFIGURATIONS

Two axis symmetric reflector configurations were considered for LFMR antenna design. One is the prime focus (single) reflector. The other one is the Cassegrain (two) reflector system. In general, the Cassegrain configuration has less axial length due to its folded optics design. However, both configurations have aperture blockage problems.

LFMR Antenna Subsystem Configuration

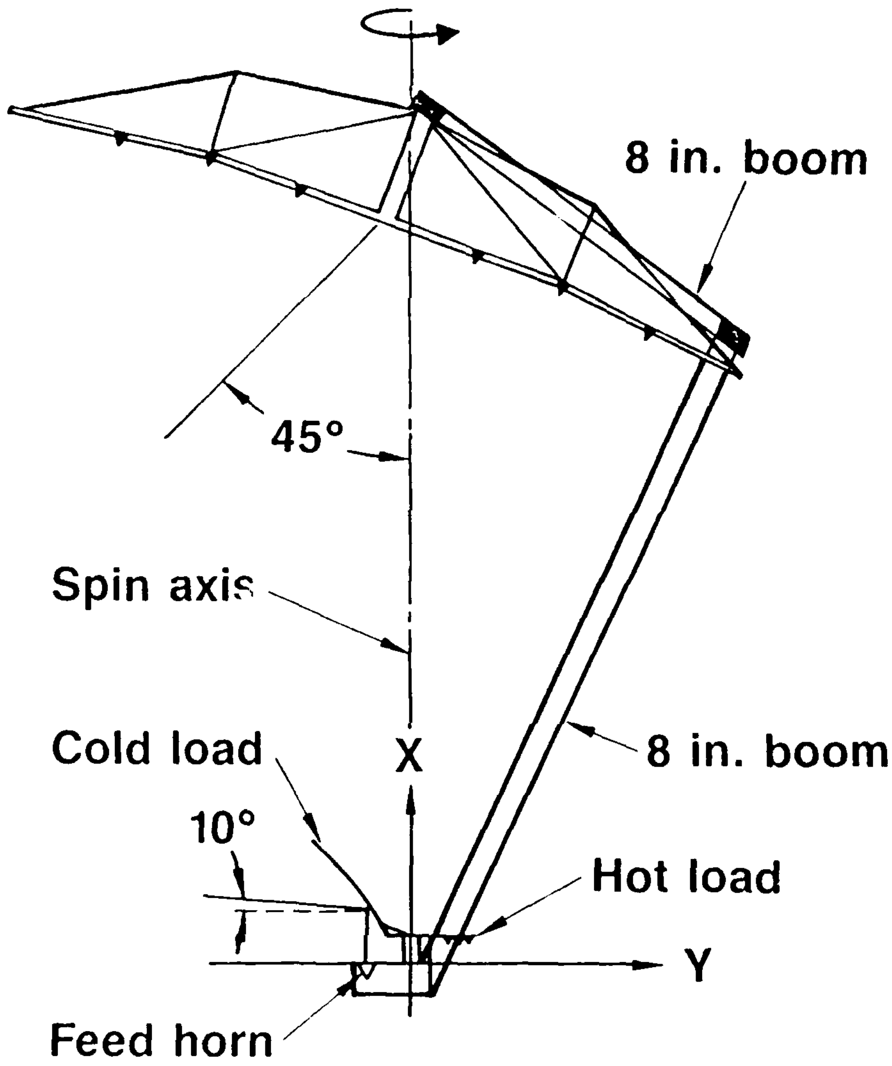

847098-19

LFMR ANTENNA SUBSYSTEM CONFIGURATION

The baseline LFMR antenna subsystem consists of an unfurlable offset reflector (with 5.9 meter projected diameter), 8 inch support boom, feed horn cluster, hot and cold calibration loads. The reflector is attached at the back of the hub by the 8 inch boom. In addition, the reflector and the feed cluster are spinning at a constant speed about the X-axis. The reflector boresight is pointed at 45° w.r.t. the spin axis (or X-axis). The hot and cold loads are supported by a shaft which is stationary, i.e. not moving with the reflector and feed cluster. The cold load is a solid offset reflector whose boresight is tilted 10° up from the horizon so that its field of view (FOV) is cleared from the other instruments on the spacecraft.

ANTENNA SUBSYSTEM

SAMPLING CONCLUSIONS

HUGHES

- INTEGRATE AND DUMP
  - EASY TO BUILD
  - HIGH GROUND SPACIAL FREQUENCIES ATTENUATED
- ANALOG FILTER
  - DIFFICULT TO STABILIZE PHASE AND AMPLITUDE RESPONSE
  - LESS ATTENUATION OF HIGH SPACIAL FREQUENCIES
- DIGITAL FILTER
  - DIFFICULT TO BUILD
  - THEORY WELL UNDERSTOOD
  - SHOULD WORK PERFECTLY

SAMPLING CONCLUSION

The integrate and dump sampling technique has been used on flight radiometers, and is easy to fabricate. The high ground spatial frequencies are attenuated, and it remains to be determined if this is a problem for the LFMR.

Two types of low pass filters are available, either analog or digital. The analog low pass filter has better theoretical performance than the integrate and dump, but the filters are difficult to build with stable phase and amplitude response. The digital low pass filter has the best response and the operational theory is well understood. No space qualified low weight and low power digital filter is available. A significant development effort would be needed to implement the digital filter technique.

RECONSTRUCTED NOISE LEVEL

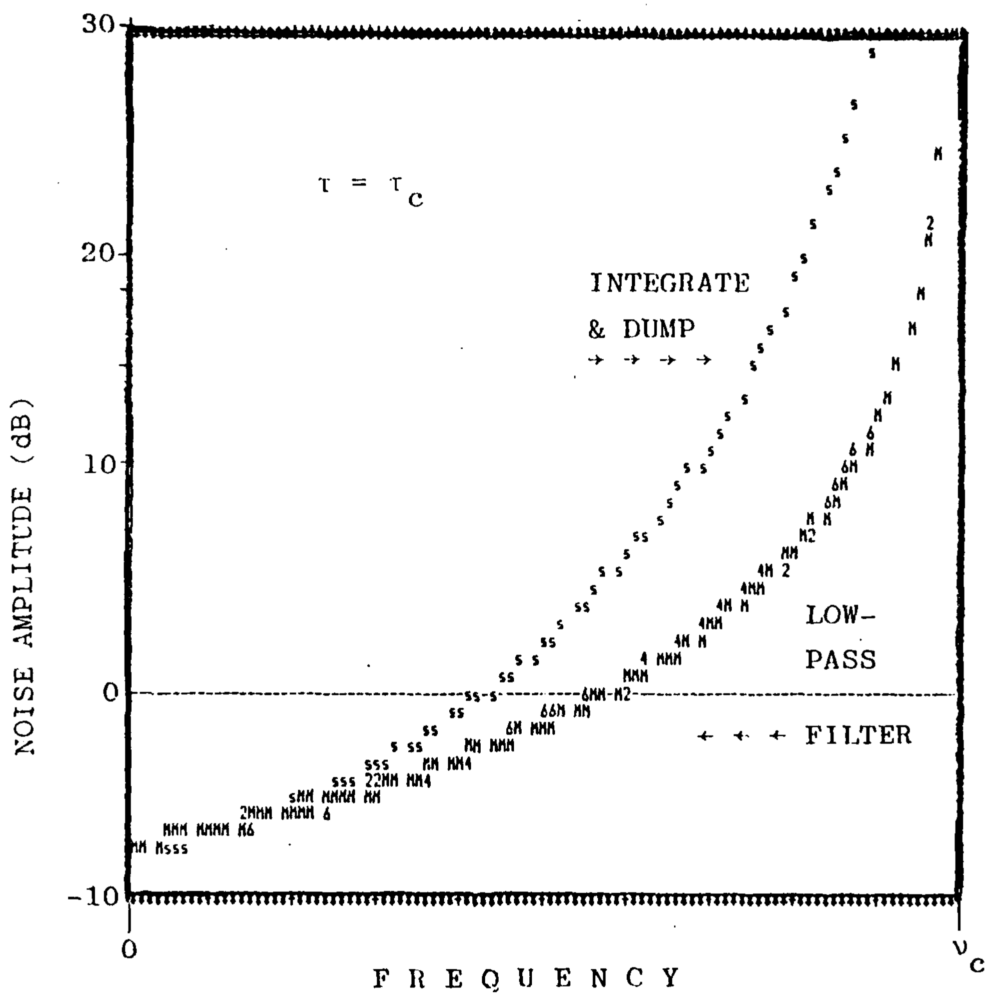

RECONSTRUCTED NOISE LEVEL

The noise amplitudes for the two different sampling techniques are shown. The integrate and dump technique allows increased noise at higher spatial frequencies with a resultant loss of spatial resolution when compared to the low pass filter technique.

RADIOMETER ANALOG OUTPUT SPECTRUM

HUGHES

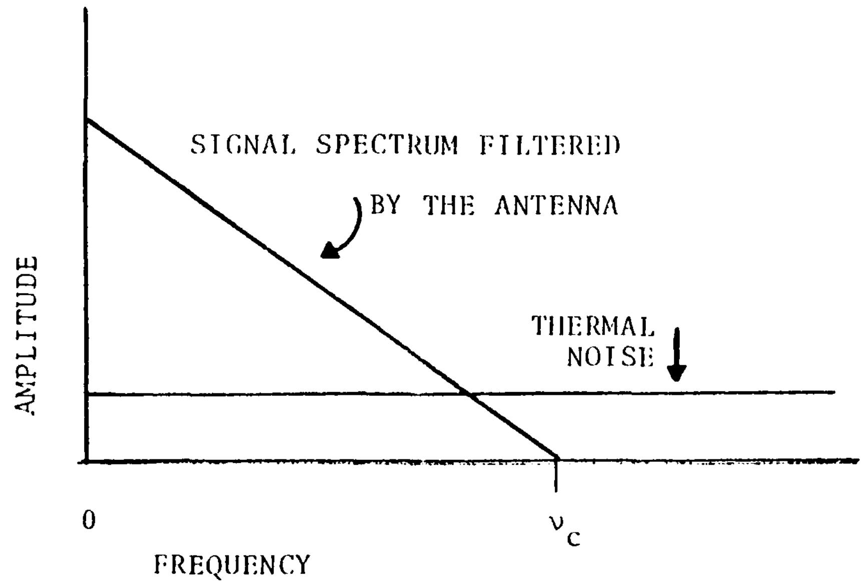

RADIOMETER ANALOG OUTPUT SPECTRUM

The higher ground spatial frequencies are attenuated by the antenna as shown here. For transmission to earth, the signal must be sampled. The two sample processes are integration for $\tau \leq 1\ \nu_C$ or filtering with a cutoff frequency of ν_C.

Results are shown in the next pages, but a more complete report is given in Appendix A.

CANDIDATE LFMR SCAN PATTERNS

HUGHES

3 FEEDS - 31.6 RPM

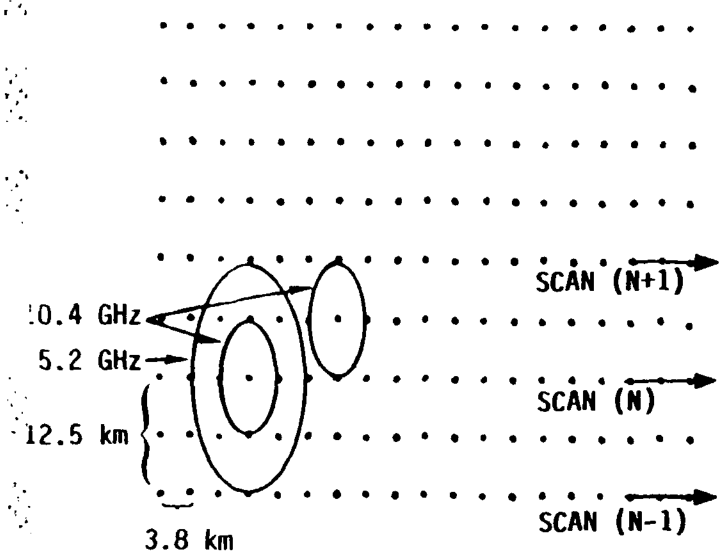

6 FEEDS - 15.8 RPM

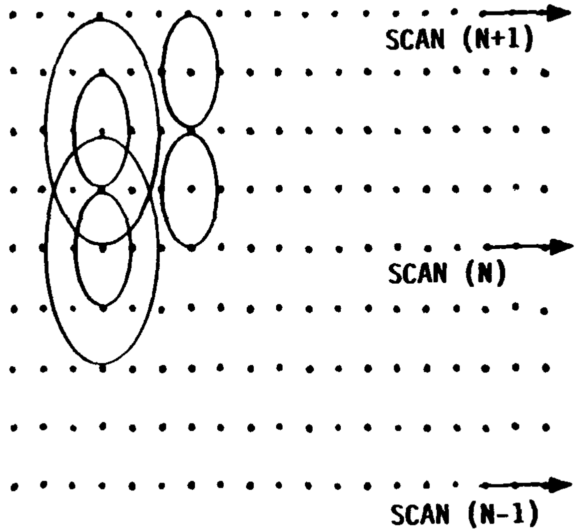

6 FEEDS - 31.6 RPM

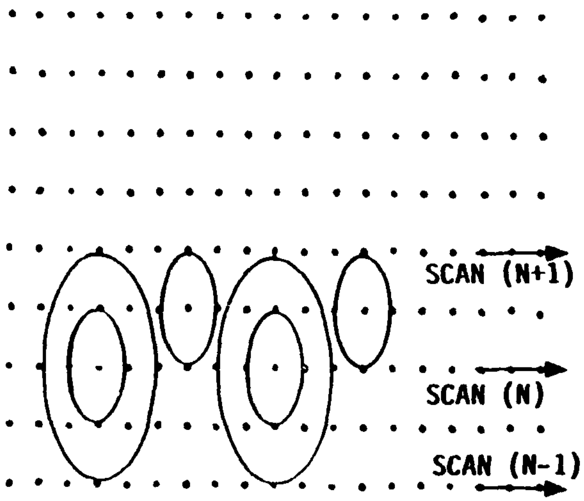

CANDIDATE LFMR SCAN PATTERNS

This chart shows scan patterns that will achieve NYQUIST sampling rates. The relative positions of the beams can be adjusted subject to the physical constraints of the feed package. Each dot on the chart represents a scene station at 10.4 GHZ. The 5.2 GHZ scene stations are every other dot in both the along track and along scan direction.

OFFSET DESIGN CONFIGURATIONS

HUGHES

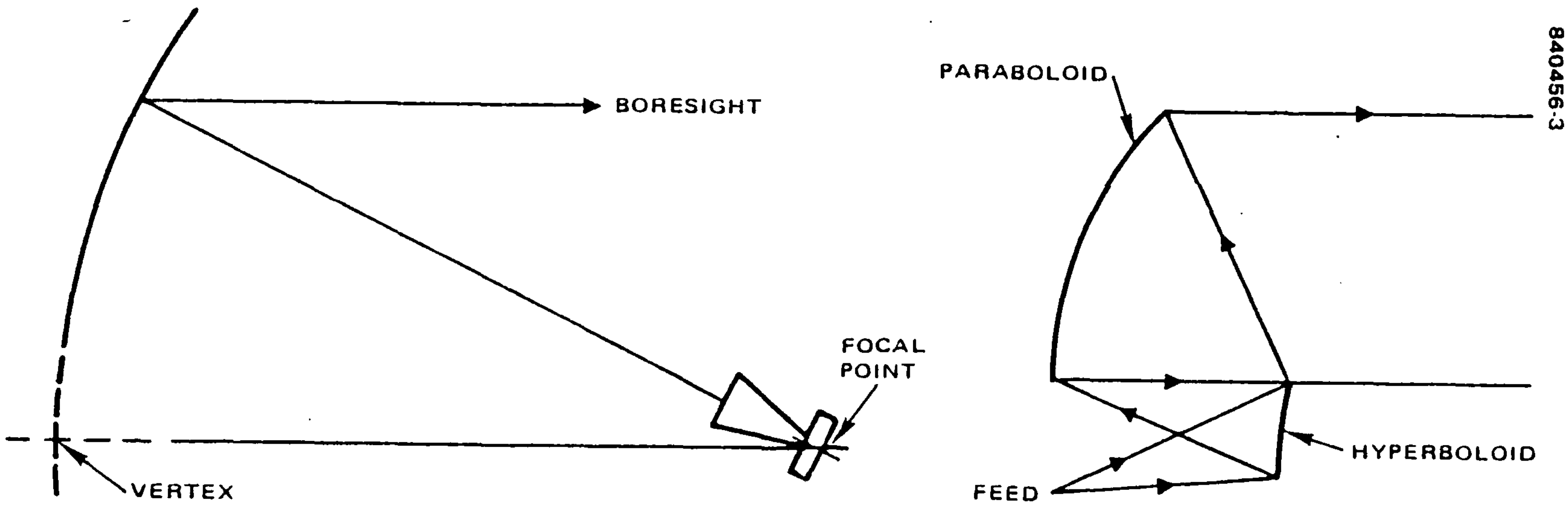

a) OFFSET REFLECTOR

b) OFFSET CASSEGRAIN

ANTENNA CONFIGURATION TRADE-OFF

The comparison of the four different reflector antenna configurations is summarized in this viewgraph. The two symmetric configurations have aperture blockage problems which result in lower beam efficiency and higher sidelobe levels and spillover loss. The cross polarization is low for axial symmetric configurations and for offset reflectors with long focal length. The alignment is easier for single reflectors and symmetric Cassegrain antennas. Except for the front-fed offset reflector, the other three configurations have difficulty accommodating the hot and cold calibration loads. Therefore, the front fed offset reflector is selected as the baseline configuration.

ANTENNA CONFIGURATION TRADE-OFF

HUGHES

	OFFSET FRONT FED	ON-AXIS FRONT FED	OFFSET CASSEGRAIN	ON-AXIS CASSEGRAIN
APERTURE BLOCKAGE	NO	YES	NO	YES
BEAM EFFICIENCY	HIGH	LESS	HIGH	LESS
SIDELOBE LEVEL	LOW	HIGH	LOW	HIGH
CROSS POLARIZATION	MEDIUM	LOW	LOW	LOW
SPILLOVER LOSS	SMALL	MEDIUM	SMALL	HIGH
ALIGNMENT DIFFICULTY	SMALL	SMALL	HIGH	MEDIUM
CALIBRATION LOADS ARRANGEMENT DIFFICULTY	SMALL	HIGH	HIGH	HIGH

GEO-TRUSS TYPE UNFURLABLE REFLECTOR

A geo-truss type unfurlable reflector, which is made by General Dynamics, is shown in the fully deployed and folded configurations. Also shown here are the supporting truss ribs of this reflector.

GEO-TRUSS TYPE UNFURLABLE REFLECTOR

HUGHES

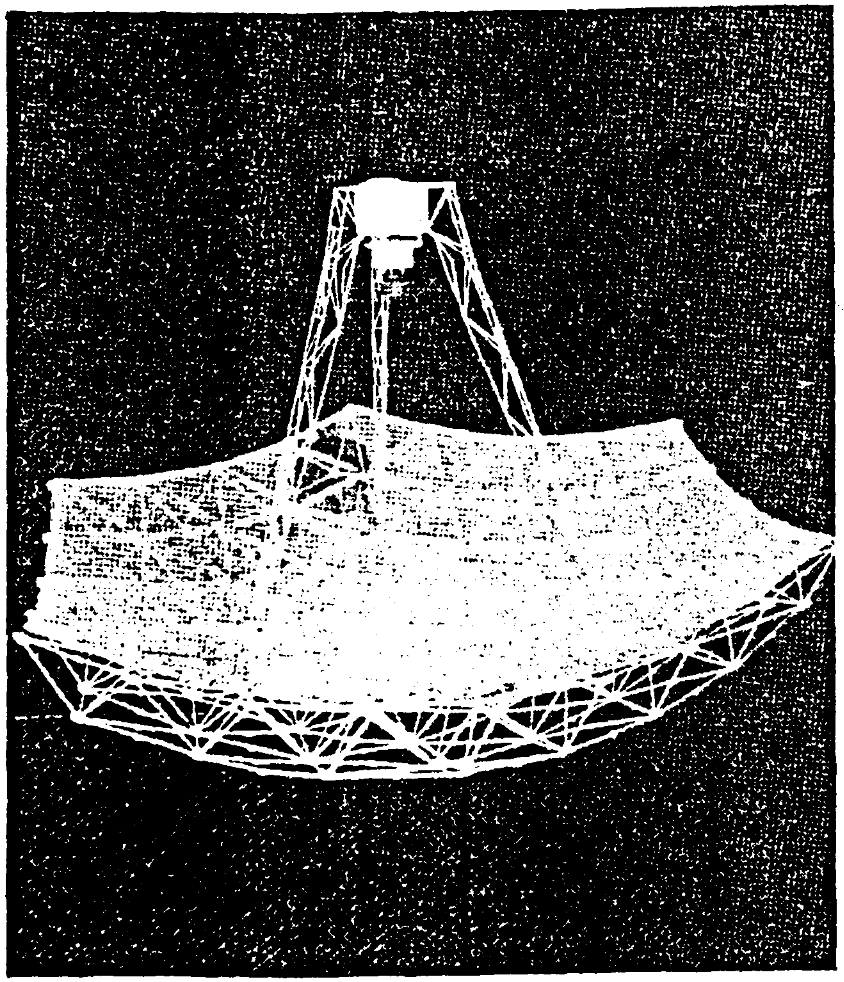

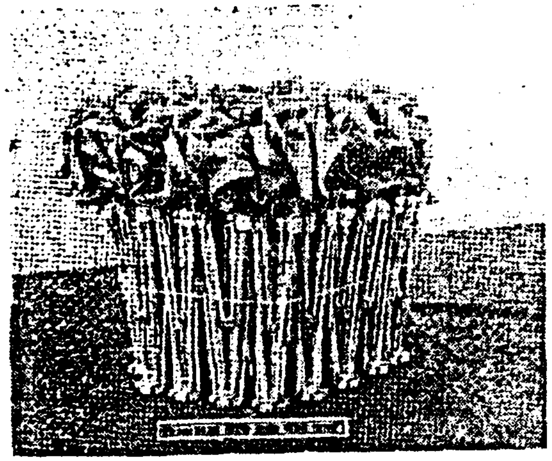

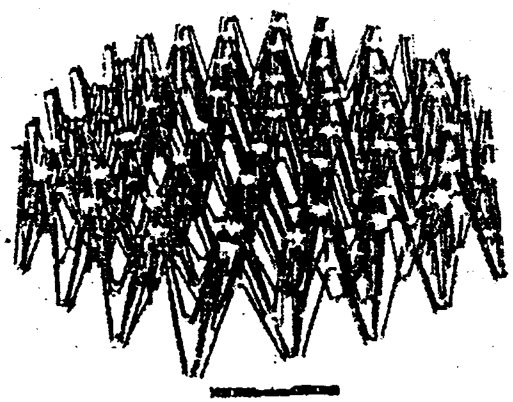

846770-9

HARRIS TRUSS RIB ANTENNA

A fully deployed truss rib antenna proposed by Harris is shown.

HARRIS TRUSS RIB ANTENNA

HUGHES

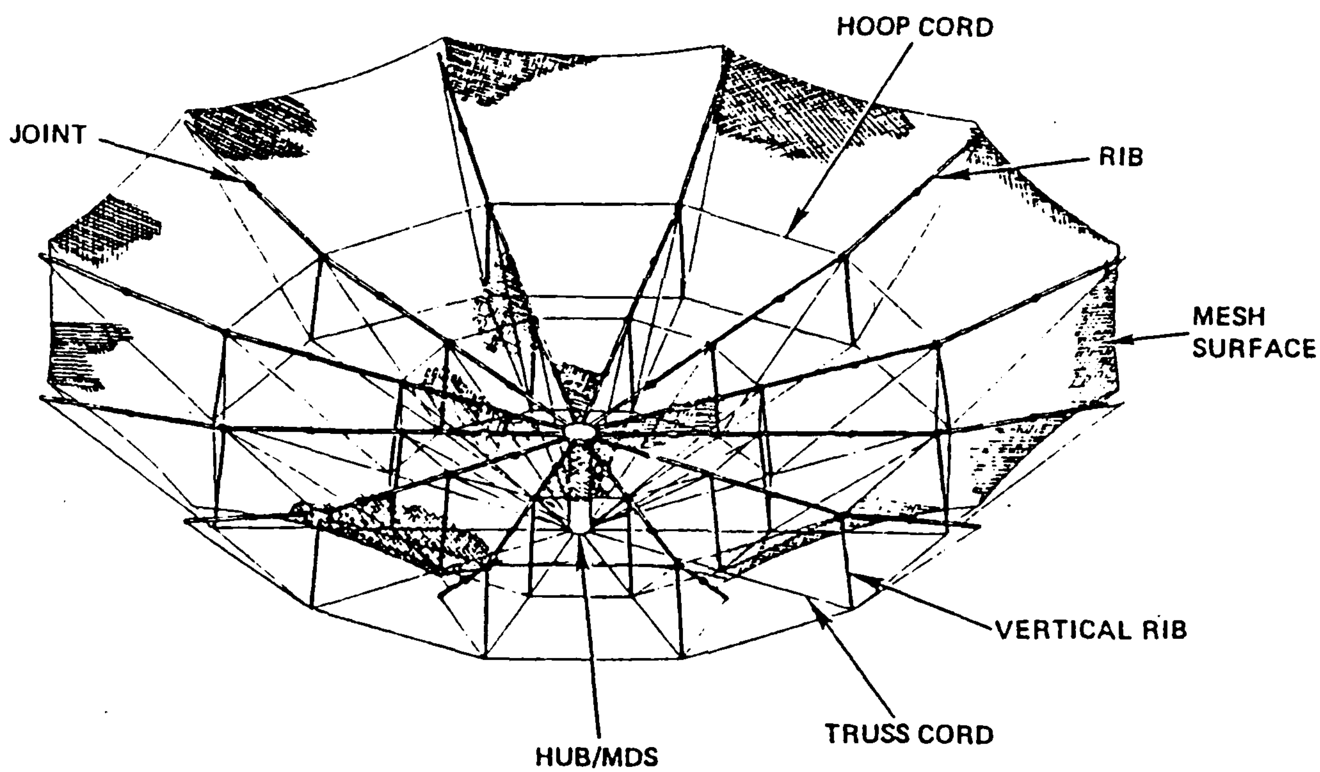

COMPARISON OF 5.9M DIAMETER MESH REFLECTOR VENDORS

The Harris and General Dynamics (GD) reflector designs, for a 5.9m diameter mesh reflector, are summarized here. Since Harris' reflector is supported at the rear center, its reflector weight, stow volume, moment of inertia and the base frequency are lower than GD's. (Note that GD's reflector is supported at the edge so its design has to be more rigid and heavier than Harris'.) The Harris reflector design will be used for the rest of the study for both mechanical and electrical tradeoff studies.

COMPARISON OF 5.9M DIAMETER MESH REFLECTOR VENDORS

HUGHES

	GENERAL DYNAMICS	HARRIS
REFLECTOR WEIGHT (LB)	75.9	37.5
REFLECTOR BASE FREQUENCY (Hz)	9	3.8
REFLECTOR MOI WRT C.G. (SLUG.FT²)	$\begin{bmatrix} 89 & 0 & 0 \\ & 96 & 25 \\ & & 158 \end{bmatrix}$	$\begin{bmatrix} 24 & 0 & 0 \\ & 24 & 0 \\ & & 46 \end{bmatrix}$
STOW DIAMETER (IN)	29.3	24
STOW HEIGHT (IN)	73.5	30
MOUNTING LOCATION	EDGE	CENTER REAR

DUAL MODE HORN

The first feed candidate is the dual mode horn which has the following features:

- good pattern symmetry
- low sidelobe, cross polarization and insertion loss
- 12% bandwidth
- proven design and manufacture
- one horn will be needed for each frequency and antenna beam

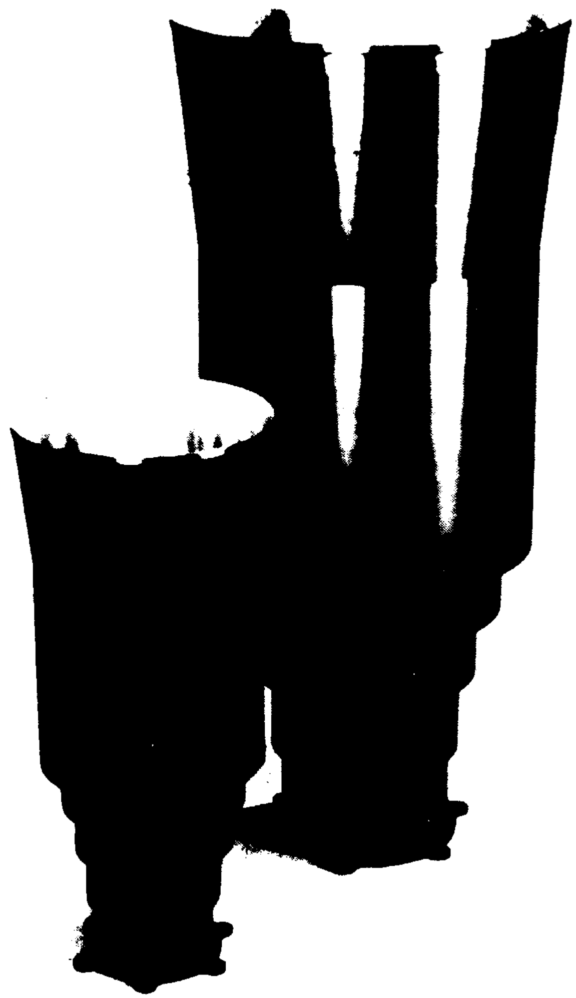

HUGHES

Dual Mode Horn

847098-17

82 16172

CORRUGATED HORN

The second feed candidate is the corrugated horn which has the following features:

- good pattern symmetry
- low sidelobe and cross polarization
- wider bandwidth than the dual mode horn
- relatively expensive and complicated to manufacture

CORRUGATED HORN

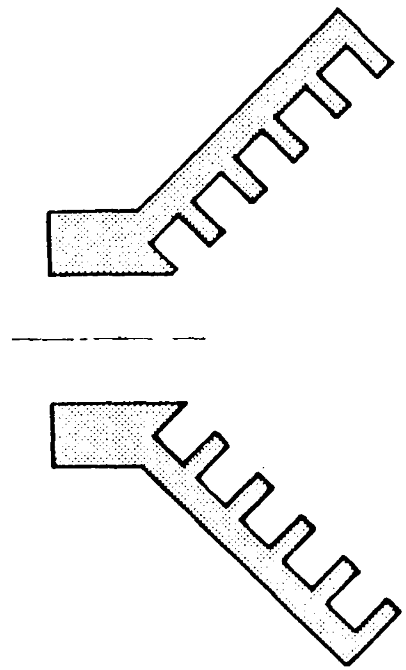

COAXIAL HORN SCHEMATIC

The third feed candidate is the coaxial horn which consists of an outer corrugated horn operated at 5.2 GHz and a center dielectric rod operated at 10.4 GHz.

MESH EMISSIVITY THEORETICAL MODELING

A simple theoretical model is used to evaluate the mesh emissivity. The mesh is modeled by periodically bonded lossy wires(with the finite conductivity of the gold). Thus the mesh emissivity is computed as the dissipative power fraction (or ohmic loss) of these lossy wires. Note that this model is valid only for meshes with thin wires and electrically small apertures.

18 OPENINGS/INCH MESH

FREQUENCY, GHz	REFLECTION LOSS, dB		
	NORMAL INCIDENCE	OBLIQUE INCIDENCE ($\theta = 30°$)	
		TM	TE
18	0.253	0.189	0.322
15.12	0.179	0.134	0.2296
8	0.0503	0.0375	0.0658

846770-4

COMPUTED REFLECTION LOSS OF 18 OPENINGS/INCH MESH

At normal incidence, the computed reflection loss of 18 openings/inch mesh agrees with Harris measured results at 8 and 15.12 GHz. Computed results are also shown for a 30° incident case and TE and TM polarized plane waves.

COMPUTED MESH CROSS POLARIZATION
NORMAL INCIDENCE

HUGHES

OPENINGS/IN.	5.2 GHZ	10.4 GHZ
31	0.11×10^{-4}	0.45×10^{-4}
18	0.46×10^{-4}	1.82×10^{-4}
10	1.8×10^{-4}	6.7×10^{-4}

COMPUTED MESH CROSS POLARIZATION, NORMAL INCIDENCE

The computed mesh cross polarization for a normally incident plane wave is very small for all the three different meshes at both 5.2 and 10.4 GHz. The values shown are fractions of total incident radiation.

COMPUTED MESH TRANSMISSIVITY
NORMAL INCIDENCE

HUGHES

OPENINGS/IN.	5.2 GHZ	10.4 GHZ
31	0.002	0.007
18	0.006	0.024
10	0.022	0.086

COMPUTED MESH TRANSMISSIVITY, NORMAL INCIDENCE

For a normally incident plane wave, the mesh transmissivity is computed for 5.2 and 10.4 GHz and 31, 18 and 10 openings/inch. Note that as the number of mesh openings/inch increases (i.e., the aperture size of the mesh becomes smaller), the mesh transmissivity decreases (i.e., less energy is transmitted through the mesh). Also for a fixed number of openings/inch at the lower frequency region (5.2 GHz), the electrical size of the mesh aperture becomes smaller, the transmissivity is again less than at 10.4 GHz. Therefore, the mesh with greater than or equal to 31 openings/inch is recommended for LFMR.

Theoretical Modeling of Mesh Transmissivity

HUGHES

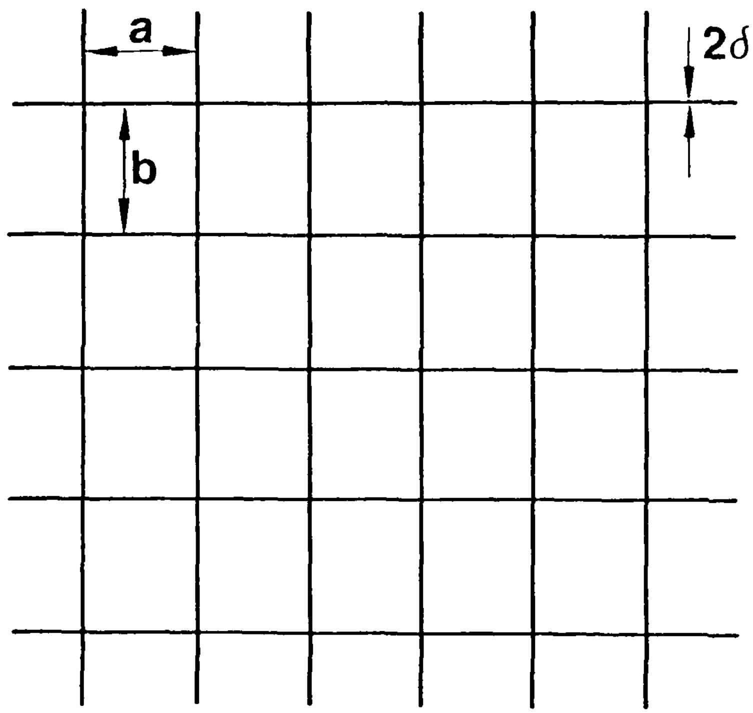

Assumptions

- Periodic lattice
- Square or rectangular opening
- Perfect conducting wire
- Plane wave illumination

847098 1

THEORETICAL MODELING OF MESH TRANSMISSIVITY

The most commonly used reflective mesh is composed of gold-plated molybdenum wire, approximately one-thousandth of an inch in diameter. Typically the mesh is knitted in a tricot manner and is characterized in terms of the number of openings per inch. To evaluate the mesh transmissivity, the simple model of a periodic lattice consisting of conducting wires is assumed. Using the integral equation technique, one may readily compute the mesh transmissivity for various openings/inch and frequencies. The mesh transmissivity is defined as the ratio of the transmitted power through the mesh divided by the total power of the incident plane wave.

FEED HORN TRADE-OFF

HUGHES

	SINGLE FREQUENCY DUAL MODE	CORRUGATED	COAXIAL	QUADRIDGE
PATTERN SYMMETRY	GOOD	GOOD	GOOD	POOR
CROSS POLARIZATION	LOW	LOW	LOW	MEDIUM
SIDELOBE LEVEL	LOW	LOW	LOW	MEDIUM
BANDWIDTH	MEDIUM	MEDIUM	HIGH	HIGH
INSERTION LOSS	LOW	MEDIUM	HIGH	HIGH
SIZE/WEIGHT	SMALL	MEDIUM	MEDIUM	MEDIUM
DESIGN/FAB. DIFFICULTY	LOW	MEDIUM	MEDIUM	HIGH

FEED HORN TRADE-OFF

The features of the four feed candidates are summarized here. The single frequency dual mode horn has all the required features for a radiometer such as good pattern symmetry, low sidelobe and cross polarization and most important low insertion loss. Therefore, it is selected for LFMR. If several antenna beams at different frequencies were needed, the corrugated, coaxial, and quadridge horn would need to be augmented by additional horns.

QUADRIDGE HORN SCHEMATIC

HUGHES

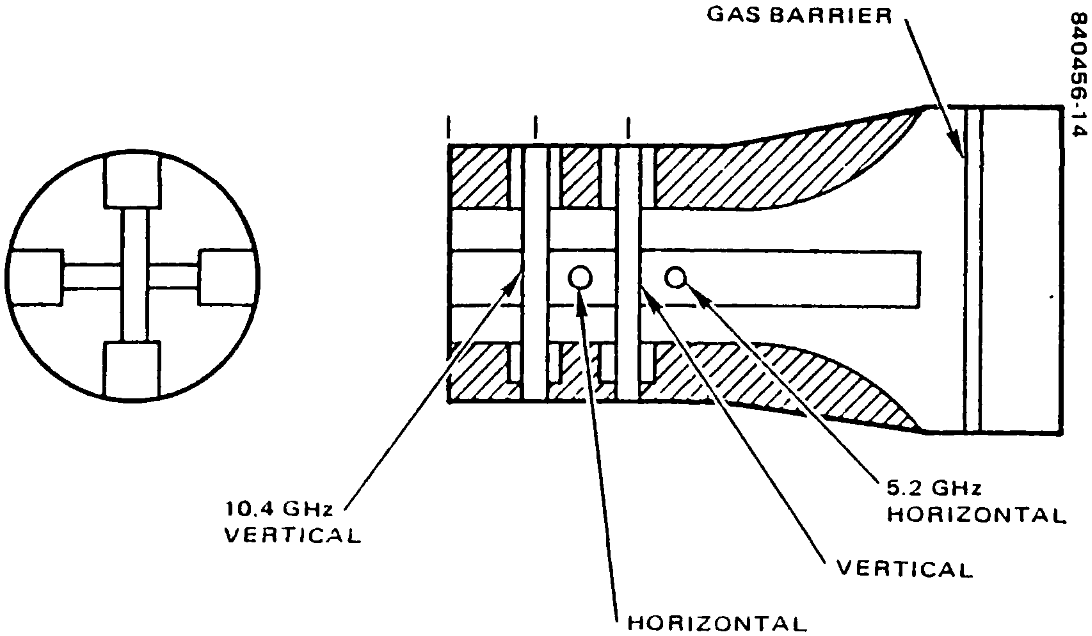

QUADRIDGE HORN SCHEMATIC

The last feed candidate is the quadridge horn which has four probes. Two front probes are operated at 5.2 GHz for horizontal and vertical polarization respectively. Two rear probes are operated at 10.4 GHz for horizontal and vertical polarization respectively.

Coaxial Horn Schematic

HUGHES

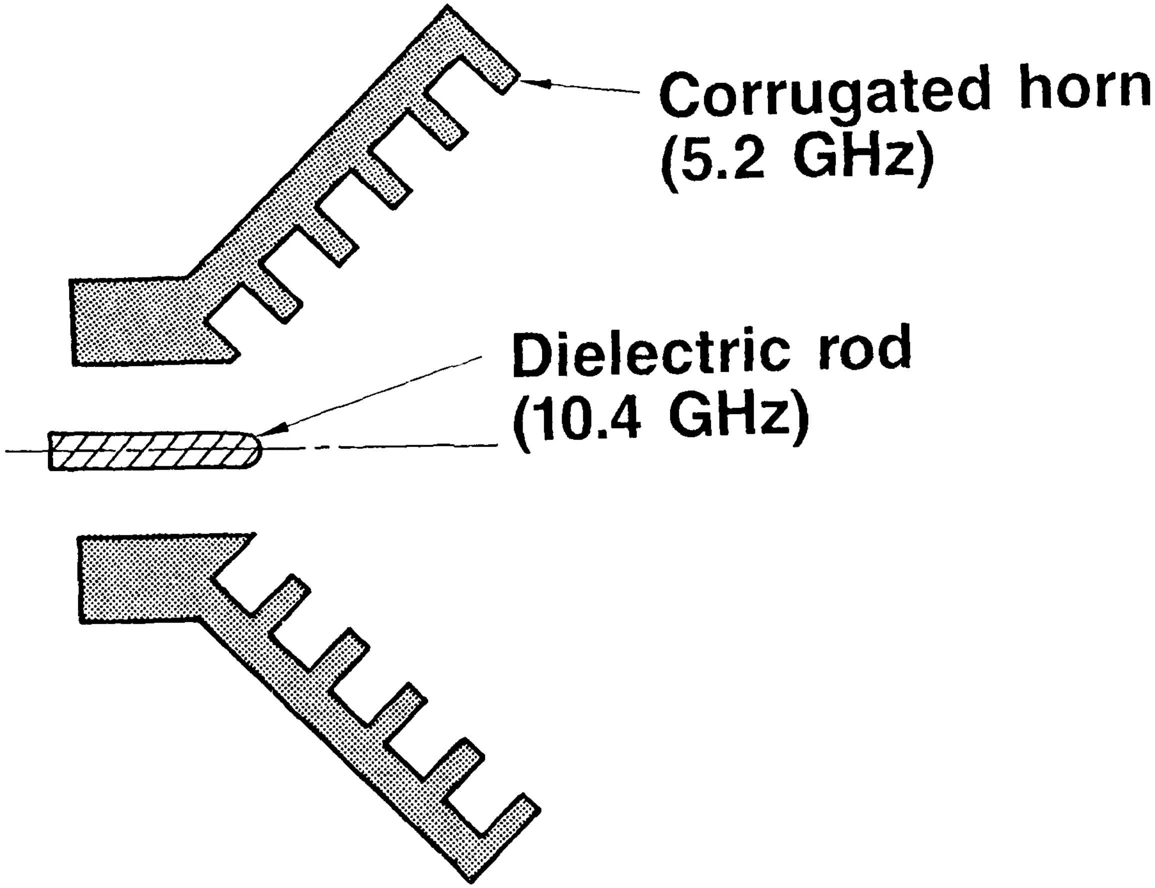

847098 2

Mesh Emissivity Theoretical Modeling

HUGHES

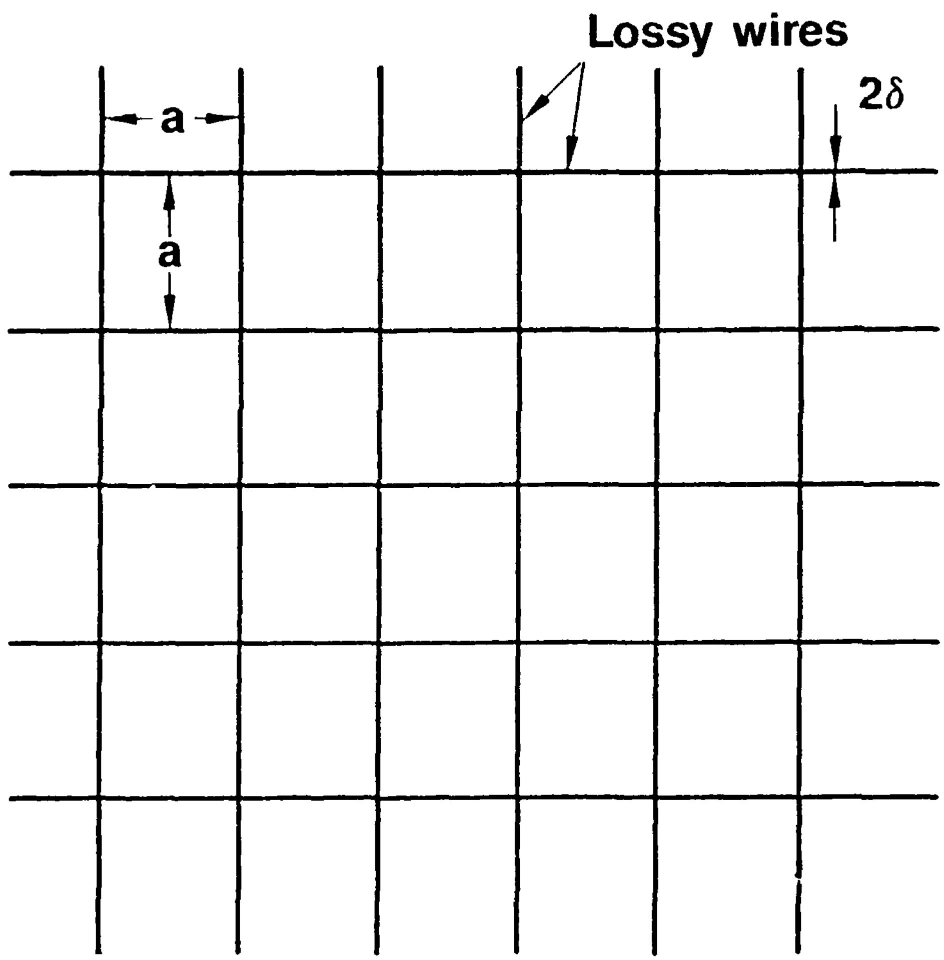

846952 9

Assumptions

- Periodically bonded lossy wires
- Square opening
- Gold-plated molybdenum wire
- 2δ is 1 mil thick
- $2\delta << a <<$ wavelength

EQUATION FOR MESH EMISSIVITY EVALUATION

Based on the assumptions shown, the equation derived by Ulrich may be used to compute the mesh emissivity. Although the accuracy of this equation needs further experimental verification, one may readily evaluate the mesh emissivity for various frequencies and openings/inch.

EQUATION FOR MESH EMISSIVITY EVALUATION

HUGHES

- $\epsilon = \frac{a}{\pi \gamma} \left| \Gamma \right|^2 \sqrt{\frac{c}{\sigma \lambda}}$
- ϵ IS THE MESH EMISSIVITY
- a IS THE PERIOD OF THE MESH
- γ IS THE RADIUS OF THE MESH WIRE
- $\Gamma = 1 / \left(1 + j \frac{2a}{\lambda} \ln \frac{a}{2\pi\gamma}\right)$
- C IS THE SPEED OF LIGHT
- λ IS THE WAVELENGTH
- σ IS THE GOLD CONDUCTIVITY IN CGS UNITS

R. ULRICH, APPLIED OPTICS, VOL 9, PP 2511-2516, NOV 1970

COMPUTED MESH EMISSIVITY (OHMIC LOSS)

The computed mesh emissivities for three different openings/inch at 5.2 GHz are very close to the preliminary measured results obtained at NASA-Langley. Also shown here are the computed emissivities at 10.4 GHz. Note that as the frequency increases the emissivity also increases. However as the number of openings/inch increases the emissivity decreases. Thus it is recommended that 31 openings/inch mesh be used for the LFMR.

Computed Mesh Emissivity (Ohmic Loss)

HUGHES

Openings/in.	5.2 GHz	10.4 GHz
31	0.0025	0.0035
18	0.0041	0.0058
10	0.007	0.0098

846952-10

COLD LOAD REFLECTOR DESIGN

The LFMR requires a cold calibration point that is best provided by sensing the background radiation present in deep space. This can be accomplished by directing the background radiation into the feeds while simultaneously blocking the beam of the LFMR reflector. A small cold load reflector of the proper dimensions can be incorporated into the design to serve these functions.

This cold load reflector will be mounted on the despun shaft of the bearing assembly and positioned so the focal point will pass over each of the feed horns as they rotate about the spin axis. The reflector must also provide acceptable electrical performance to enable five calibration samples to be collected during each rotation.

The cold load reflector must have a field of view that avoids radiation from the sun, earth and spacecraft components which would invalidate the cold calibration measurement. To avoid extraneous radiation from the sun, the cold load reflector must look away from the sun and is therefore restricted to the -Z-direction. Earth radiation can be avoided by directing the cold load reflector in the -Y-direction. This reduces the field of view to the III quadrant of the Y-Z plane. The only potential spacecraft interferences within this quadrant are the scatterometer antennas which can be avoided by requiring the cold load reflector to look up 10° out of the Y-Z plane. Although it is likely the cold load reflector will sometimes see the moon, these occasions can be accurately predicted and result in an acceptable increase in the cold calibration measurement.

Cold Load Reflector FOV

HUGHES

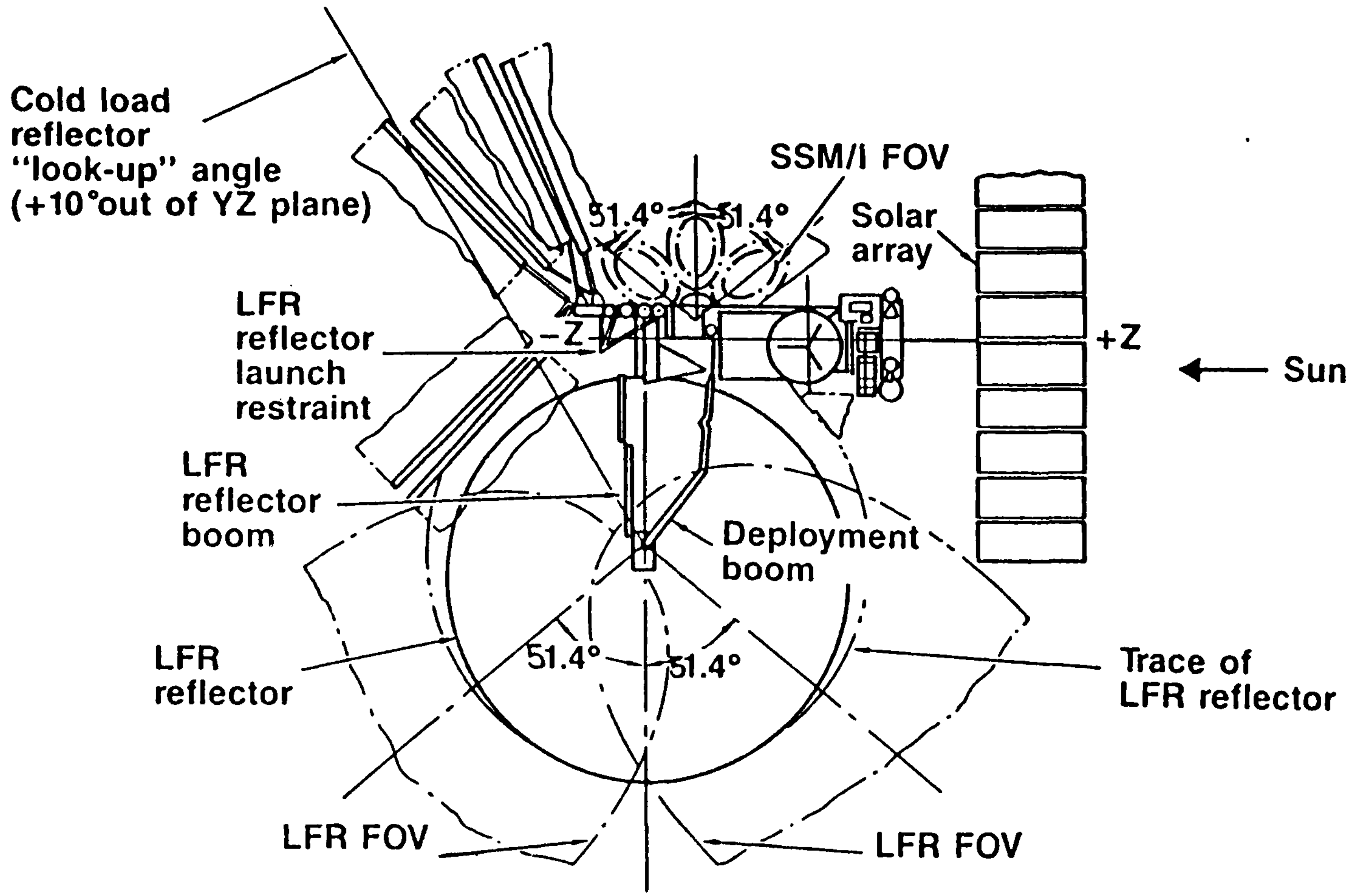

847098-10

CAD-ASSISTED COLD LOAD DESIGN

A study was performed to investigate the design parameters associated with the cold load reflector. Several variables were considered in determining the optimum design. Firstly, it is desirable to have a cold load reflector with a long focal length and small offset for satisfactory electrical performance. In addition, the reflector diameter must be large enough to insure the complete blockage of the LFMR reflector. In contrast to these needs the reflector should be as compact as possible for low mass and to avoid interference with the LFMR reflector in both the stowed and deployed configuration.

Three cold load reflector designs were examined making extensive use of CAD technology. Use of CAD was required to determine when interference with the LFMR reflector field of view occurred. The study was conducted using the baseline LFMR configuration incorporating a focal length of 175.6 inches with an F/D ratio equal to 0.36.

CAD-Assisted Cold Load Design

Focal length, 175.6 in.

F/D = 0.36

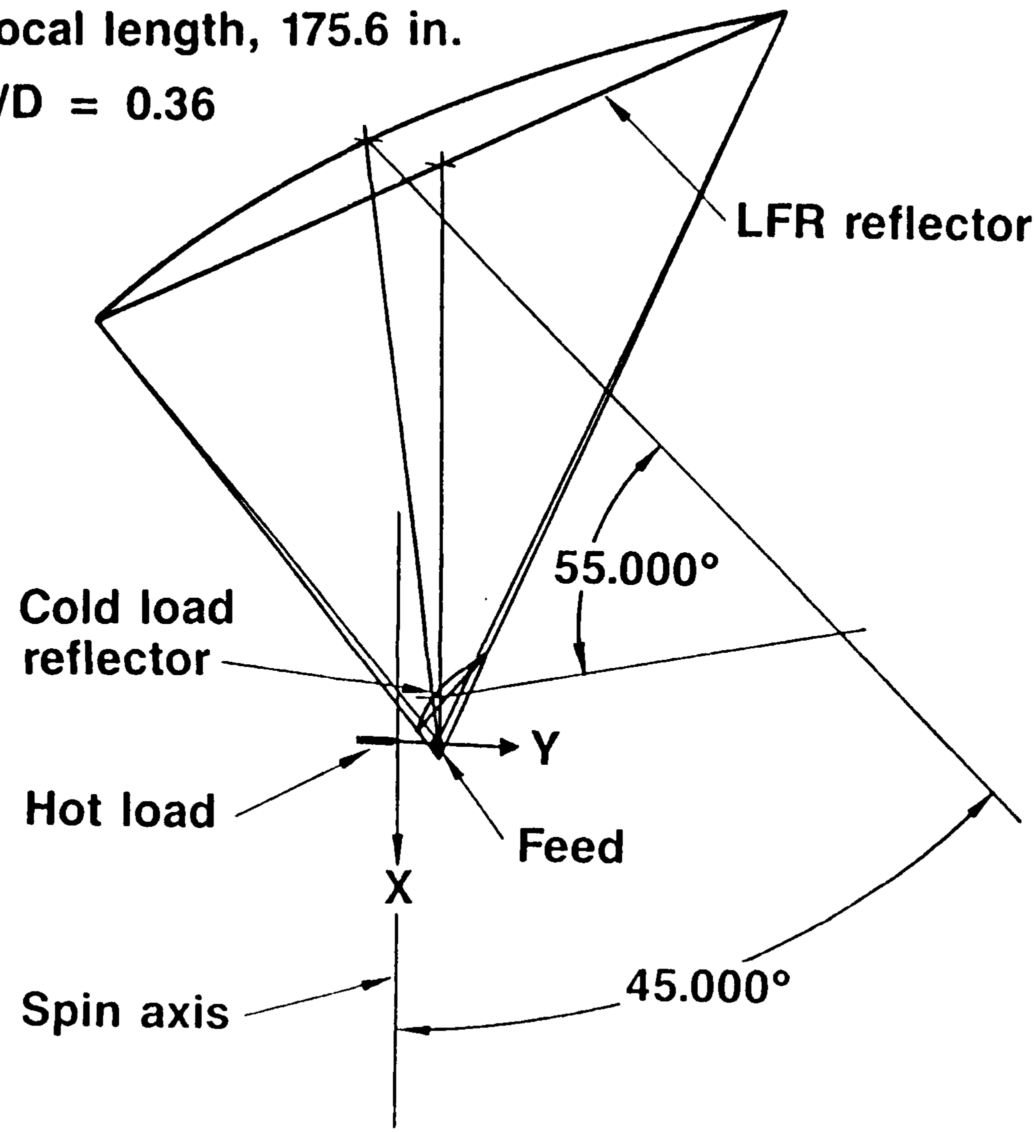

847098-11

HOT AND COLD LOAD CONFIGURATION

This is a typical view created by the CAD operator and used to determine the correct reflector diameter. The worst-case configuration occurs when the 5 GHz horn (5.4 inch aperture diameter) is aligned with the cold load reflector. Lines are inserted *about the horn* aperture to the perimeter of the LFRM reflector. Sections are then created to insure complete blocking of the LFMR reflector by the cold load reflector during calibration.

HUGHES

Hot and Cold Load Configuration

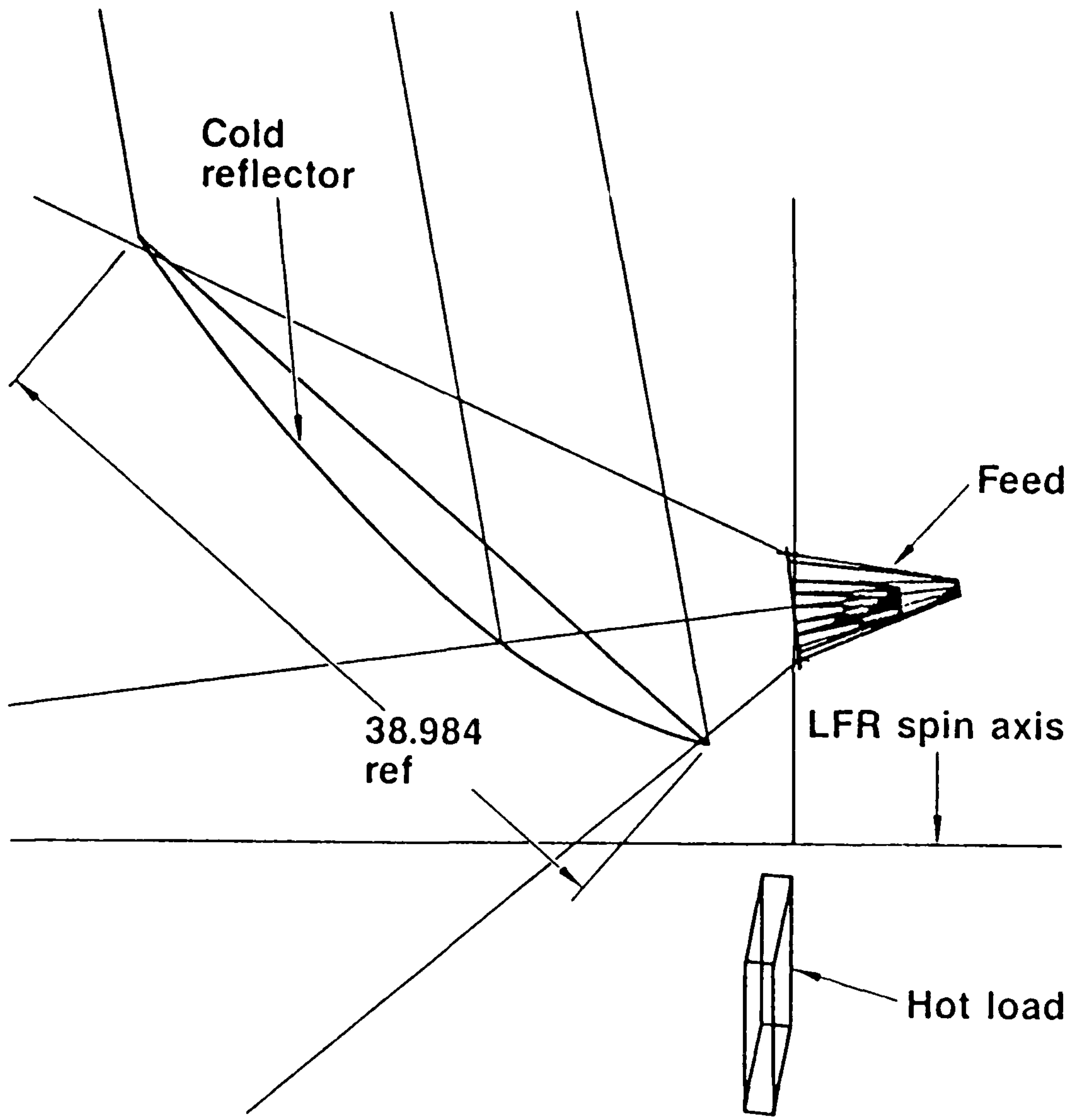

847098-12

TRUE END VIEW

The method used to determine when the cold load reflector intersects the field of view of the secondary beam (i.e., parallel to the boresight) of the LFMR reflector is demonstrated here. The top diagram shows the cold load reflector positioned directly over the feed. The bottom diagram shows the cold load reflector as it begins to rotate out of the field of view. A complete series of views is examined, and from this information it is possible to determine the impact of various cold load reflector configurations on the active scan. Additional views along the primary beam (i.e., from the feeds to the LFMR reflector) are examined at the point of interference with the secondary beam. In all configurations it was determined that the primary beam field of view is unaffected by the cold sky reflector if the secondary beam field of view is unobstructed.

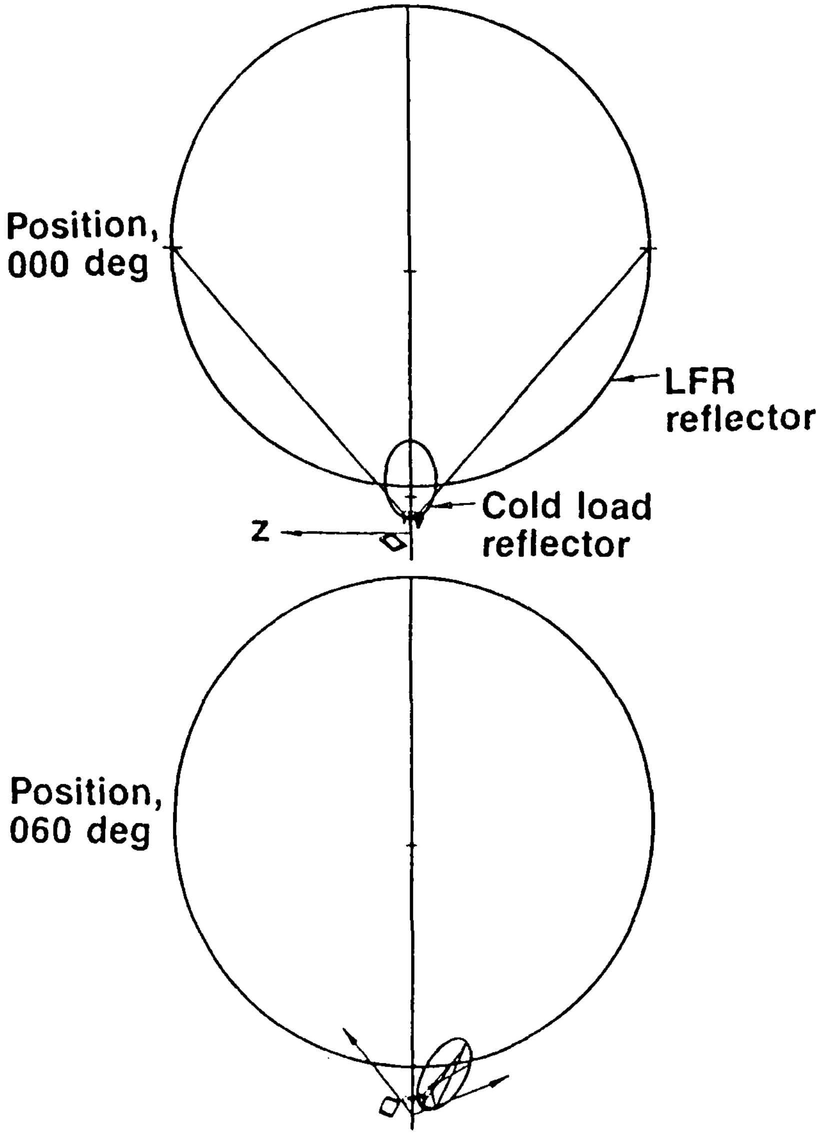

HUGHES

True End View
Secondary Beam

847098-13

HOT AND COLD LOAD FOV

The following page lists the three cold load reflector configurations examined. The next three pages show the results of the investigation and the effects on the active scan angle available for SST data acquisition. Also shown in the figures is the hot load and its required calibration angle. The hot load, constructed of a RF absorbent material, provides an additional calibration point near 300K. The feed horn aperture passes over it, and like the cold load reflector, is of sufficient size to provide five calibration samples each pass.

The results of the study indicate all three configurations examined provide a sufficient angle for the active scan (102.4° *being the minimum*). The advantages of a small cold load reflector in both stowed and deployed configurations indicates a reflector having a focal length of approximately 7 inches and a projected diameter of approximately 24 inches. A reflector of these *dimensions* provides acceptable electrical performance and allows a sufficient margin for design maturity.

AD-A153 691 LFMR DEFINITION STUDY(U) HUGHES AIRCRAFT CO EL SEGUNDO 2/3
CALIF SPACE AND COMMUNICATIONS GROUP APR 85
N00014-84-C-2290

UNCLASSIFIED F/G 5/1 NL

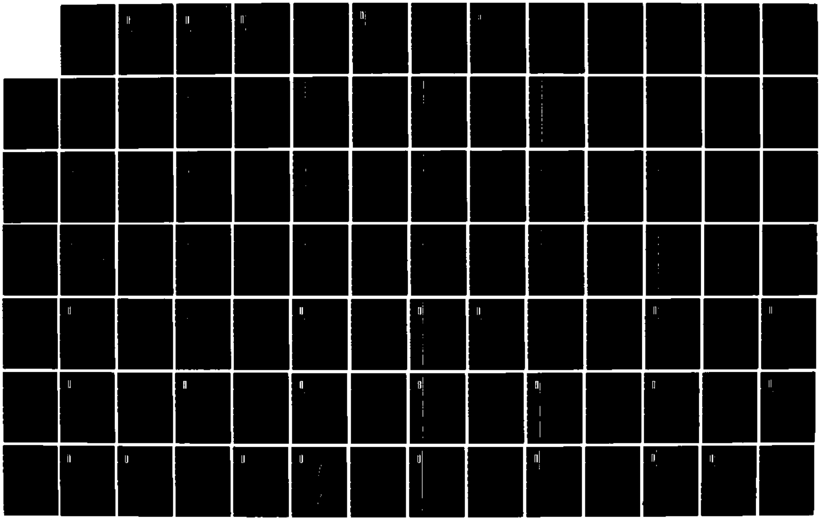

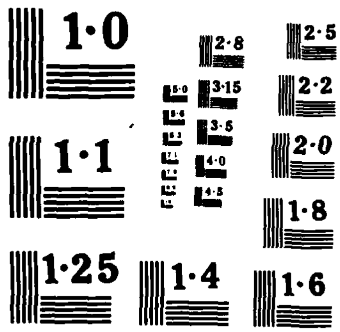
1·0
2·8
2·5
3·15
2·2
3·5
1·1
4·0
2·0
4·5
1·8
1·25
1·4
1·6

Hot and Cold Load FOV

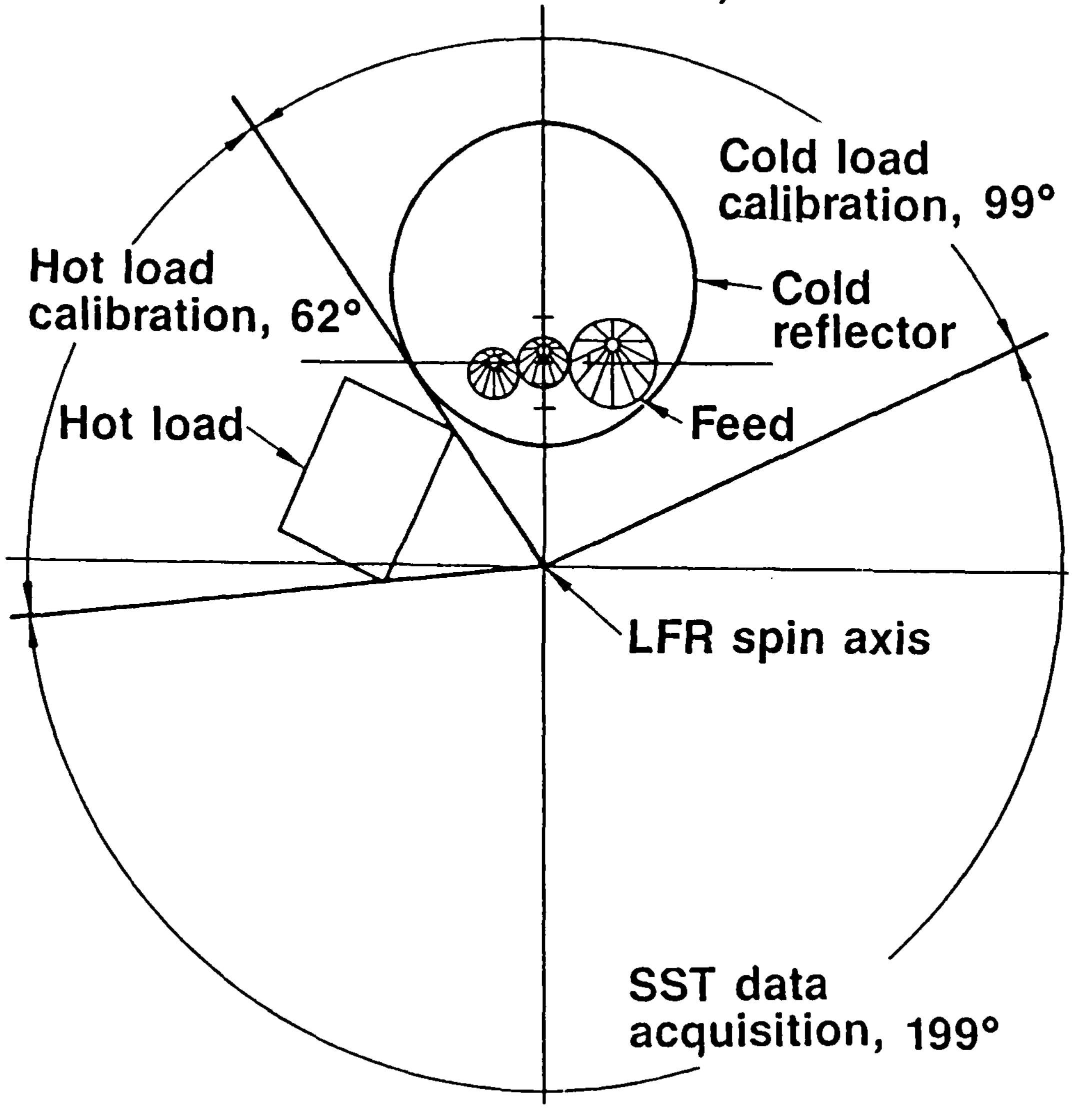

HUGHES

847098-14

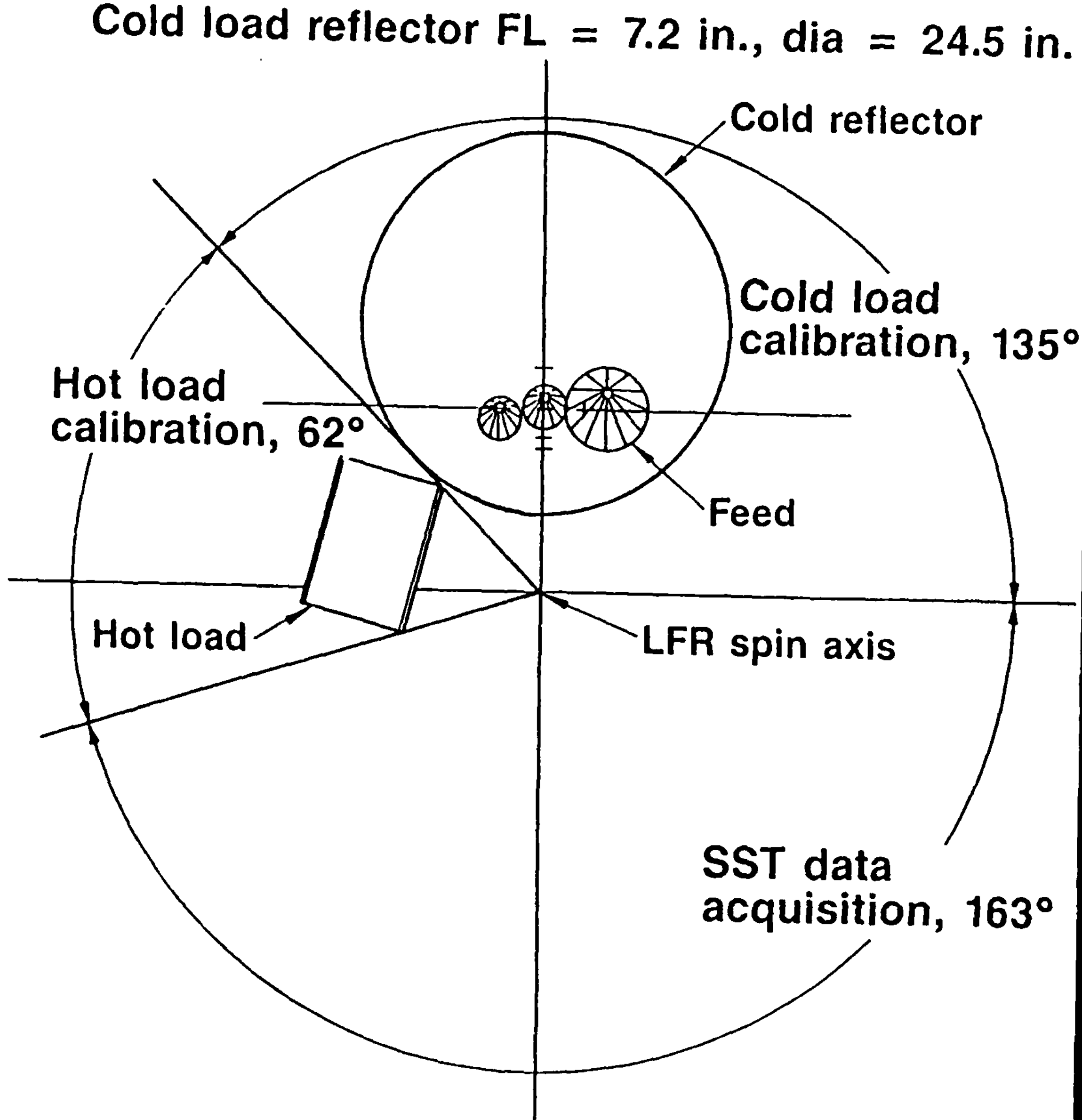

HUGHES

Hot and Cold Load FOV

847098-15

PREVIOUS PAGE IS BLANK

HUGHES

Hot and Cold Load FOV

Cold load reflector FL = 9.54 in., dia = 30.5 in.

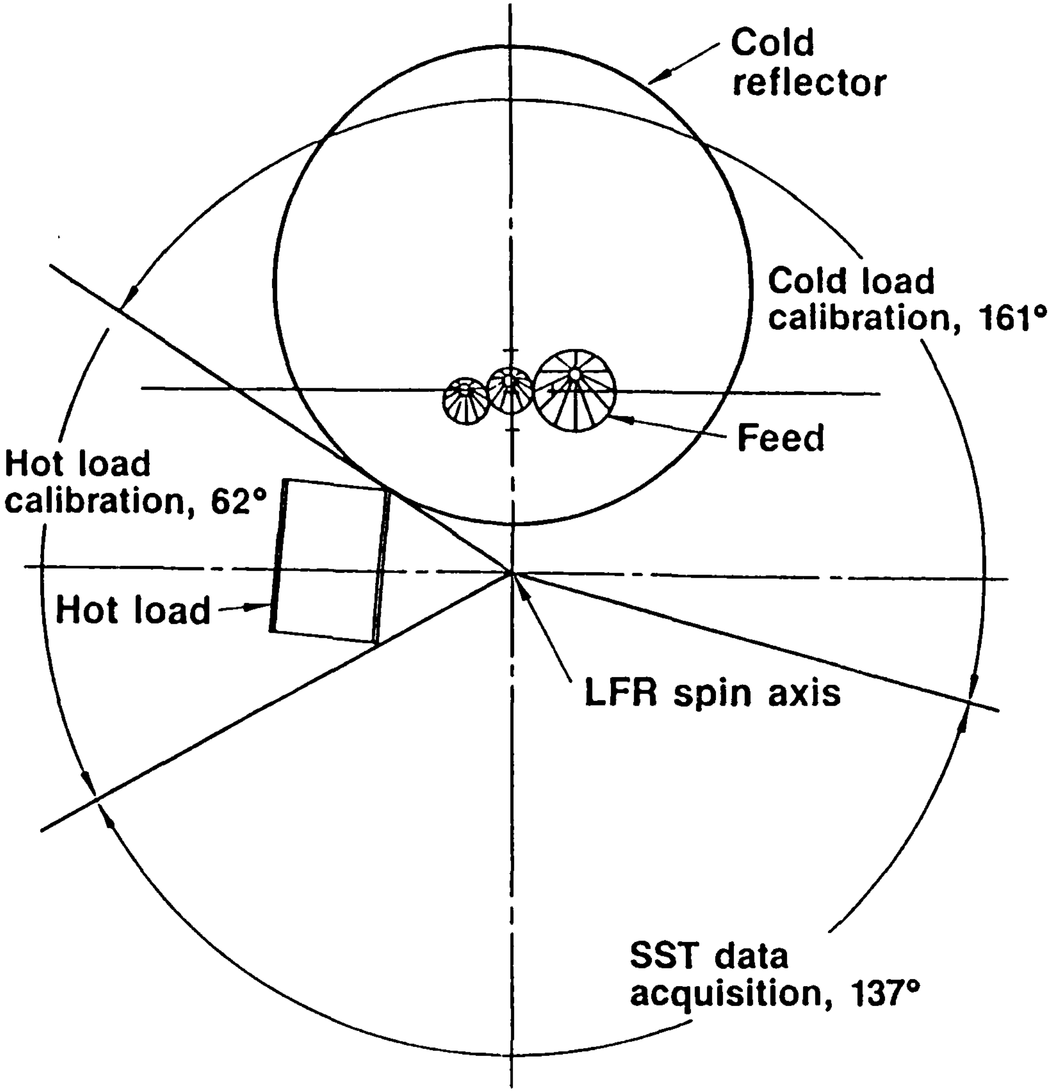

PREVIOUS PAGE IS BLANK

847098-16

COLD LOAD ELECTRICAL EVALUATION

Three offset reflectors were considered for the cold calibration load. They are placed at three different distances from the feed horn. The cold load reflector diameter is designed via CAD to be large enough so during calibration the feed will not see any part of the main reflector, and small enough so the cold load will not block the main reflector during the active scan. As the distance increases the potential coupling between the feed and cold load reflector decreases.

COLD LOAD ELECTRICAL EVALUATION (INCHES)

HUGHES

	REFLECTOR NO.		
	1	2	3
PROJECTED DIAMETER	18.5	24.5	30.5
MAJOR DIAMETER	29.2	39.0	48.6

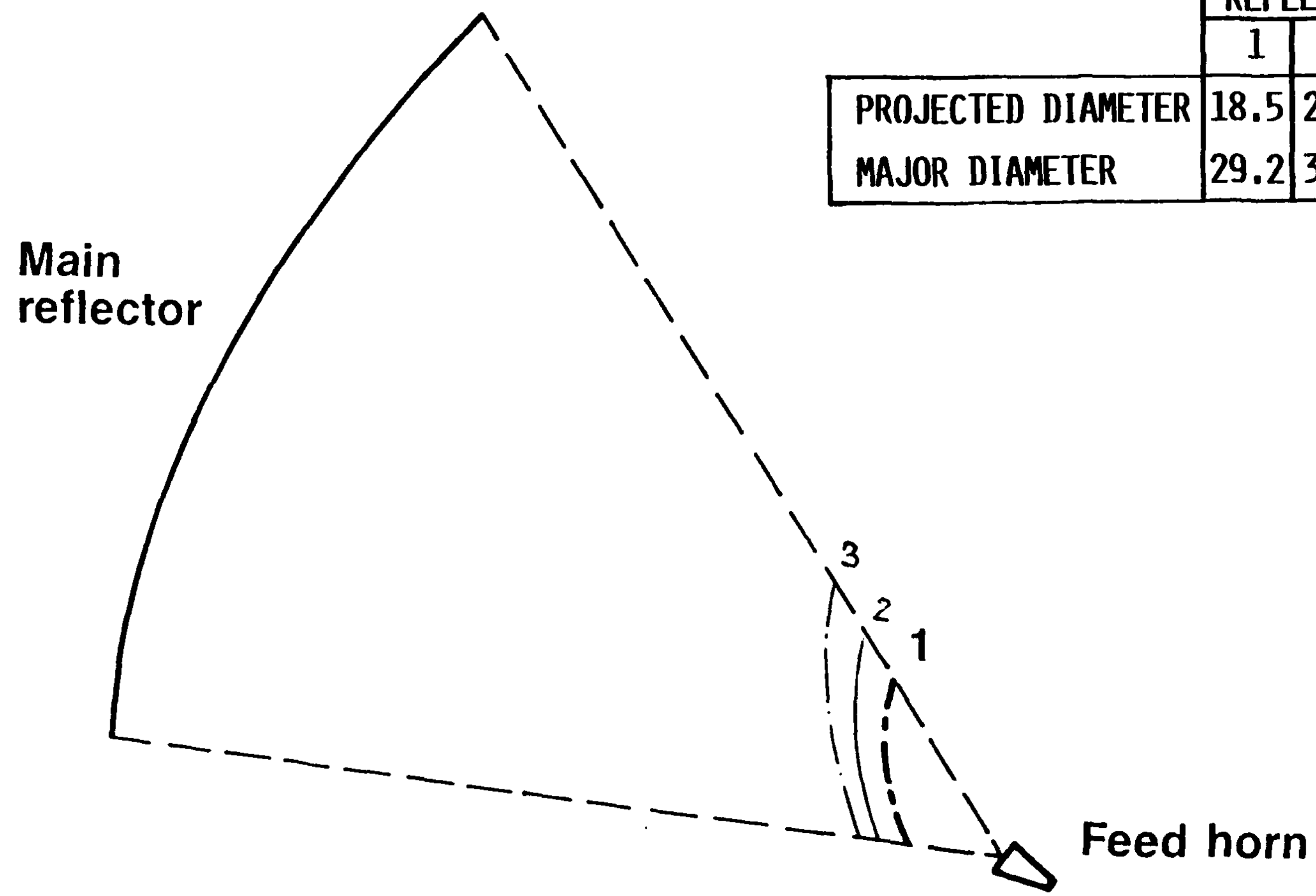

COLD LOAD REFLECTOR PATTERN, 10.4 GHz

A typical radiation pattern of the cold load reflector (24.5" diameter) is shown with a dual mode horn feed (3" diameter) at 10.4 GHz. The sidelobe level is below -40 dB due to the high edge taper of the feed.

Cold Load Reflector Pattern

10.4 GHz

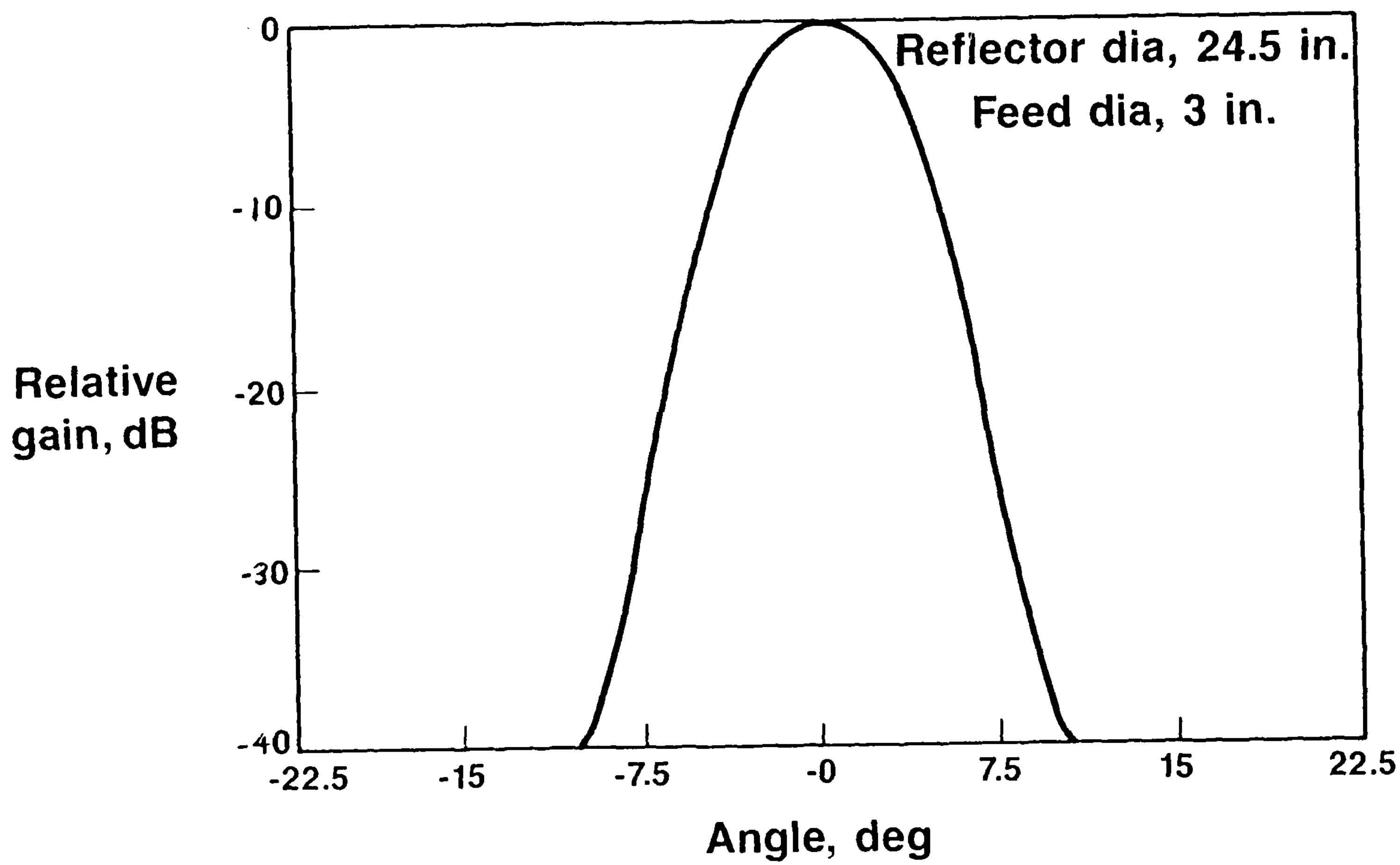

847098-4

COLD LOAD REFLECTOR PERFORMANCE TRADE-OFF (3" DIAMETER POTTER HORN FEED, 10.4 GHz)

The electrical performances of the three cold load reflectors are summarized. The half power beamwidth decreases as the reflector diameter increases. The sidelobes are all below -40 dB, and the cross polarization is less than -17 dB.

HUGHES

COLD LOAD REFLECTOR PERFORMANCE TRADE-OFF
(3" DIA. POTTER HORN FEED, 10.4 GHZ)

PROJECTED APERTURE DIAMETER (IN.)	18.5	24.5	30.5
HPBW (°)	8	5.2	3.5
CROSSPOLARIZATION (-dB)	<-17	<-17	<-17
SIDELOBE LEVEL (-dB)	<-40	<-40	<-40

COLD LOAD REFLECTOR PATTERN WITH FEED DISPLACEMENT

Since the cold load reflector provides cold calibration for a feed horn cluster, radiation patterns are plotted for those feed horns which are laterally displaced from the focal point. Note that no serious pattern deterioration occurs even as the feed is displaced 1.4" away from the focal point. However the beams are deflected 3° and 6° for 0.7" and 1.4" displacements respectively.

Cold Load Reflector Pattern With Feed Displacement

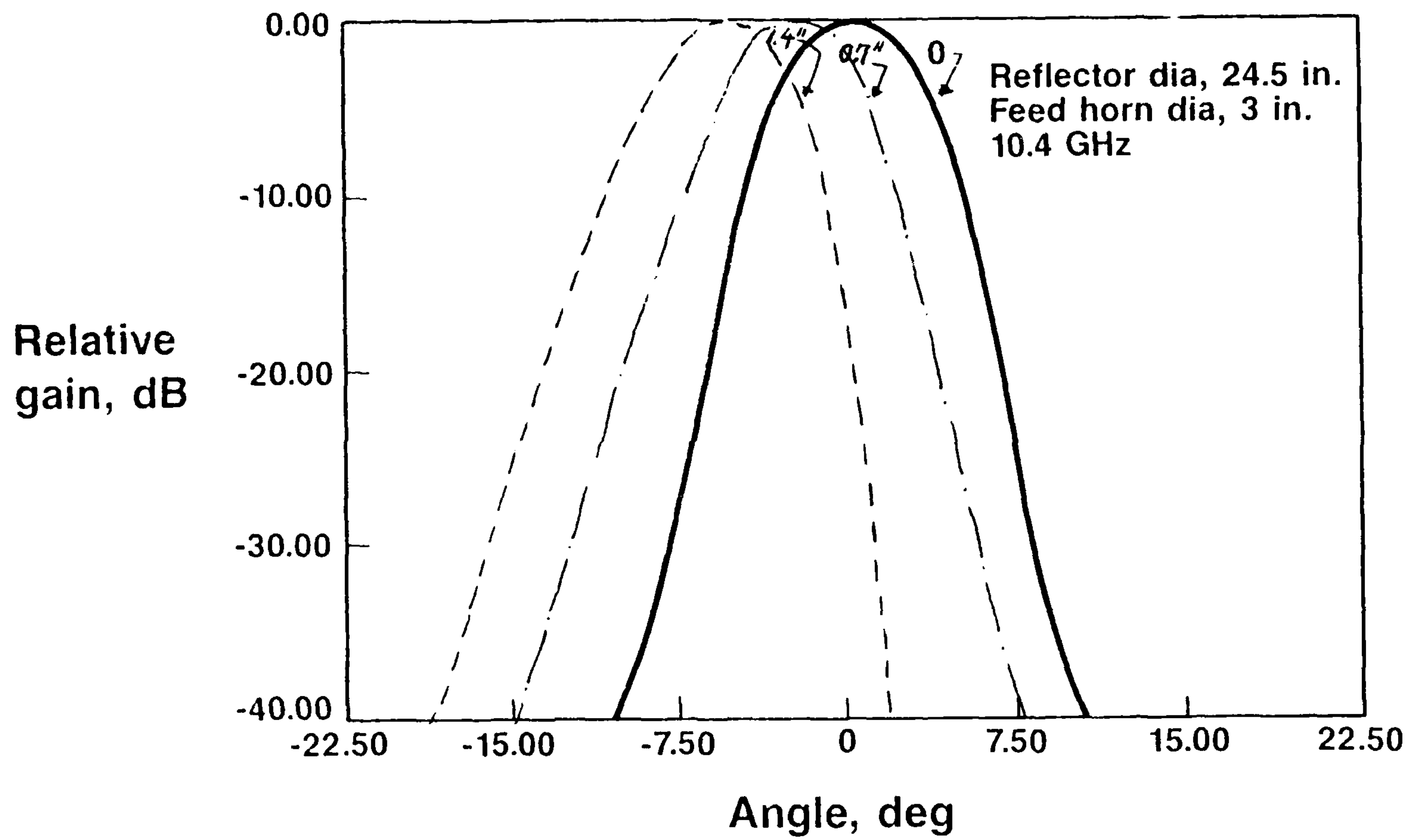

847098 5

REFLECTOR EVALUATION

Basic mesh antennas under consideration have degraded performance when compared to equivalent solid reflectors. The primary parameters affected are beam efficiency and sidelobe levels.

Two primary distortion mechanisms are inherent to both gore and geo-truss structures: (1) periodic surface distortions and (2) random or statistical surface distortions.

Originally periodic distortions were thought to have a significant effect on antenna electrical performance, but after discussions with both General Dynamics and Harris it was discovered the effect had been eliminated by design technique. The periodic distortion analysis is shown in an appendix and could be used during reflector construction if required.

PARAMETRIC INVESTIGATIONS

HUGHES

PURPOSE:

- TO ESTABLISH OPTIMUM DESIGN BASED ON TRADEOFFS
- TO MEET LFMR SPECS:

$\eta_B > 90\%$

HPBW (AVG) $\leq 0.34°$ @ $F = 10.4$ GHZ

XPOL ≤ 20 dB

CONDITIONS:

- $F_o = 10.4$ GHZ $D = 5.9$M $\varepsilon_{RMS} = 0.022''$
- POTTER'S HORN FEED

PARAMETRIC INVESTIGATIONS

Parametric studies were undertaken in an effort to establish an approach to an eventual point design. Design requirements are reviewed and conditions under which the study is done are presented.

RESULTS AND CONCLUSIONS

- RMS SURFACE ERRORS RESULT IN DEGRADED BEAM EFFICIENCIES AND SLL'S.
- XPOL UNAFFECTED.
- HIGH EDGE TAPERS CAN COMPENSATE FOR RMS ERRORS SLIGHTLY.

RANDOM DISTORTION CONCLUSIONS

The conclusions of the previous charts are presented.

XPOL LEVEL vs RMS SURFACE ERROR

F_O = 10.4 GHZ F/0′ = 0.360 h/0 = 0.065 D = 5.3M

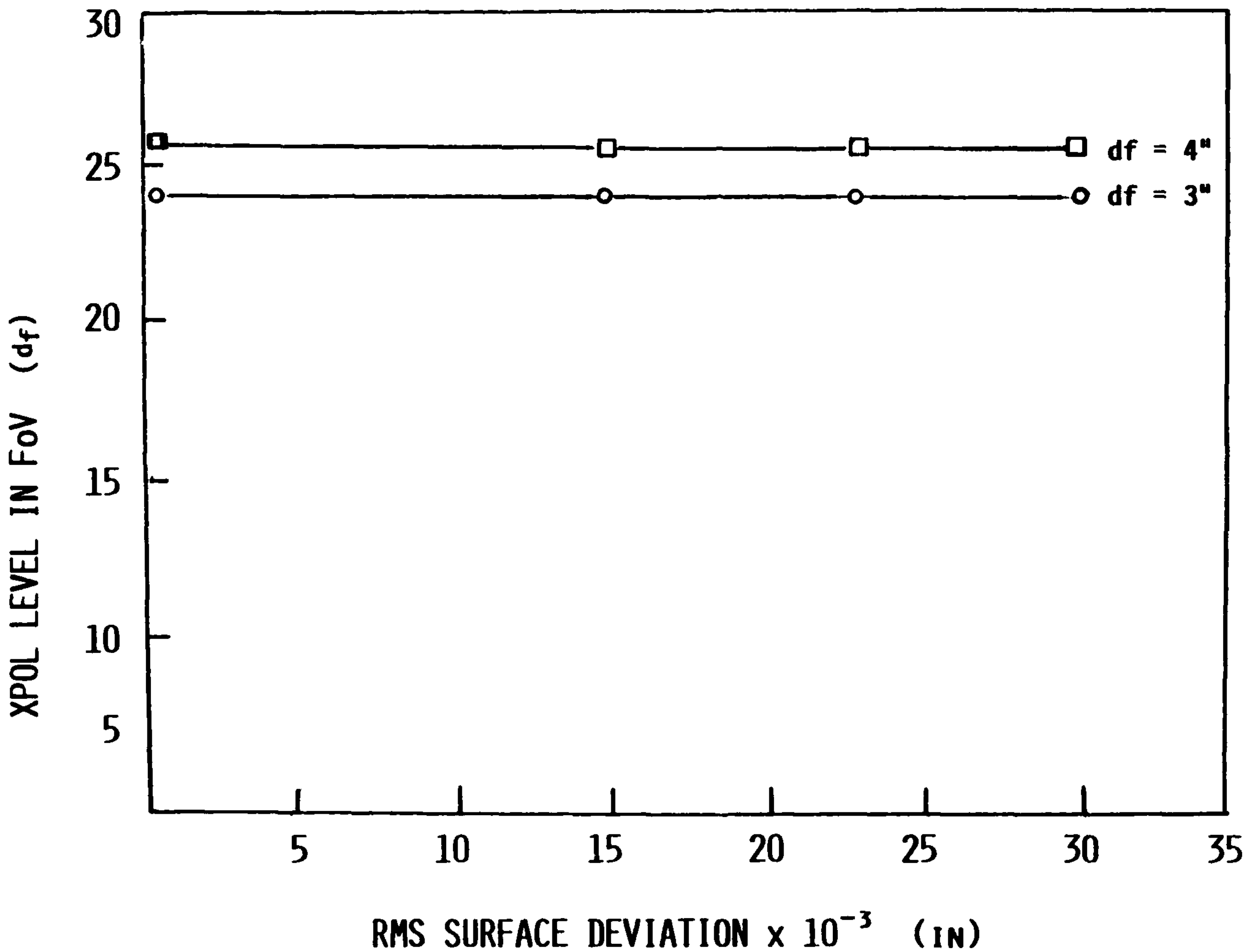

CROSS POLARIZATION

Cross polarized energy in the field of view vs. RMS surface deviation is depicted. The results show that these levels are invariant with respect to increasing RMS surface deviations.

HUGHES

RELATIVE SIDELOBE LEVEL vs RMS SURFACE ERROR

F_o = 10.4 GHZ F/0' = 0.360 h/0 0.065 D = 5.3M

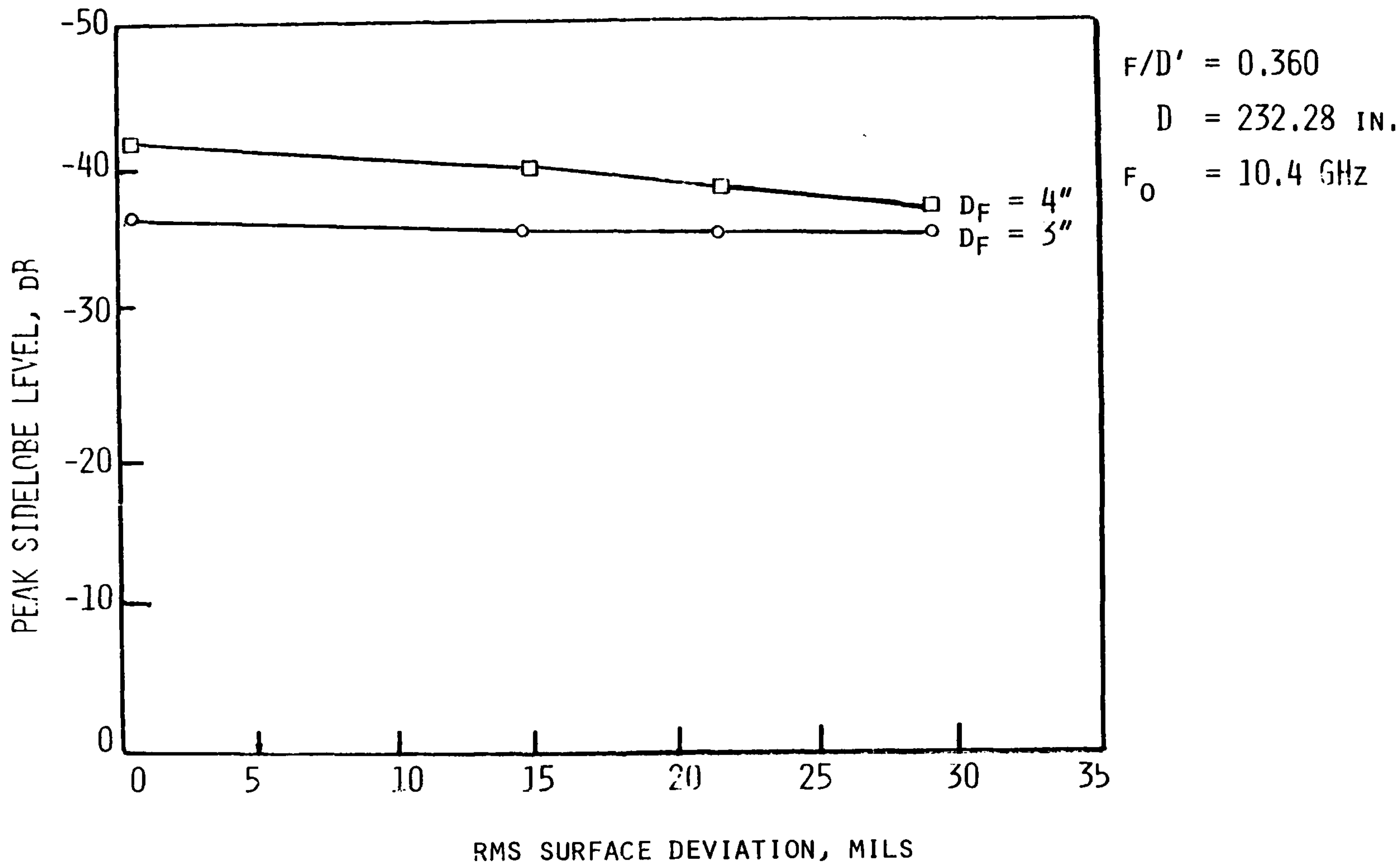

SIDELOBE LEVEL vs SURFACE DEVIATION

The peak sidelobe level vs. RMS surface deviation is depicted. The plot indicates that a higher edge taper results in lower overall sidelobe levels, but relative sidelobe level degradation is more extreme as a function of increasing RMS surface deviation for the higher edge taper.

HUGHES

BEAM EFFICIENCY vs RMS SURFACE ERROR

F_0 =10.4 GHZ F/D'=0.360 h/D = 0.065 D = 5.9M

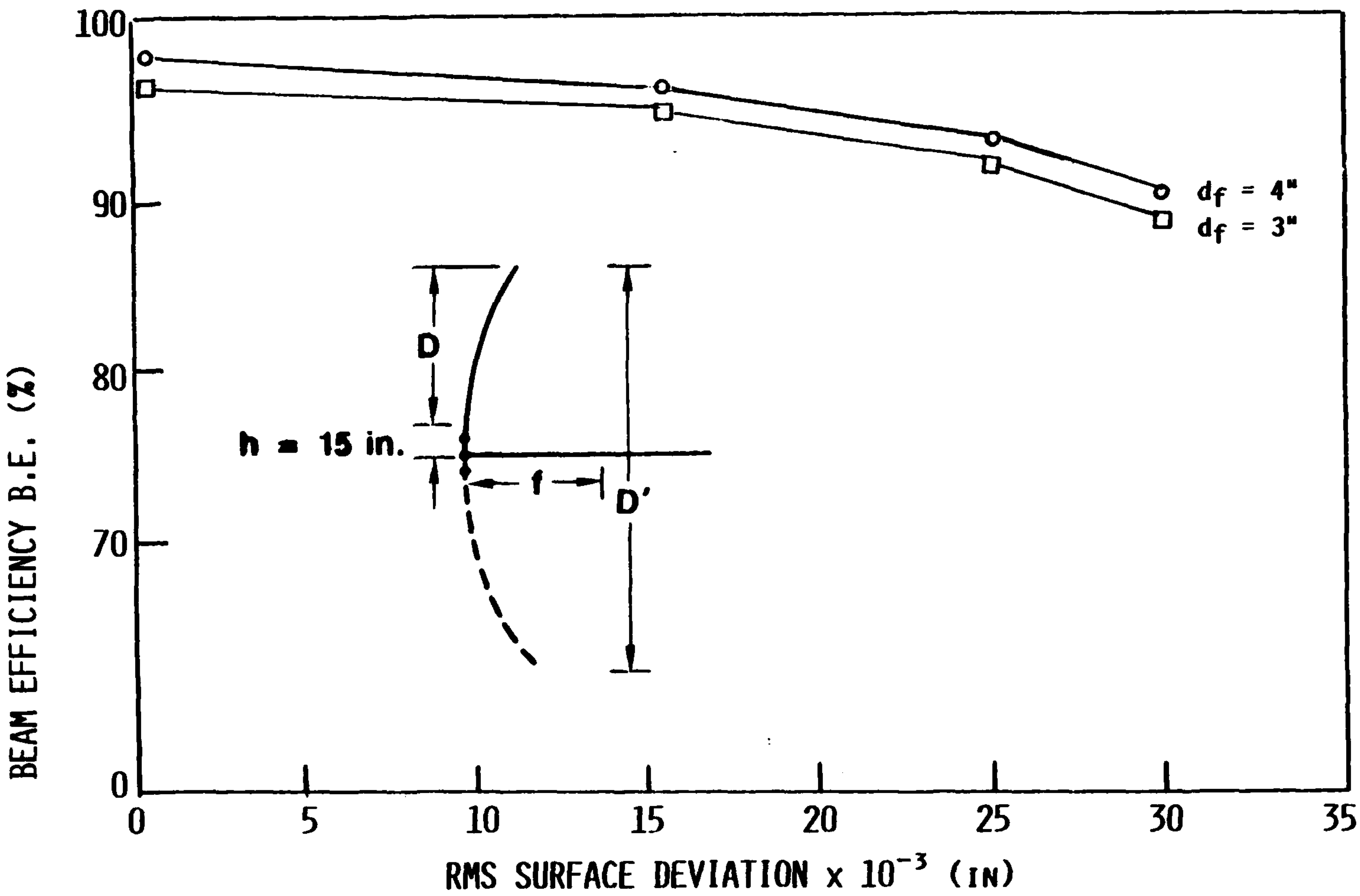

BEAM EFFICIENCY vs SURFACE ERROR

Beam efficiency degradation as a function of increasing RMS surface deviation is shown for two feed horn diameters. Offset reflector geometry variables used in the study are also shown for reference. The plot indicates that for the chosen horn diameter of d_f=3" an upper limit of 0.025" is tolerable to meet the specification of 90% beam efficiency.

PROJECTED APERTURE

HUGHES

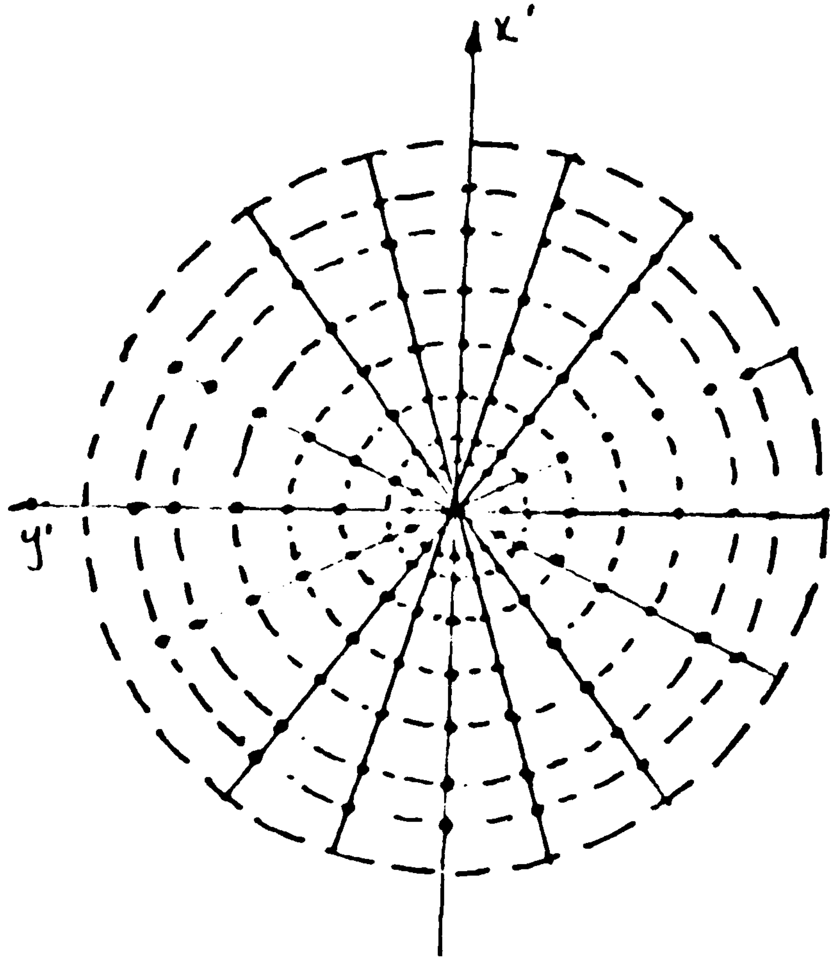

- EQUISPACED POLAR ANGLES
- RADII = GAUSS QUAD. ABCISSAS

PROJECTED APERTURE

A depiction of the projected aperture is presented. Integration grid points are equally spaced angularly and radially spaced according to Gauss Quadrature abcissas.

RANDOM DISTORTIONS

HUGHES

DISTORTION MODEL

- BASED ON NORMALIZED UNIFORM DISTRIBUTION
- P.O. CURRENTS ON DISCRETE SURFACE POINTS
- DISTRIBUTION NORMALIZED TO INPUT RMS
- VALIDITY OF MODEL: (< 5% ERROR)

RUZE: $G = G_0 e^{-\left(\frac{4\pi\epsilon}{\lambda}\right)^2}$

$\epsilon \triangleq$ RMS SURFACE DEVIATION

CONDITIONS:

- f/D' = 0.36 D = 5.9M F_O = 10.4 GHZ

d = HORN DIAMETER h/D = 0.065

RANDOM DISTORTIONS

Random or statistical surface distortions have been determined to be of primary importance according to vendor inputs. In order to address this topic, a statistical solid reflector distortion model was developed based on a normalized uniformly distributed random number generator. The standard integration grid for the reflector projected aperture would now be axially deviated in a plus or minus direction relative to the "ideal" surface, the value of which is normalized to an input RMS value. The validity of this model has been established via comparison with Ruse's well known equation expressing gain reduction due to surface distortion. Results of the model agree with Ruse well within 5%. Condition for radiometric parameters vs. RMS surface deviations are set.

BEAM EFFICIENCY AND CROSS POLARIZATION

Beam efficiency and cross polarized energy in the field of view are depicted for three various f/D ratios as a function of feed horn diameter. The design driver here is minimized horn diameter for:

1. Minimum weight
2. Beam scan degradation. It indicates for f/D = 0.360 and d_f = 3.0" design specifications are met under worst case surface deviation of 0.022" rms surface error.

BEAM EFFICIENCY AND CROSS POLARIZATION

HUGHES

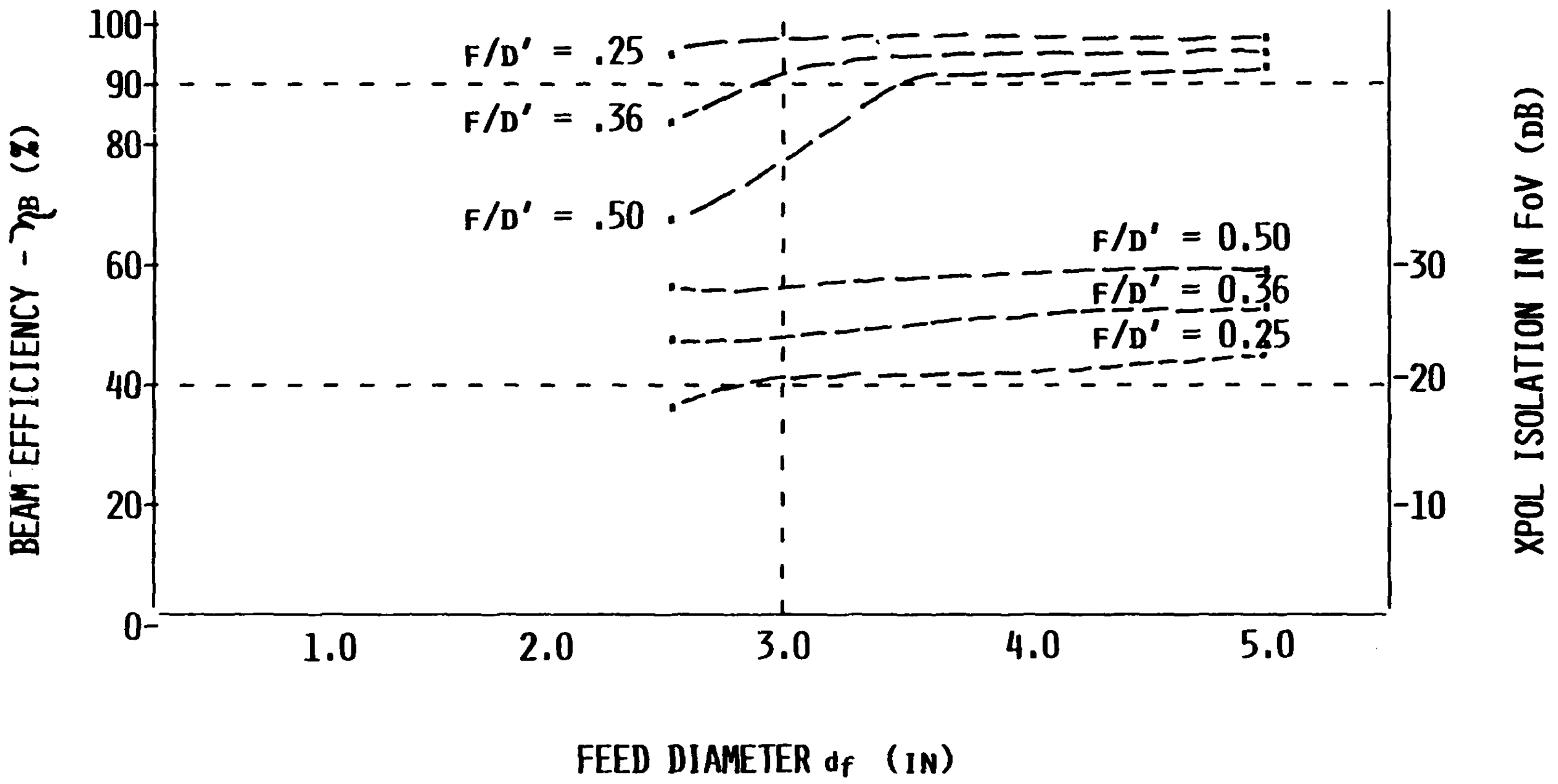

EDGE TAPER vs. FEED DIAMETER

Reflector edge illumination vs. horn diameter is depicted for the three f/D ratios to translate feed horn diameters to the more commonly used edge taper terminology.

EDGE TAPER VS. FEED DIAMETER

HUGHES

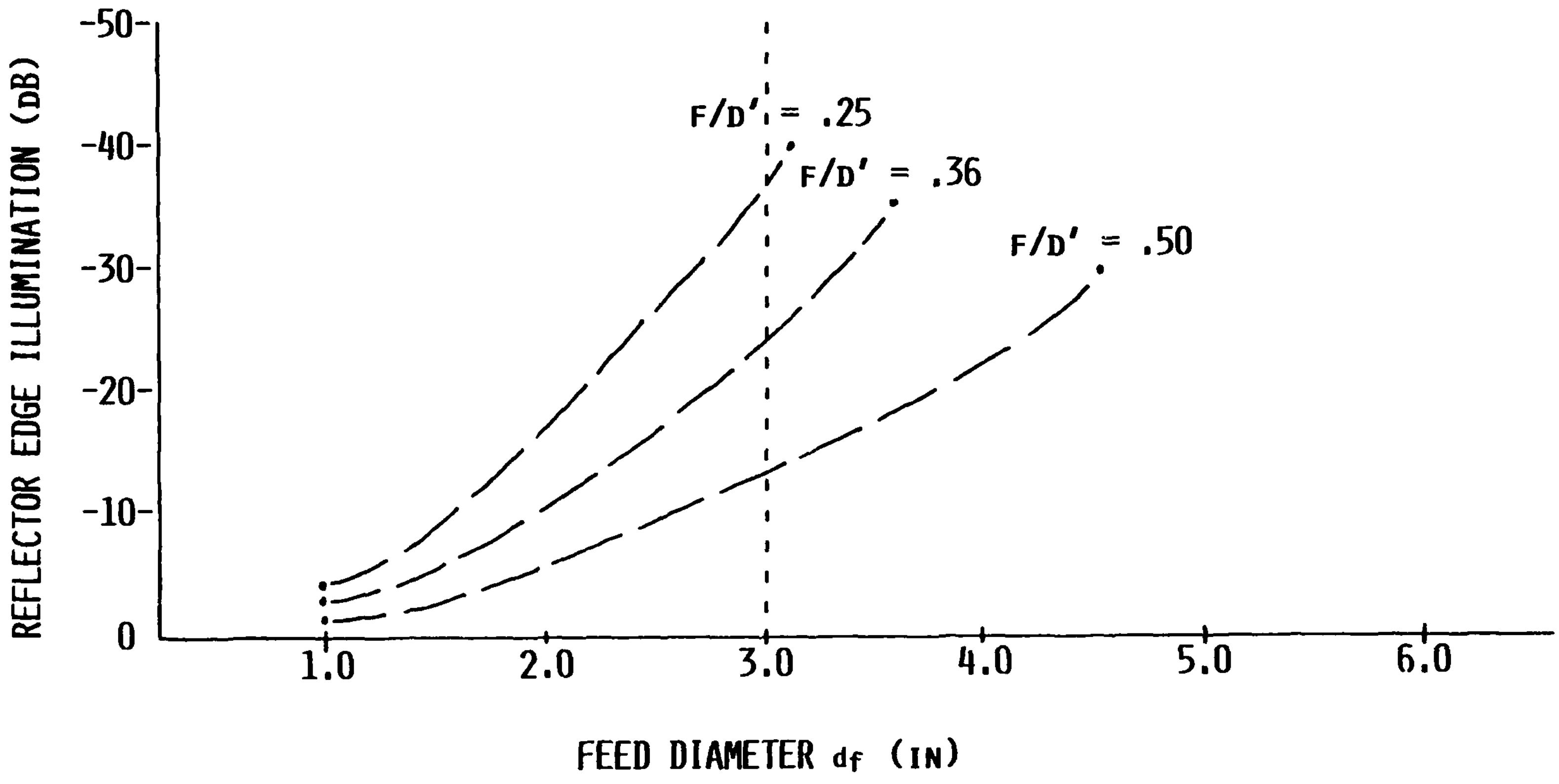

HALF POWER BEAMWIDTH vs FEED DIAMETER

Secondary pattern half power beamwidth (HPBW) is depicted as a function of feed horn diameter for the three f/D ratios. The plot indicates that for the chosen f/D ratio of 0.36 and a feed diameter of 3.0" the specification requirement is met.

HPBW vs. FEED DIAMETER

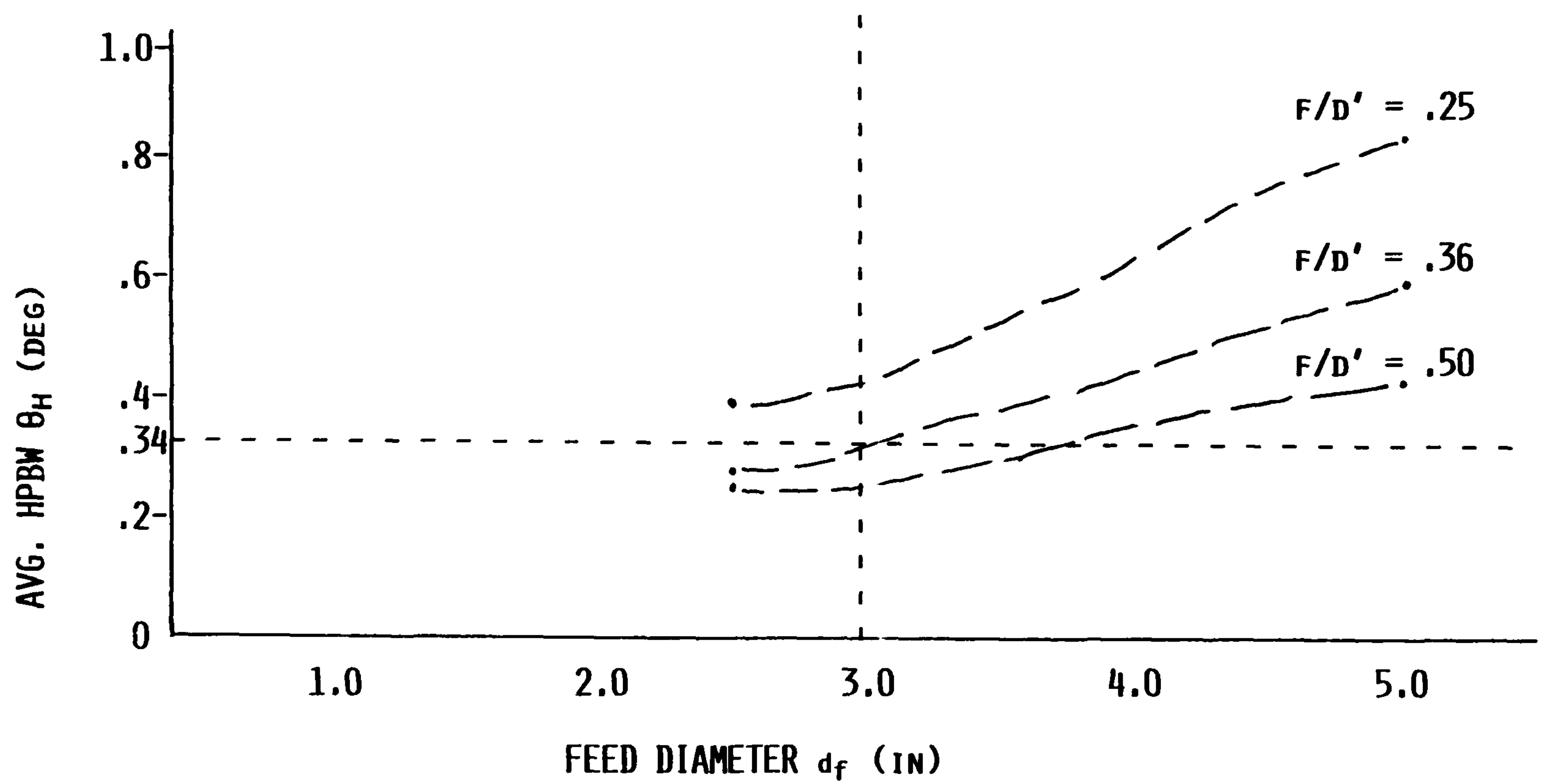

BEAM EFFICIENCY, CROSS POLARIZATION vs OFFSET

Reflector offset effects on design parameters such as beam efficiency, cross polarized energy in the field of view and secondary pattern half power beamwidth were investigated. Depicted in the initial plot is beam efficiency and cross polarized energy vs. offset height for two f/D ratios. Results indicate that for the smaller f/D ratios, beam efficiency is relatively insensitive to small increases in offset height while cross polarized energy is constant for small f/D ratios.

η_B AND XPOL vs. OFFSET

HUGHES

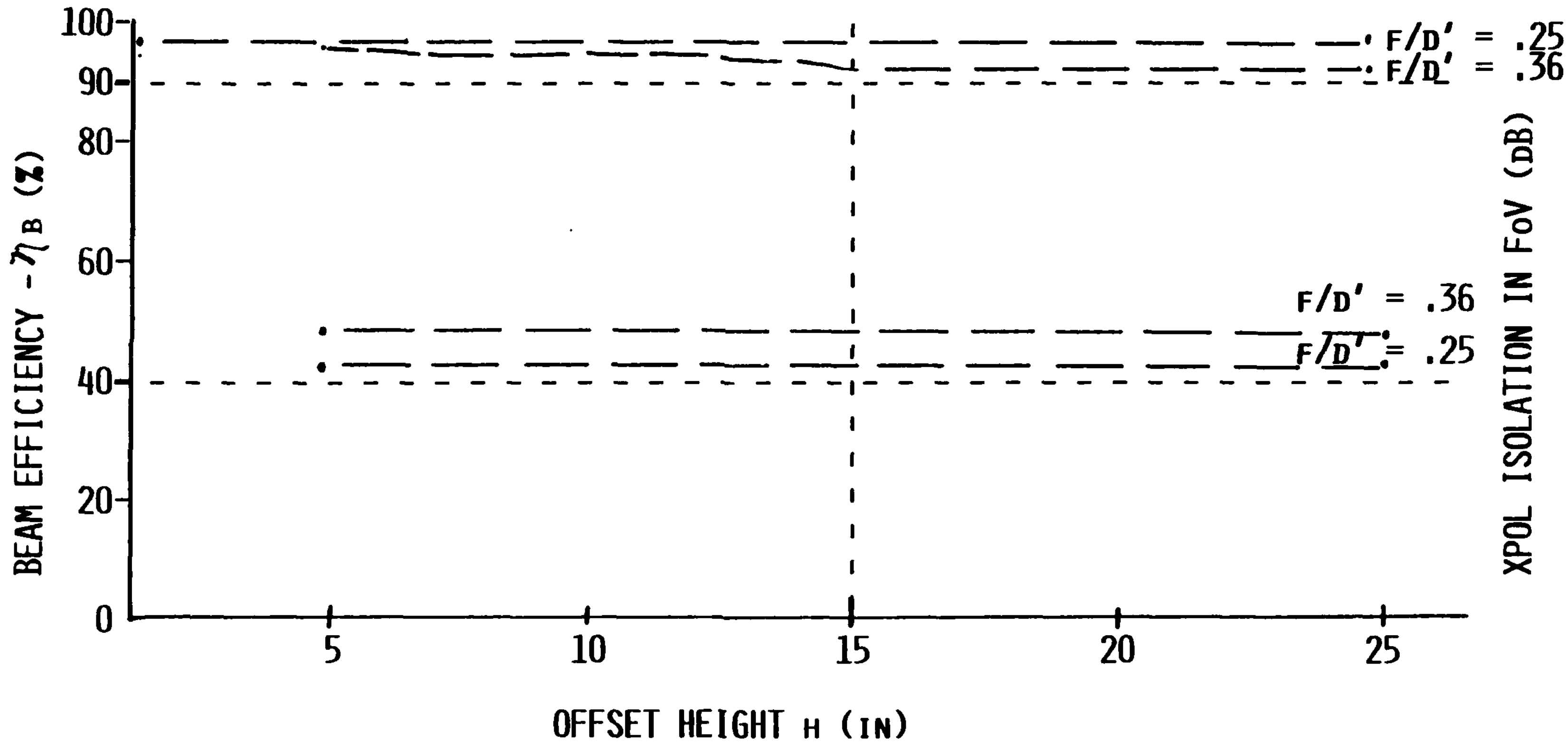

HALF POWER BEAMWIDTH vs OFFSET

Secondary pattern half power beamwidth is depicted as decreasing as a function of height for two f/D ratios. This is due to the fact that *for a set horn diameter, increasing h/D ratio (or offset height)* reduces the effective subtended angle, thus increasing edge taper towards uniform illumination.

HPBW vs. OFFSET

HUGHES

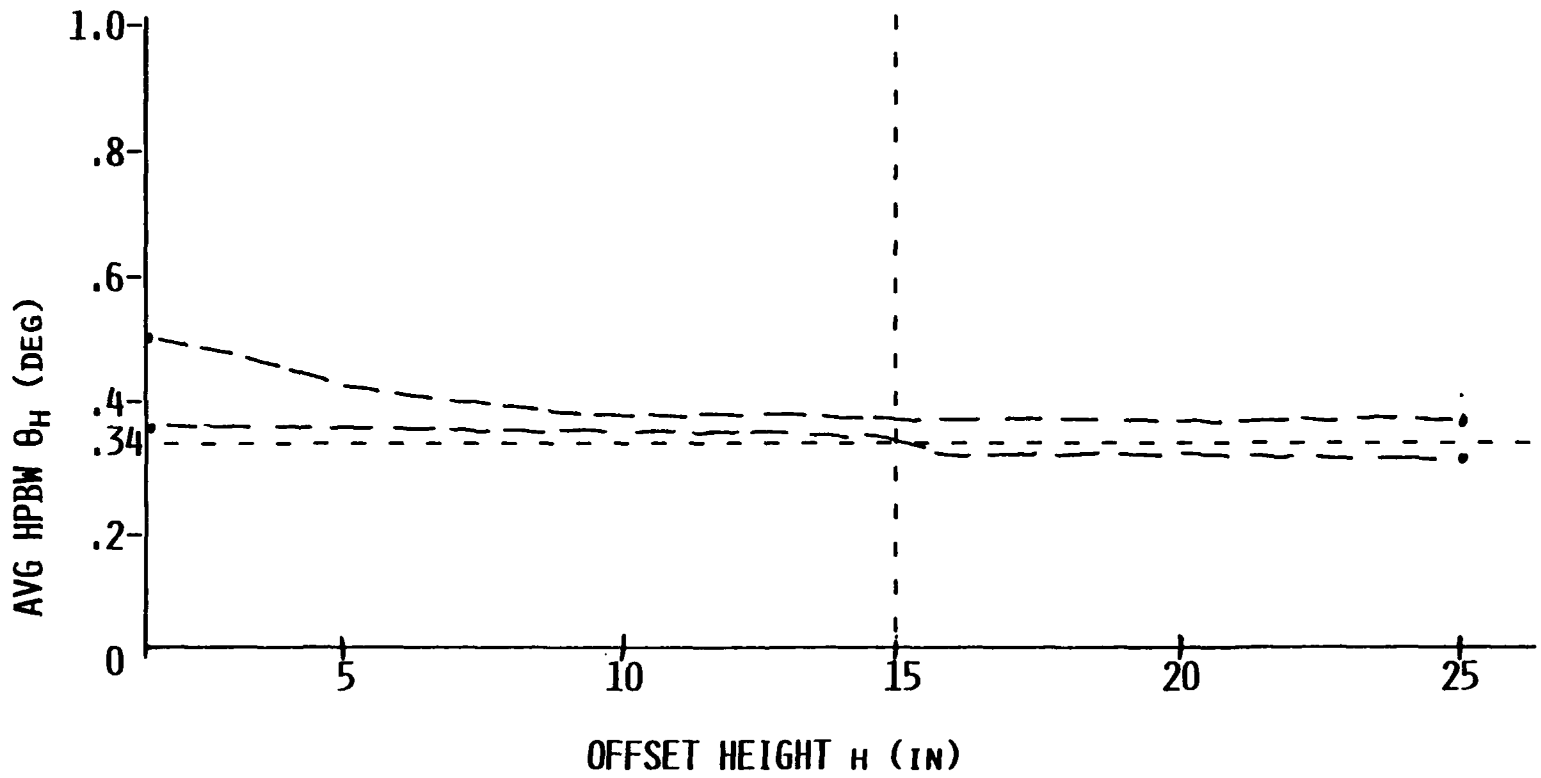

SUMMARY AND CONCLUSIONS

A tabular summary of the qualitative results of the f/D ratio tradeoffs is presented. As indicated, the current choice of f/D=0.36 meets design requirements although a smaller f/D ratio of approximately 0.30 could be used to allow additional margin for beam efficiency at the expense of a slightly higher half power beamwidth. In addition, a minimized horn diameter is recommended as a primary design driver.

PARAMETRIC INVESTIGATIONS
SUMMARY AND PRELIMINARY CONCLUSIONS

F/D'	ADVANTAGE	DISADVANTAGE
0.25	• HIGH η_B • SMALL d_f's	• HIGH XPOL • BROAD HPBW's
0.36	• MEETS ALL REQUIREMENTS W/RMS ERRORS	• MARGINAL HPBW @ CHOSEN d_f
0.50	• LOW XPOL • NARROW HPBW's	• LOW η_B • LARGER d_f's

- DESIRE $0.25 < F/D' < 0.36$
- DESIRE SMALL d_f TO MINIMIZE WEIGHT

LATERAL FEED DISPLACEMENT STUDY

The effects of lateral feed displacements in the focal plane are studied to determine the feasibility of 15 rpm and 30 rpm feed configurations. The general effects of beam scanning on radiometric performance are degraded beam efficiencies and increased sidelobe levels. The conditions of the study are presented delineating the antenna parameters used as the baseline.

LATERAL FEED DISPLACEMENT

HUGHES

PURPOSE:

- STUDY SCANNED BEAM EFFECT ON N_B, HPBW, XPOL & SLL's
- UTILIZATION IN MULTIBEAM APPLICATION

CONDITIONS:

- $F/D' = 0.360$ $H/D = 0.065$ $D = 5.9$M $F_O = 10.4$ GHZ
- NO SURFACE DISTORTION
- PLANE OF SYMMETRY: ± Y - DIRECTED DISPLACEMENT
- PLANE OF ASYMMETRY: ± X - DIRECTED DISPLACEMENT
- POTTER'S HORN FEED

31.6 RPM FEED LAYOUT

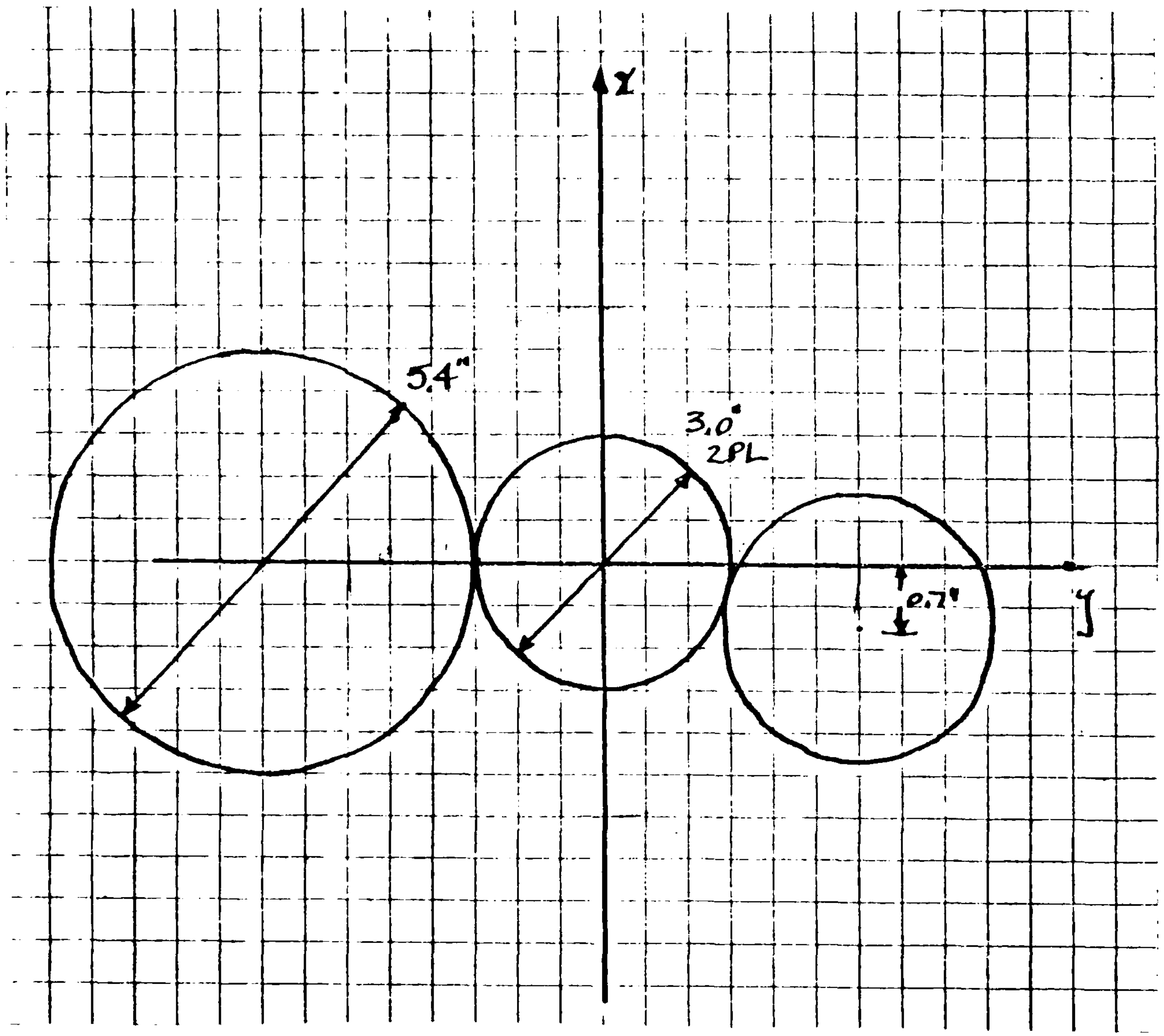

31.6 RPM FEED LAYOUT

A depiction of a representative feed cluster layout is presented which meets the required ground coverage for a 31.6 rpm system. The figure indicates a single dual mode feed horn operating at 5.2 GHz and two dual mode horns operating at 10.4 GHz.

HUGHES

ASYMMETRY PLANE DISPLACEMENT (±X) (CONT'D)

SLL vs FEED DISPL

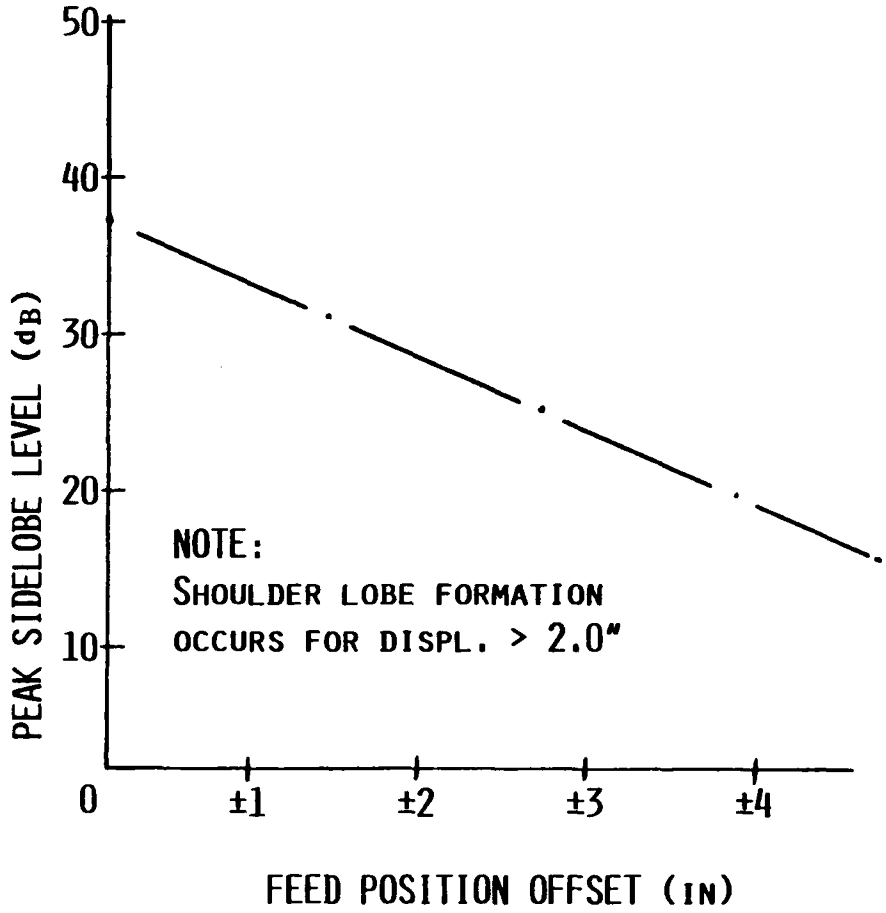

XPOL vs FEED DISPL.

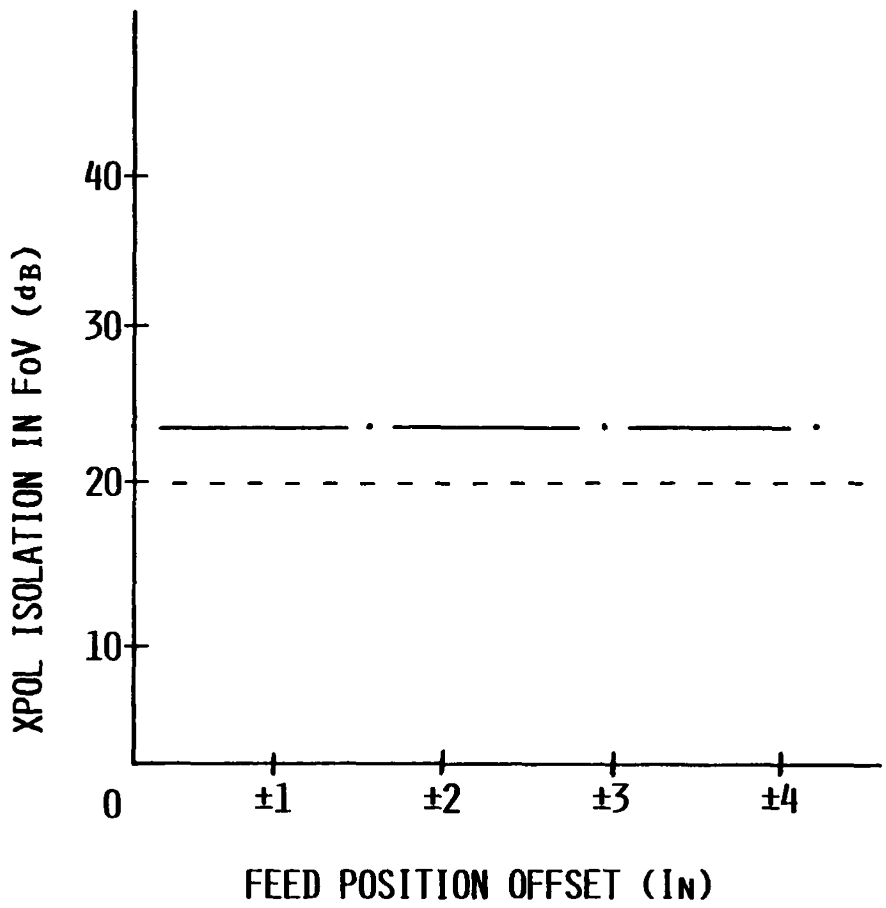

ASYMMETRY PLANE DISPLACEMENT (CONT'D)

Phase errors in the aperture due to feed displacements in the plane of asymmetry result in sidelobe degradation as a function of scan. These effects are manifested as shoulder lobe formation for scan angles of more than 2 beamwidths. These effects are not evident on cross polarized energy in the field of view.

ASYMMETRY PLANE DISPLACEMENT (±X)

HUGHES

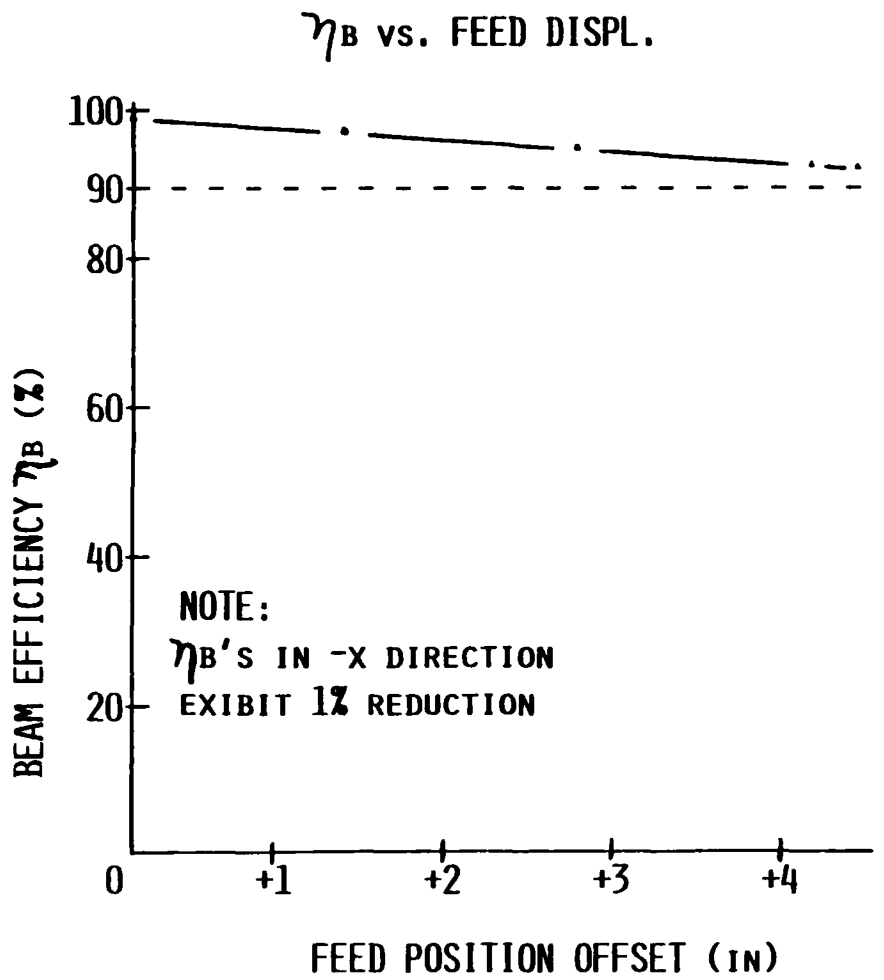

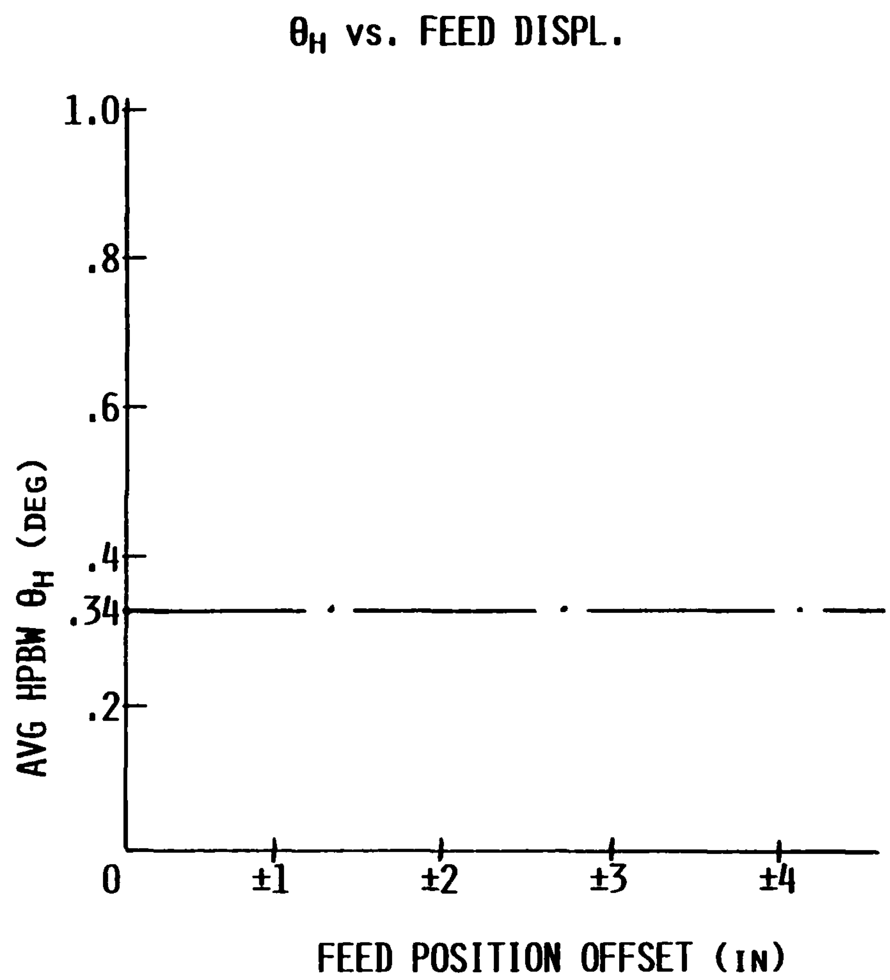

ASYMMETRY PLANE DISPLACEMENT

Feed displacements in the plane of asymmetry (i.e. elevation plane) are studied to determine the effects of the offset geometry on scan degradation. Depicted is the fact that although beam efficiency exhibits graceful degradation as a function of beam scan, this degradation is lower as the feed is displaced toward the offset reflector. This is quantitatively expressed as a 1% overall reduction in beam efficiencies observed as compared with feed displacement away from the reflector. As in the case of feed displacement in the azimuth plane, displacements in the elevation plane do not affect secondary pattern half power beamwidths.

HUGHES

SYMMETRY PLANE DISPLACEMENT (±Y) (CONT'D)

SLL vs DISPL.

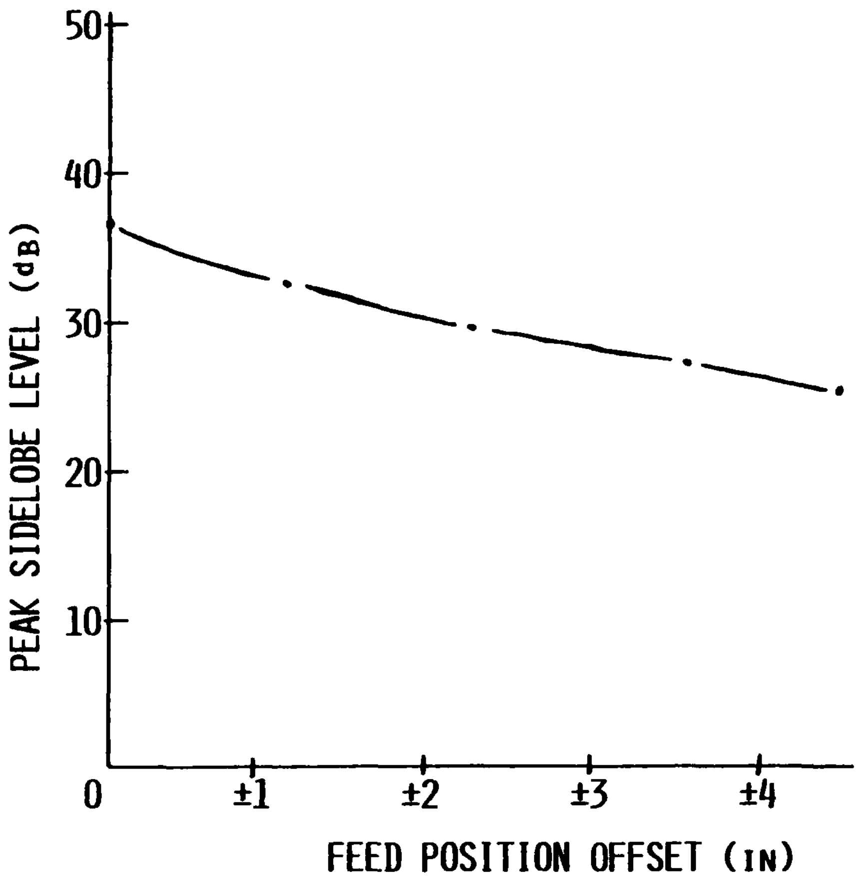

XPOL vs DISPL

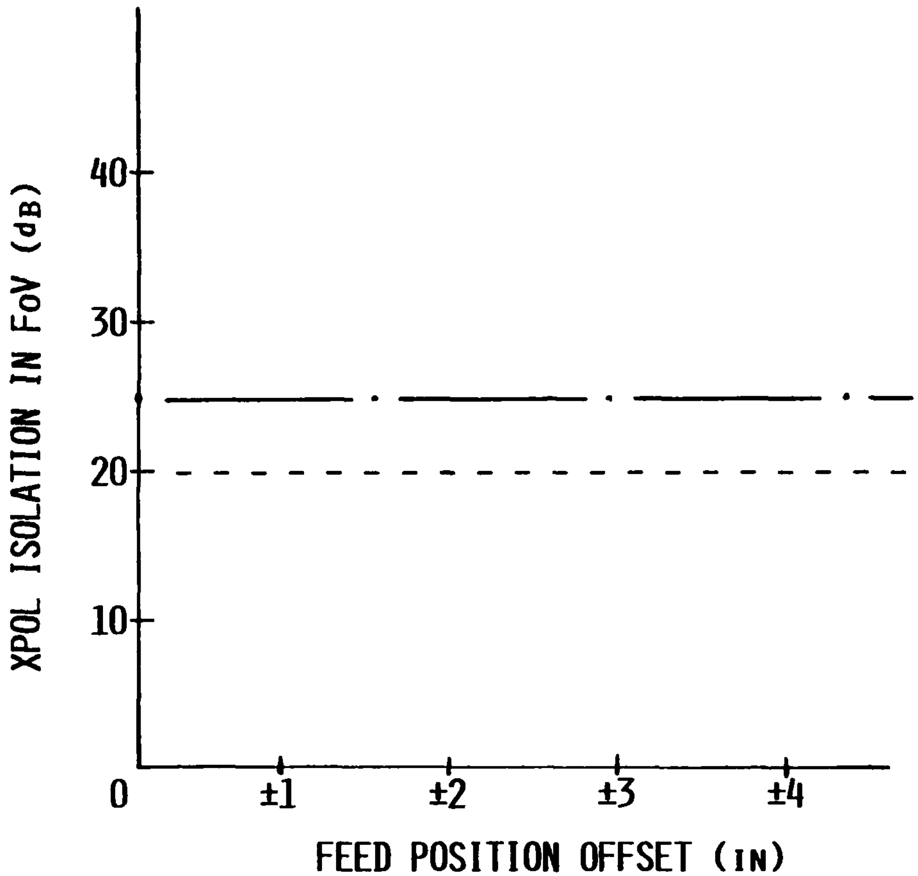

SYMMETRY PLANE DISPLACEMENT (CONT'D)

Graceful degradation of sidelobe levels is shown as a function of feed displacement while cross polarized energy of levels in the field of view is shown to be invariant with beam scan for feed displacement in the azimuth plane.

SYMMETRY PLANE DISPLACEMENT (±Y)

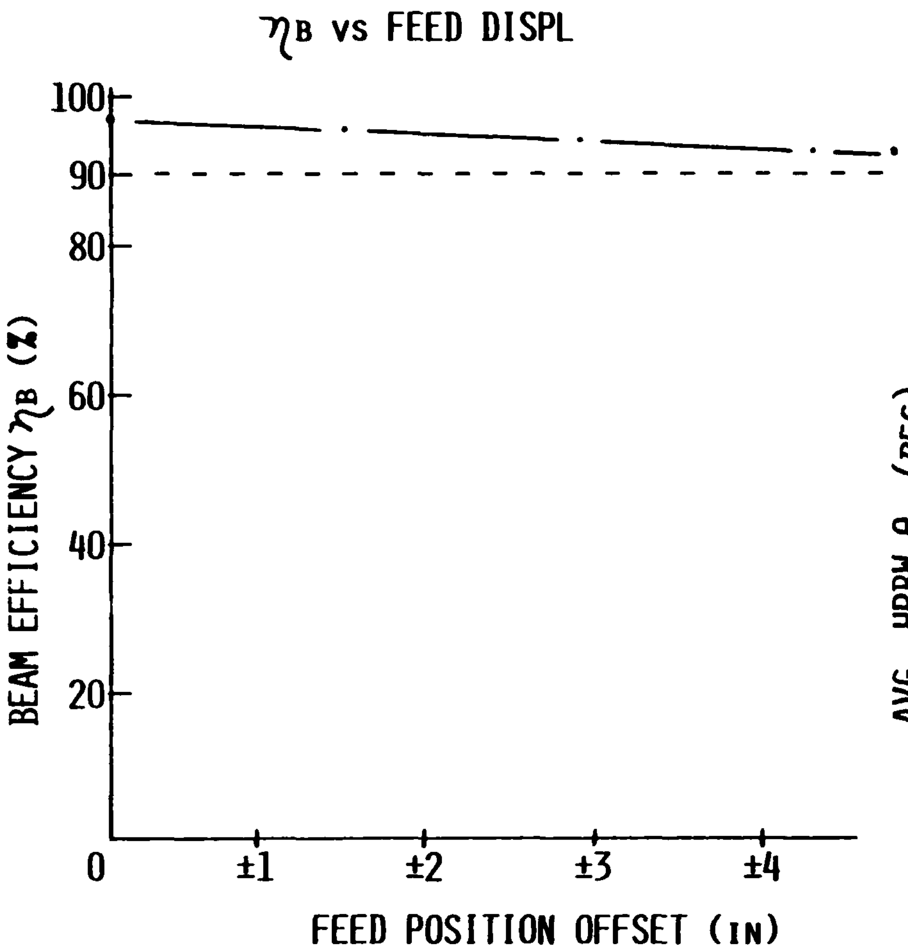

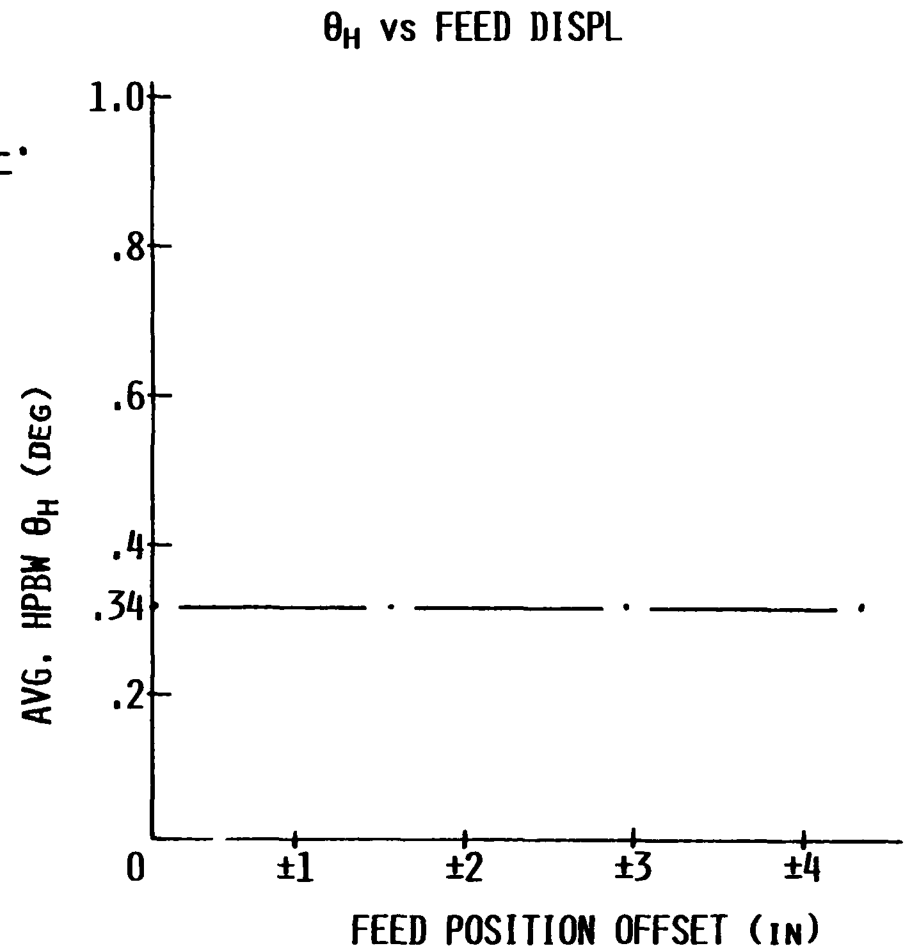

SYMMETRY PLANE DISPLACEMENT

Feed displacement in the plane of symmetry (i.e. azimuth plane) results in a graceful degradation of beam efficiency with scan angles up to 4.5 beamwidths. Due to the fact that scanning takes place in the plane of symmetry, this degradation is independent of direction (+ or -) of displacement. Also depicted is the invariance of secondary pattern half power beamwidth with feed displacement.

ABSOLUTE BEAM SCAN ANGLE

HUGHES

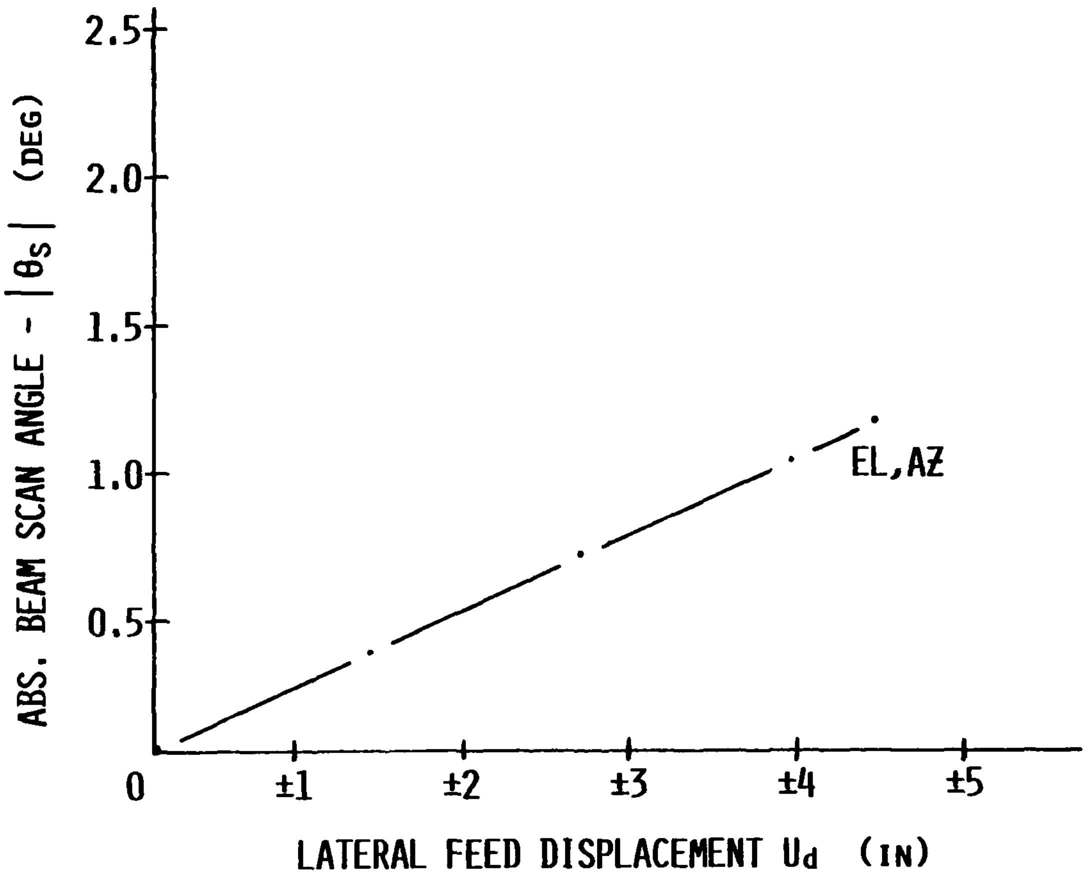

ABSOLUTE BEAM SCAN ANGLE

Absolute beam scanning angle as a function of lateral feed displacement is depicted. Scanning is a linear function independent of whether the feed is displaced in either the elevation or azimuth planes for small displacements. In addition, displacements of up to 5λ will result in scan angles of 1.5° (Or 5 beamwidths).

LATERAL FEED DISPLACEMENT COORDINATES

HUGHES

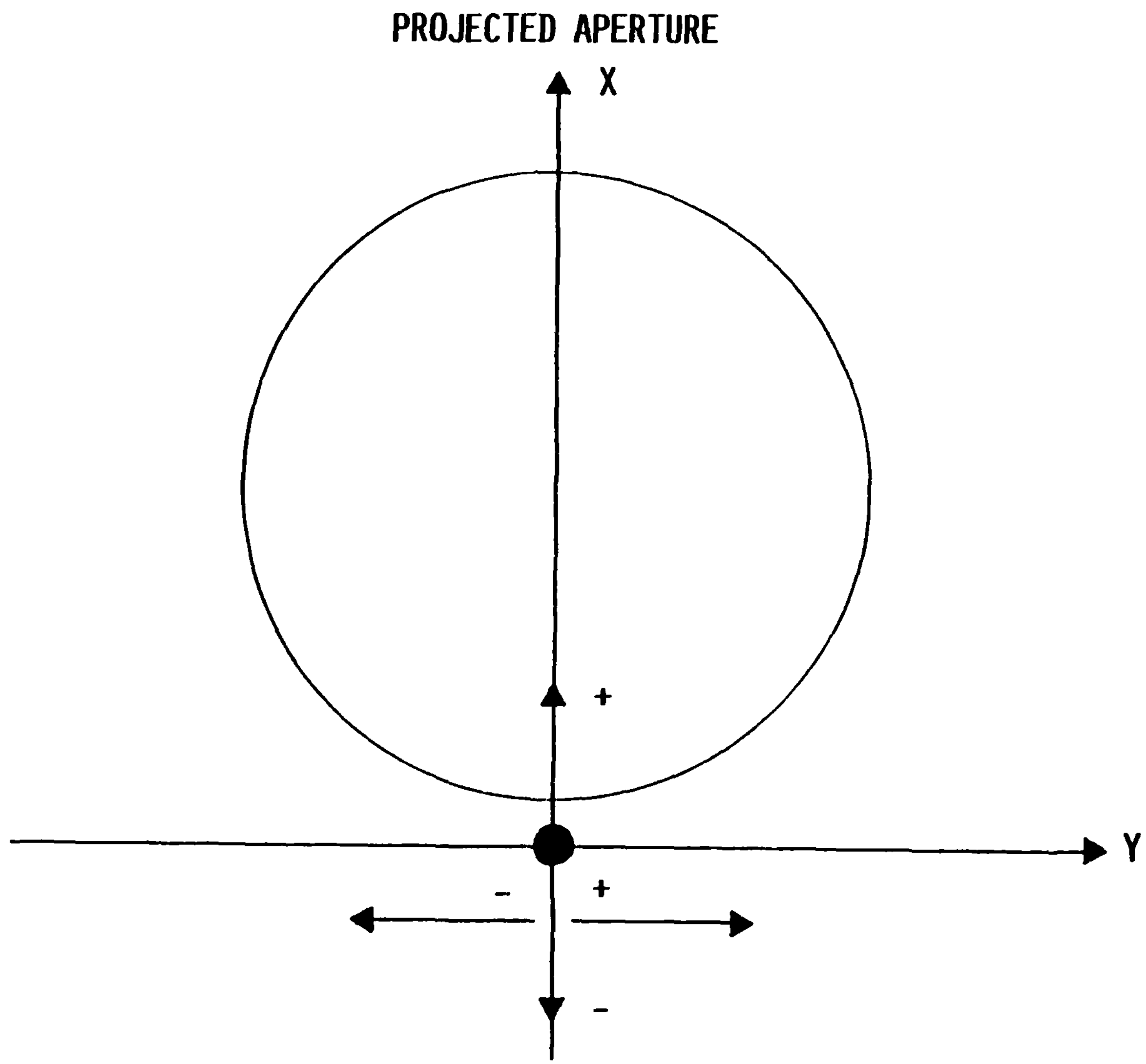

LATERAL FEED DISPLACEMENT COORDINATES

A pictorial presentation of the focal plane coordinate system used to relate relative feed positioning in both azimuth and elevation planes.

31.6 RPM ANTENNA PERFORMANCE CHARACTERISTICS

Specific worst case performance results for the 31.6 rpm configuration are tabulated. A comparison between smooth and RMS deviated reflector surfaces is also presented to establish a relationship between ideal and actual performance. Parameters of interest are beam efficiency, cross polarization and secondary pattern half power beamwidth. The parameter which shows a significant degradation with surface inaccuracies is beam efficiency at 10.4 GHz. Worst case denotes the performance of the feed displaced furthest from the focal point.

31.6 RPM ANTENNA PERFORMANCE CHARACTERISTICS

HUGHES

FREQ (GHZ)	REFLECTOR SURFACE ACCURACY (IN. RMS)	η_B (%)	θ_H (DEG)	XPOL (dB)
5.2	0	93.62	.684	23.5
10.4	0	95.57	.353	24.3
5.2	.022	92.72	.684	23.5
10.4	.022	91.83	.354	24.3

15.8 RPM FEED LAYOUT

A six element feed cluster comprising four 10.4 GHz dual mode horns and two 5.2 GHz dual mode horns is depicted as a representative layout which meets the ground coverage requirement at 15.8 RPM. This layout minimizes the offsets for the 10.4 GHz feeds. Other layouts are feasible which would minimize the 5.4 GHz offsets.

15.8 RPM FEED LAYOUT

HUGHES

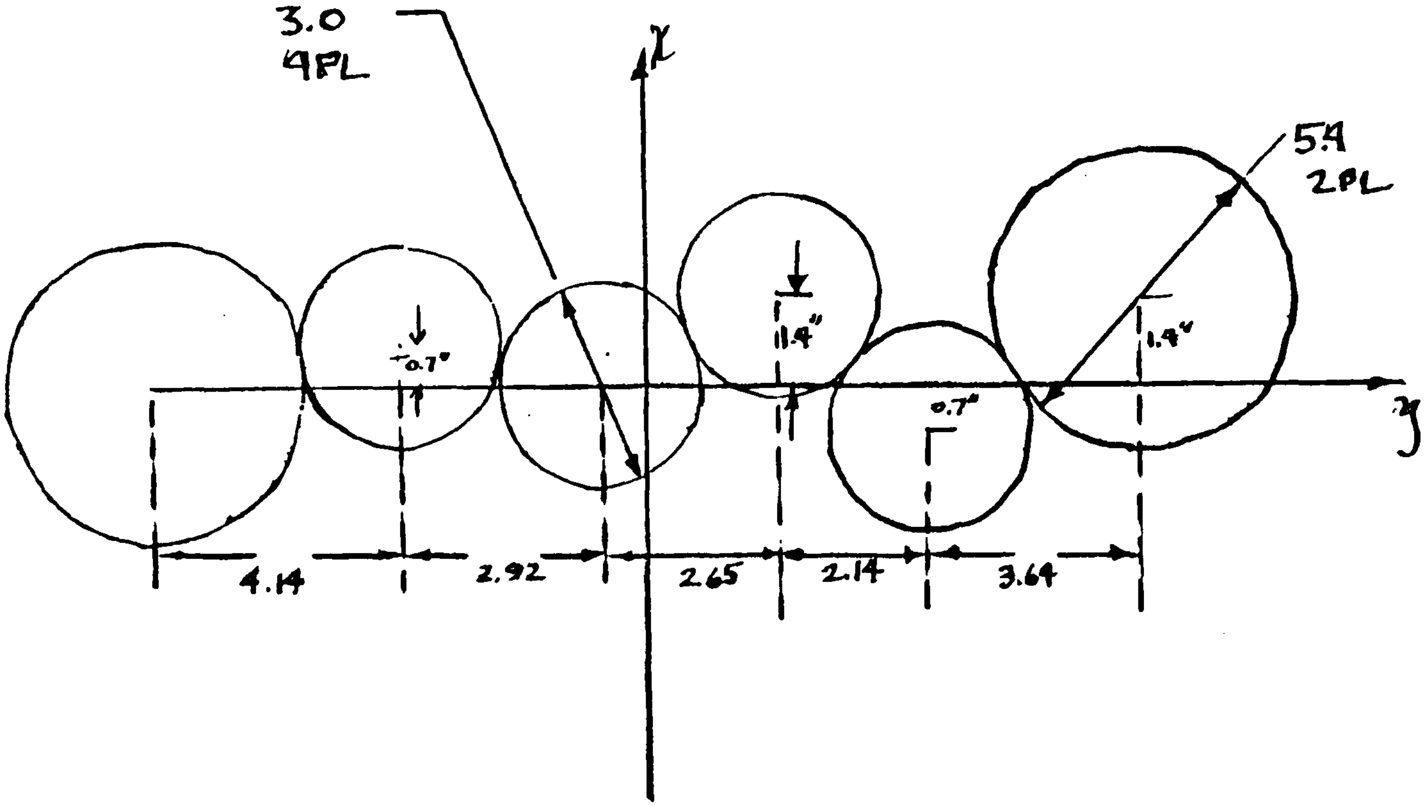

15.8 RPM ANTENNA PERFORMANCE CHARACTERISTICS

Specific worst case performance results for the 15.8 rpm configuration are tabulated. A comparison between smooth and RMS deviated reflector surfaces is also presented to establish a relationship between ideal and actual performance. As before, parameters of interest are beam efficiency, cross polarization and secondary pattern half power beamwidth. The six feed cluster results in larger displacements of the feeds from the focal point as compared to those of the 31.6 rpm configuration.

15.8 RPM ANTENNA PERFORMANCE CHARACTERISTICS

HUGHES

FREQ (GHZ)	REFLECTOR SURFACE ACCURACY (IN. RMS)	η_B (%)	θ_H (DEG)	XPOL (dB)
5.2	0	91.20	.697	23.7
10.4	0	95.22	.371	24.4
5.2	.022	90.36	.698	23.7
10.4	.022	91.46	.371	24.4

FEED DISPLACEMENT SUMMARY AND CONCLUSIONS

A summary is presented of the general trends exhibited in the lateral feed displacement studies. These trends point to feed cluster layouts in the azimuth plane for best overall performance.

LATERAL FEED DISPLACEMENT STUDIES

HUGHES

SUMMARY AND CONCLUSIONS

- SCANNED BEAM WITHIN SPEC TO $\theta_S = 1.5°$
- DISPLACEMENT IN ASYMMETRIC PLANE SLIGHTLY FAVORS + X.
- PHASE ERRORS IN ASYMMETRIC PLANE RESULTS IN SHOULDER LOBES.
- FEED DISPLACEMENT IN SYMMETRIC PLANE DESIRABLE.

DYNAMICS

LFMR DYNAMIC ANALYSIS OVERVIEW

A structural model of the LFMR was constructed to determine the effect on system weight, angular momentum and pointing accuracy due to various balancing techniques, configurations, spin rates, and antenna F/D ratios.

Using NASTRAN, a model of a deployable mesh reflector was developed and integrated into an overall LFMR NASTRAN model. The effect of the S/C-to-LFMR boom was also included in the study.

A *conceptual* balance study was also *performed on each* of the *eight* LFRM system concepts studied in order to determine whether significant differences exist in the complexity of the static and dynamic balancing subsystems required.

ASSUMPTIONS

The assumptions were necessitated by limited available information and computational ease. No attempt has been made to optimize the weight/strength of booms by variation of cross-sectional geometry or by examining alternate viable material candidates.

CONSTRAINTS

These constraints are self-imposed such that candidate alternatives could be compared on an equal basis. The 3X spin rate fundamental frequency was assumed to be the minimum allowable flexibility to minimize structural interaction to spin servo distrubances.

ASSUMPTIONS AND CONSTRAINTS

HUGHES

ASSUMPTIONS

- RIGID INERTIAL SPACECRAFT
- CIRCULAR CROSS SECTIONS ON ALL BOOMS
- T300 GRAPHITE

CONSTRAINTS

- FIRST FREQUENCY OF STRUCTURE MUST BE AT LEAST 3X SPIN RATE
- MINIMUM FIRST FREQUENCY OF 1 Hz

CONFIGURATIONS STUDIED

The Baseline configuration was examined in two structural variations: F/D = .36 and F/D = .25. Furthermore two spin rates were studied: 31.6 RPM and 15.8 RPM. Using the constraints of the preceding pages, the fundamental frequency of the structure was lowered to 1.0 Hz for the case of 15.8 RPM spin rate. This assumption will be examined in subsequent pages. A 1.6 Hz model was maintained for the higher spin rate.

The Alternate configuration was also studied in these variations. A total of eight variations (four of each configuration) were studied.

All candidate alternatives were modeled using a Hughes Aircraft Company representation of the Harris 5.9m reflector. No attempt in modeling a General Dynamics reflector was made during this analysis.

CONFIGURATIONS STUDIED

HUGHES

BASELINE

- RCA PROPOSED SIDE MOUNTED CONFIGURATION
- F/D = .36
- HARRIS REFLECTOR 5.9M
- HUB MOUNTED REFLECTOR

ALTERNATIVES

- SPIN MOTOR LOCATED ON BACK-SIDE (TOP) OF REFLECTOR
- F/D = .25

F/D = .36

HUGHES

	BASELINE		ALTERNATE	
	15.8 RPM	31.6 RPM	15.8 RPM	31.6 RPM
UNBALANCED MASS (LBM)	142.6	155.0	168.1	163.1
BALANCE WT (LBM)	15	15	5	5
BALANCED SYSTEM MASS (LBM)	157.6	170.0	173.1	168.1
UNBALANCED SPIN MOI (SL FT^2)	67.1	75.2	72.0	72.0
BALANCED SPIN MOI (SL FT^2)	74.4	82.0	73.3	73.3

SPIN RATE COMPARISON

This table shows a comparison between the baseline and alternate for both the 15.8 and 31.6 RPM cases. Although the suspended weight on the antenna boom is lower in the alternate case, the increased boom length causes the overall boom weight to be higher. The increased frequency of the antenna boom in the baseline case causes the higher weight in the 31.6 RPM case. This analysis fixed the antenna boom at 50.1 lbs. as a minimum, thus the 15.8 RPM case is heavier by the amount of the electronics.

SPIN RATE STUDY 15.8 RPM vs 31.6 RPM

HUGHES

- EFFECT ON SURFACE DISTORTION
  - LARGER SPIN RATE INDUCES LARGER REFLECTOR DISTORTIONS
  - DETAILED HARRIS MODEL IS REQUIRED
- MOMENTUM COMPENSATION
  - LARGER SPIN RATE REQUIRES LARGER MOMENTUM COMPENSATION
- BALANCING CONSIDERATION
- POINTING ERROR SENSITIVITY

SPIN RATE STUDY

The higher spin rate induces larger deformation and thus decreases RF performance. The detailed Harris model is required to determine surface distortion under spinning and dynamic distrubance conditions.

The size of the momentum wheel is decreased for lower spin rate. The actual difference in momentum compensation is discussed elsewhere (system analysis).

Balancing and pointing error sensitivity addresses the initial assumption that a lower spin rate implies a lower allowable structural fundamental mode.

ALTERNATE BALANCING

HUGHES

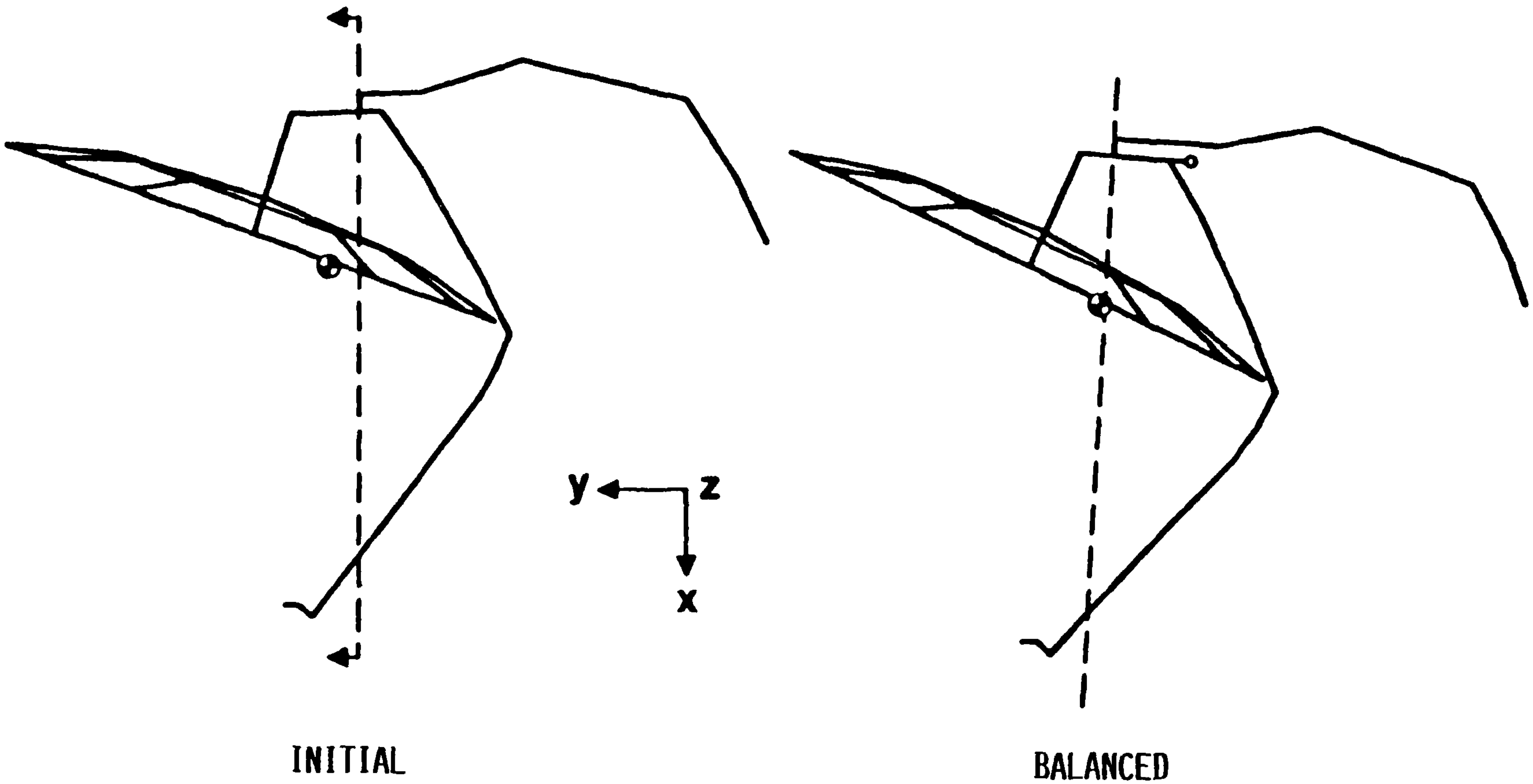

ALTERNATE BALANCING

For the Alternate configuration, it is apparent that the spin axis should lie to the right of the centroid to obtain zero dynamic imbalance at the BAPTA. This position is favorable since the balance weight is only 5 lbs in this case and the length of the boom is much reduced. Note also that the feed/horn assembly acts as a balancing weight.

BASELINE BALANCING STUDY

BASELINE

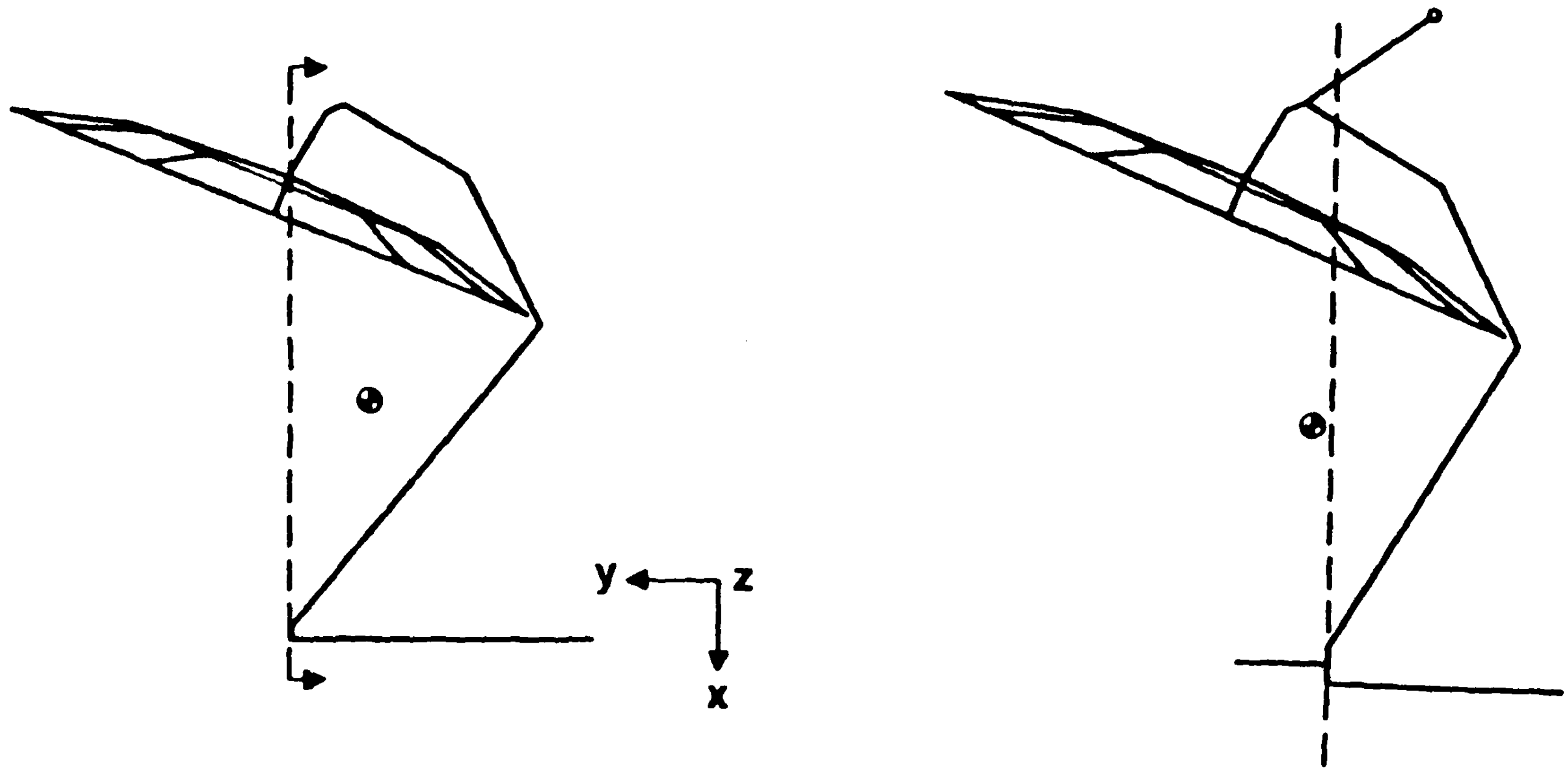

INITIAL

BALANCED

BASELINE BALANCING

The vertical dashed lines in these depictions indicate the initial and final position of the spin axis.

A careful examination of the structure reveals a preferable position of the spin axis exists such that the dynamic imbalances (cross-inertial terms) with respect to the BAPTA are equal to zero. This can be seen in the following equation:

$$I_{xy} = I_{x'y'} - m y_o x_o$$

where $I_{x'y'}$ = cross-product of inertia about the centroid

I_{xy} = cross-product of inertia about the BAPTA

m = mass

x_o = distance along x-axis from BAPTA to centroid

y_o = distance along y-axis from BAPTA to centroid

Clearly this position lies to the left of the centroid. In this configuration, however, to statically balance that system would require a balance weight from the BAPTA extending into the field of view of the reflector. This would violate one of the predescribed constraints. Any other location (x not equal to 0) of this balance weight would create a dynamic imbalance.

Given the above arguments, the figure on the right indicates the probable position of the spin axis and associated balance weight. The weight of the balance is fifteen pounds. Note that in this case it is necessary to mount the feed horns onto a boom. The weight and lengths associated with the balanced configuration are tabulated in the Summary. For these analyses all balance booms were assumed massless.

BALANCING STUDY

HUGHES

OBJECTIVES

- BALANCE SYSTEM STATICALLY AND DYNAMICALLY
- MINIMIZE BALANCE WEIGHT
- MINIMIZE BOOM LENGTH

CONSTRAINT ASSUMPTIONS

- KEEP WEIGHTS OUT OF SIGNAL PATH
- NO WEIGHTS ON REFLECTOR EDGE
- MAXIMUM WEIGHT OF 15 LBS.
- SPIN AXIS CAN BE MOVED LATERALLY

METHODOLOGY

- CALCULATE LOCATION AND MAGNITUDE OF WEIGHT(s) TO STATICALLY AND DYNAMICALLY BALANCE SYSTEM
- IF THE ABOVE CONSTRAINTS ARE VIOLATED, MOVE THE SPIN AXIS
- ITEERATE TO OPTIMIZE WEIGHT AND POSITION

BALANCING STUDY

The objectives of the study were to achieve both static and dynamic balance. The weight of the balance weight and the balance weight boom length were to be kept to a minimum. No weight was assigned to the balance weight boom in this analysis.

The constraints are listed on the chart along with the methodology.

LFMR MATH MODEL REPRESENTATION

HUGHES

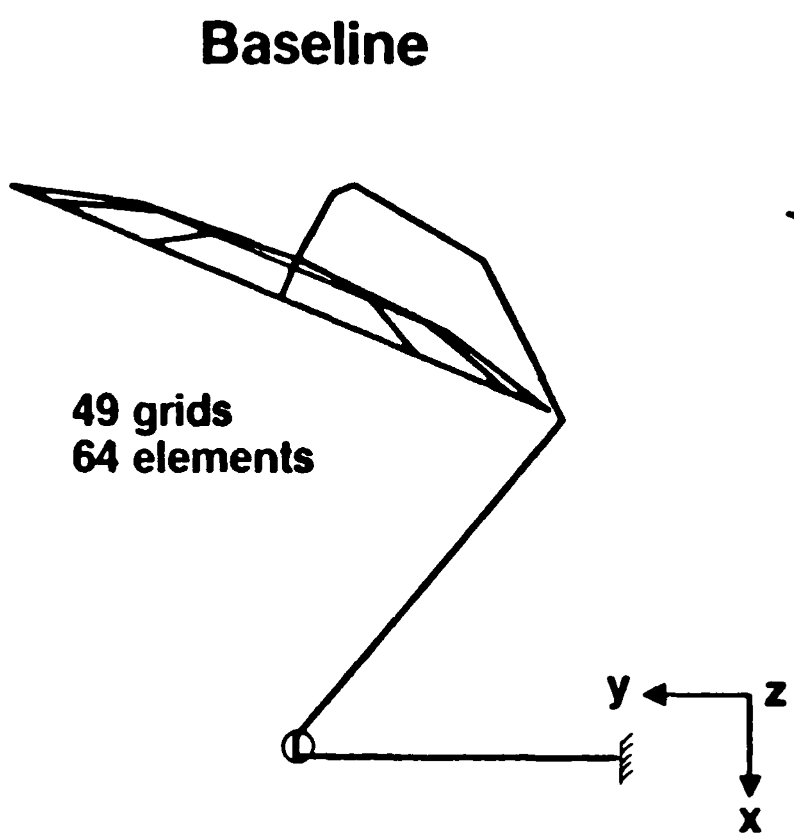

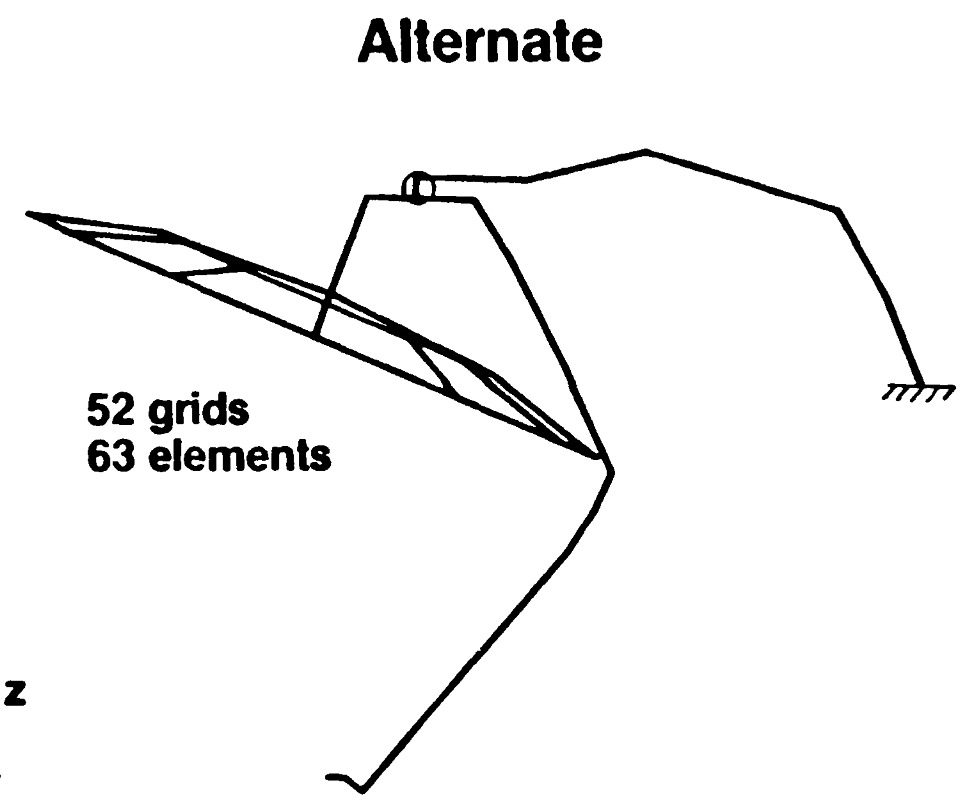

847090-1

LFMR MATH MODEL REPRESENTATION

The facing page illustrates the two different configurations with an F/D = .36. The F/D = .25 variation is illustrated on succeeding pages. The BAPTA (Bearing and Power Transfer Assembly) is located at the circle. Spacecraft is located by ground.

For the Baseline case, the feed/horns and hot and cold loads are located in the vicinity of the BAPTA. In the Alternate case the feed/horns and hot and cold loads are located at the tip of the spun booms (circle to lower tip of boom beneath the reflector). For the latter case a despun motor is required to de-spin the cold loads.

In the baseline configuration, wall thicknesses of despun booms (circle to ground) as well as spun booms (circle to reflector) were varied to achieve the desired frequency. As opposed to the Baseline case, the Alternate configuration spun boom does not carry the inertial loading of the reflector. For the Alternate case only the despun boom (circle to ground) thickness was varied. This was for convenience in balancing the system and can be justified since the actual load carried by the spun boom is much less than in the Baseline configuration.

REFLECTOR MATH MODEL REPRESENTATION

HUGHES

REFLECTOR

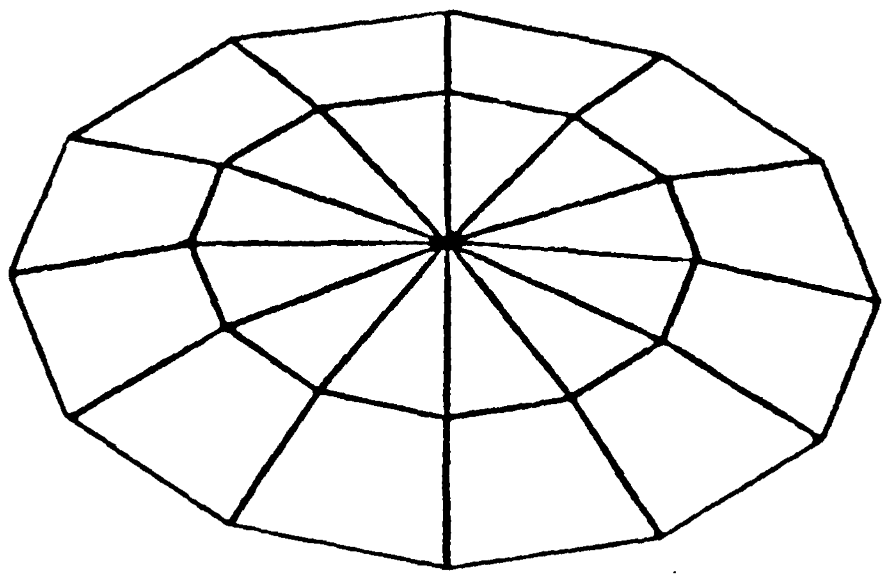

WEIGHT = 37.0 LBS

$$[I] = \begin{array}{cccc} X & Y & Z & \\ 24.0 & 0.0 & 0.0 & X \\ 0.0 & 24.0 & 0.0 & Y \\ 0.0 & 0.0 & 46.0 & Z \end{array}$$

MODE	FREQ HUGHES	HARRIS
1	3.79	3.53
2	3.79	3.79
3	4.11	3.98

REFLECTOR MATH MODEL REPRESENTATION

At the time this analysis was performed, a Harris Reflector Model was unavailable. Based upon preliminary numbers from a publication from Harris titled "NROSS MICROWAVE RADIOMETER SSM/I" (dated 9 Sept. 1982), and via telephone conversation, a finite element model was developed. Mass properties and structural frequencies were obtained to match those estimated by Hughes and Harris. All models were developed on NASTRAN and the refelctor was modeled using the lower reflective surface.

Subsequent to this analysis a Harris Reflector Mass and Stiffness representation was obtained. Mass properties indicate an approximately 32% reduction in mass moment of inertia in comparison to the Hughes finite element representation. The impact of this new information on these results shall be discussed in the conclusion.

POINTING ERROR COMPARISON

The following pages illustrates the pointing error transmissibility curve for a 1-g sine-z acceleration at the spacecraft interface.* Clearly the pointing error is dependent on structural flexibility. For the Baseline case, reducing the first fundamental mode from 1.6 Hz to 1.0 Hz results in a increase in pointing error sensitivity by a factor of 5. Since input excitation at the spacecraft may not always be periodic in nature, the pointing error should be classified as dynamic instability, that is, it can not be predicted from cycle to cycle. Clearly the pointing error sensitivity will determine the flexibility of the system, not the spin rate.

* z-base excitation yields the largest pointing error.

POINTING ERROR COMPARISON

HUGHES

Baseline

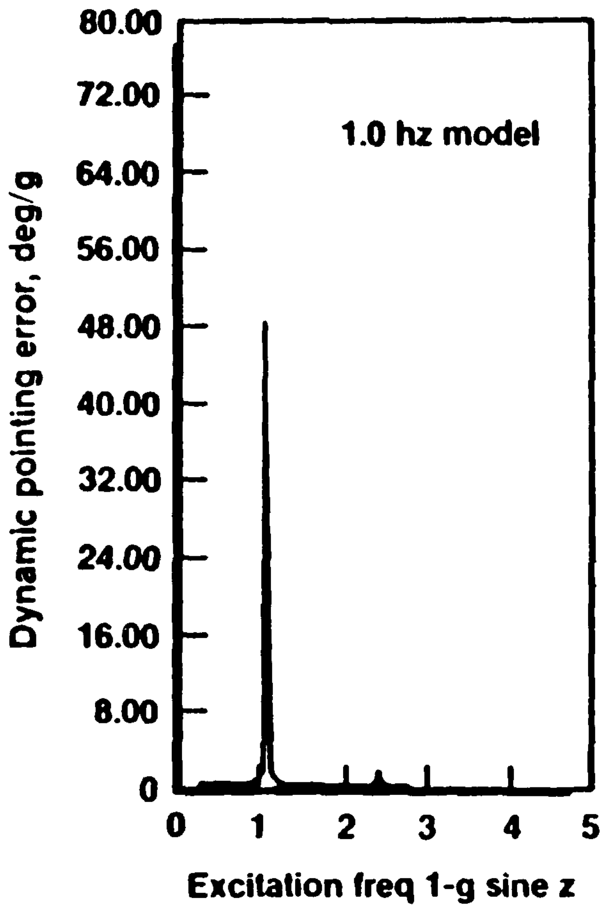

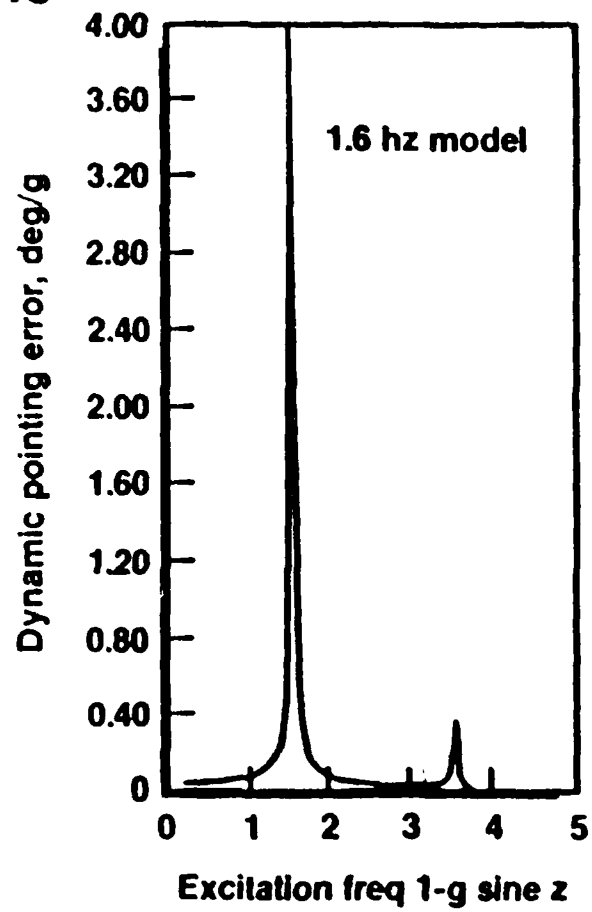

847090-4

POINTING ERROR COMPARISON (CONT'D)

HUGHES

Alternate

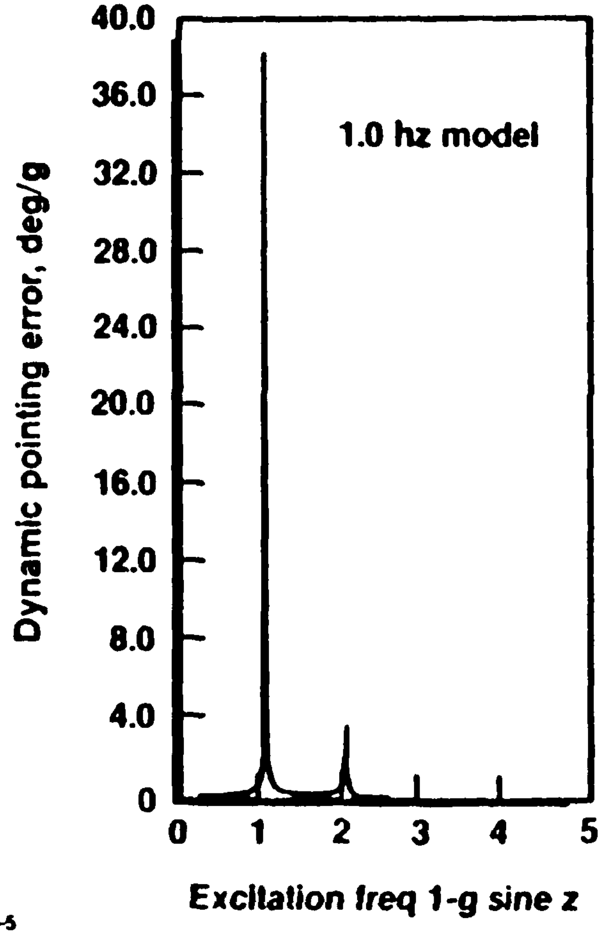

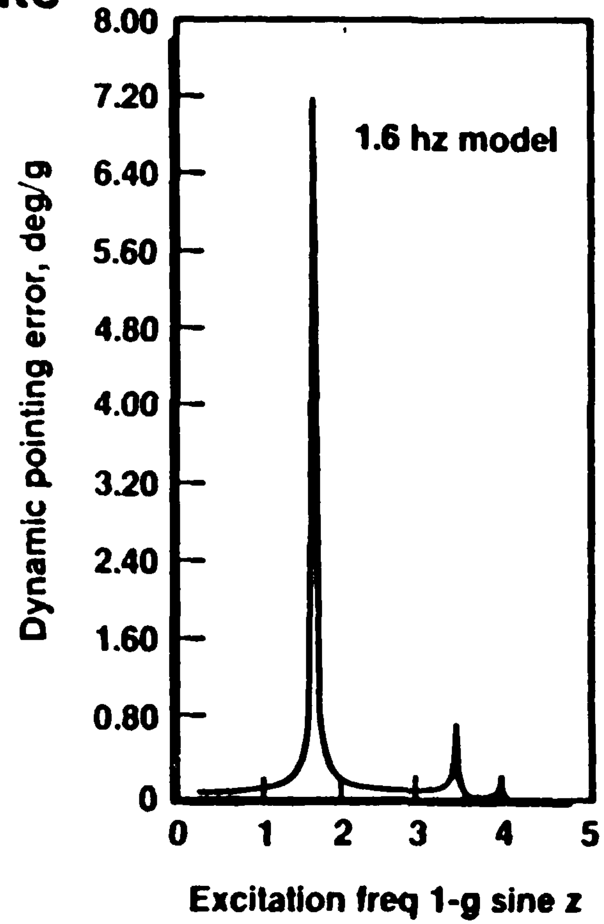

847090-5

PREVIOUS PAGE IS BLANK

F/D VARIATION

The facing page illustrates the balanced configuration of the Baseline and Alternate with an F/D = .25. Advantages of the Baseline are that the feed/horn boom has been eliminated and overall boom lengths shortened. The disadvantage of the Alternate is that a longer balance boom is needed with added weight (see Summary). In this case, the feed/horn assembly no longer acts as an effective balance weight.

F/D Variation Study

HUGHES

Baseline

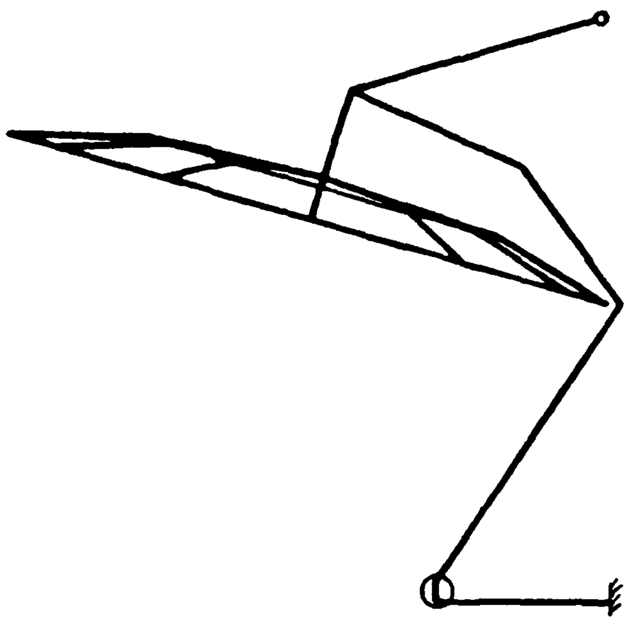

Alternate

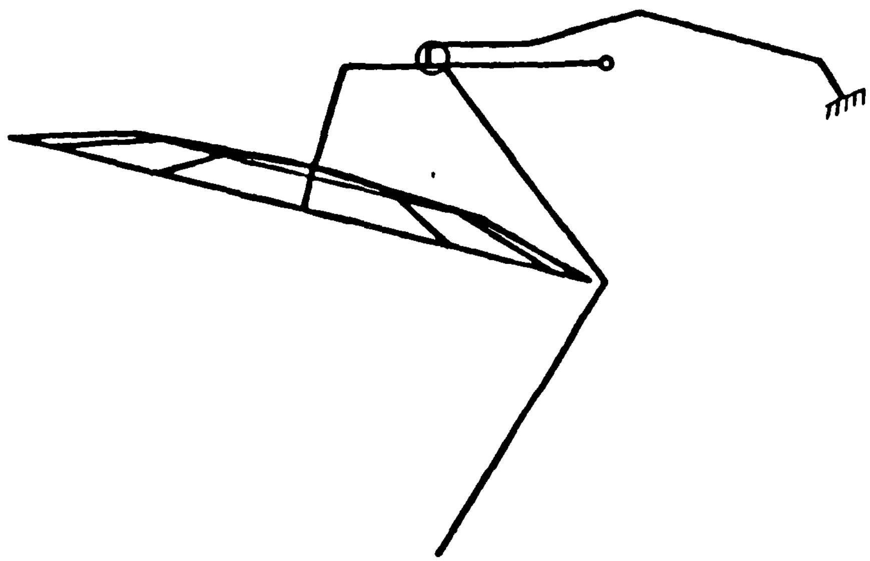

847090-6

F/D Variation Study (CONT'D)

HUGHES

Baseline

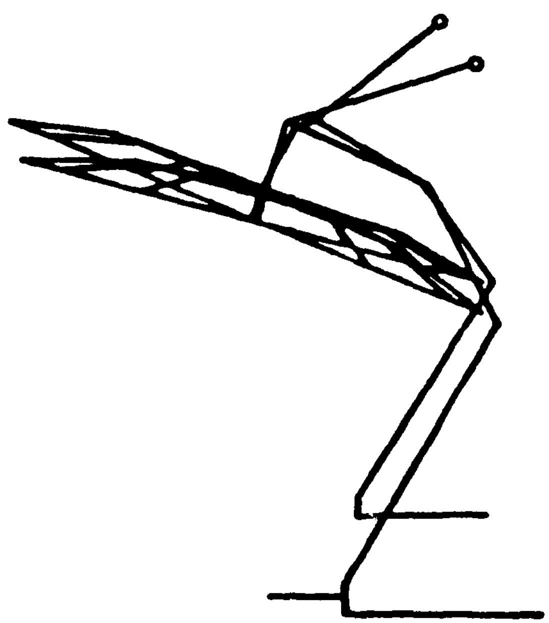

Alternate

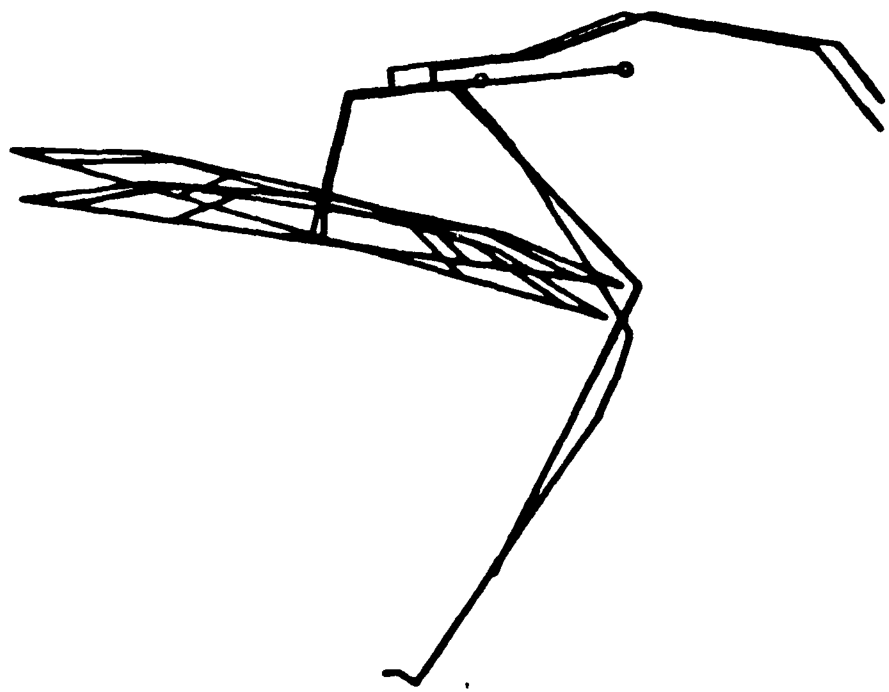

847090-7

F/D VARIATION STJDY SUMMARY

The following charts illustrate the fact that a smaller F/D ratio produces a shorter antenna boom which lowers the overall weight of the LFMR. The electrical requirements will then dictate the F/D ratio but it will be biased toward the lower end of the F/D range.

F/D VARIATION STUDY SUMMARY

HUGHES

F/D = .25

	BASELINE		ALTERNATE	
	1.0Hz	1.6Hz	1.0 Hz	1.6Hz
UNBALANCED MASS (LBM)	126.6	131.0	155.1	150.1
BALANCE WT (LBM)	15	15	15	15
BALANCED SYSTEM MASS (LBM)	141.6	146.0	170.1	165.1
UNBALANCED SPIN MOI (SL FT^2)	65.6	69.4	72.7	72.7
BALANCED SPIN MOI (SL FT^2)	89.0	85.5	90.2	90.2

SPIN RATE AND F/D SUMMARY

The chart is a summary of the spun weight, MOI, balance weight, balance boom length, and S/C boom weight for F/D of .25 and .36, for spin frequency of 15.8 and 31.5 RPM, and the baseline and alternate.

It is clear that as the structural frequency is increased from 1.0 Hz to 1.6 Hz the weight of the spun portion increases for the baseline. The reduction of 5 lbs for the alternate when the spin rate increases from 15.8 to 31.8 RPM is due to the increased number of radiometer channels for the 1.0 Hz (15.8 RPM case).

As the F/D increases from .25 to .36 the weight also increases for the baseline, but the balance boom length decreases which may be an important consideration.

SPIN RATE AND F/D SUMMARY

HUGHES

	1.0 Hz (15.8 RPM)				1.6 Hz (31.6 RPM)			
	BASELINE		ALTERNATE		BASELINE		ALTERNATE	
F/D	.25	.36	.25	.36	.25	.36	.25	.36
SPUN WEIGHT (LBS)	141.6	157.6	170.1	173.1	146.0	170.0	165.1	168.1
MOI (SL FT^2)	89.0	75.0	90.2	73.3	85.5	82.0	90.2	73.3
BALANCE WEIGHT (LBS)	15	15	15	5	15	15	15	5
BAL. BOOM LENGTH (IN.)	118	77	68	10	106	97	68	10
S/C BOOMWEIGHT (LBS)	19.9	28.0	36.0	37.2	29.7	38.4	80.3	83.7

CONCLUSIONS

Clearly the Baseline configuration with F/D = .25 appears the most attractive. The only apparent disadvantage is the weight and length of balance boom. As noted earlier, however, the Harris reflector has a considerably smaller moment of inertia than assumed in the study. This would reduce the balance weight and/or the length of the balance boom.

The higher spin rate does not have any advantage over the lower spin rate from a dynamic standpoint. At this point, it appears spin rate will be governed by electrical or system considerations. The structural flexibility will not be determined by spin rate.

CONCLUSIONS

HUGHES

BASELINE vs ALTERNATE

- BASELINE ADVANTAGES
  - LOWER OVERALL WEIGHT
  - SHORTER BOOMS
- ALTERNATE ADVANTAGES
  - EASIER TO BALANCE

15 RPM vs 30 RPM

- LOWER SPIN RATE APPEARS ATTRACTIVE
- LOWER SPIN RATE DOES NOT IMPLY LOWER FREQ

BALANCING

DYNAMIC BALANCING

The LFMR requires dynamic balancing to maintain alignment and minimize spacecraft distrubance effects due to mass imbalance. The method proposed to accomplish this task involves a combination of balancing on earth with the additional capability of in-space balancing using a dynamic balance mechanism (DBM).

The main advantage of balancing on earth is the ease in which adjustments of the balance masses can be made, but this is offset by the deflection uncertainties when working in a one-G environment and the effects of aerodynamic loading on the spinning section. A DBM is recommended to remove the residual unbalance. It is necessary to balance the subsystem on earth within the limits of the DBM.

AD-A153 691 LFMR DEFINITION STUDY(U) HUGHES AIRCRAFT CO EL SEGUNDO CALIF SPACE AND COMMUNICATIONS GROUP APR 85 N00014-84-C-2290 3/3

UNCLASSIFIED F/G 5/1 NL

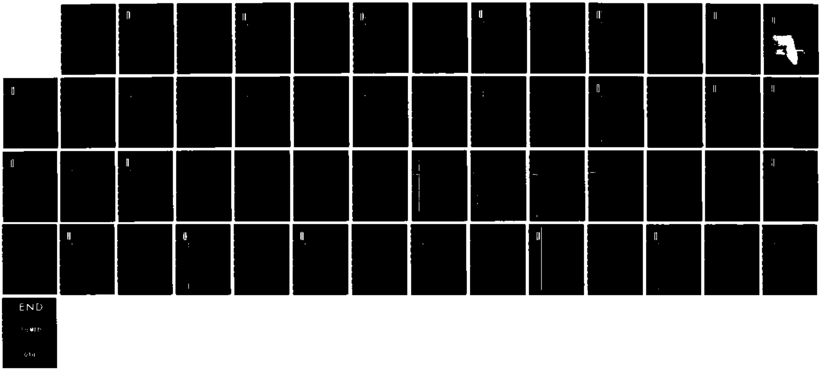

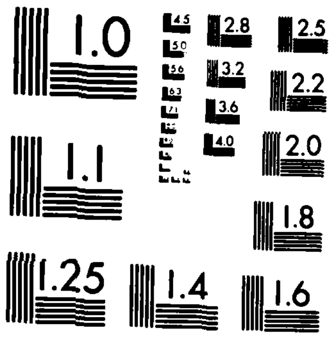

MICROCOPY RESOLUTION TEST CHART
NATIONAL BUREAU OF STANDARDS-1963-A

DYNAMIC BALANCING

HUGHES

- GROUND BALANCING
- DYNAMIC BALANCE MECHANISM (DBM) USED IN SPACE TO ELIMINATE:
  - ONE-G EFFECTS
  - AERODYNAMIC EFFECTS
  - STRUCTURAL MODELING UNCERTAINTIES

PREVIOUS PAGE IS BLANK

DYNAMIC BALANCE SETUP

The spinning section can be balanced either right side up or inverted. The spin axis must be oriented parallel to the local gravity vector. The actual implementation will depend on the difficulty of implementation in either case.

Dynamic Balance
Setup

HUGHES

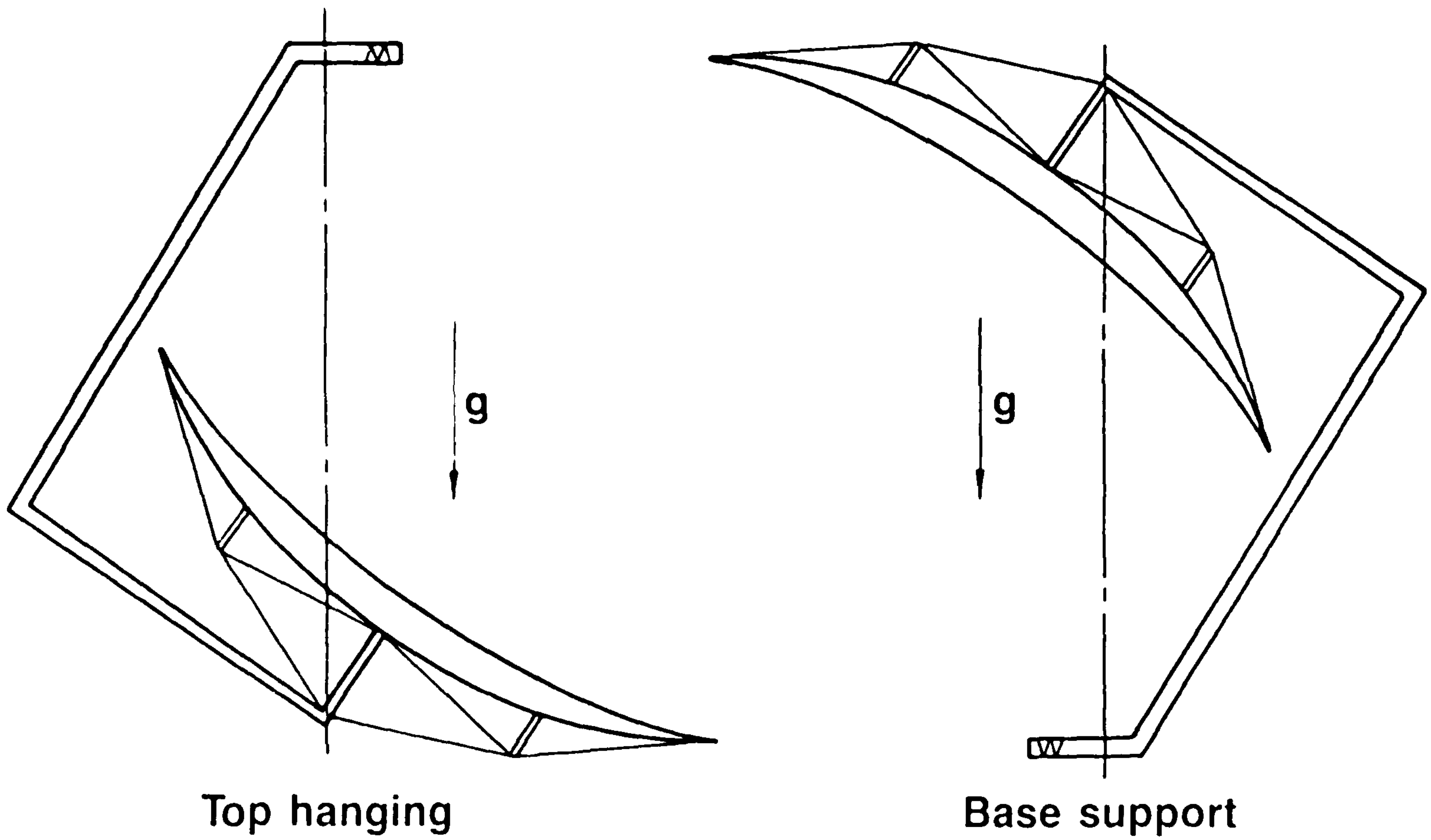

847098 8

TOP HANGING DEFLECTIONS

Shown here are the magnitude of the LFMR deflections (calculated using finite element modeling techniques) due to both gravity which exists only on earth and rotational forces existing both on earth and in space. During balancing on earth it is desirable to remove as much of the deflections due to gravity as possible without effecting deflections due to rotation. The method proposed employs the use of a zero-G fixture which consists of a series of thin cables suspended from a support structure and attached to critical points on the spinning section. Analysis indicates a dynamic imbalance of 11.3 lb-in-s^2 for a configuration completely uncorrected for deflections due to gravity. It is estimated that correcting 80% of this imbalance due to gravity by using the described zero-G fixture is reasonable. This results in an uncertainty of 2.3 lb-in-s^2 which is well within the limits of the proposed DBM budget.

Dynamic Balance
Top Hanging

HUGHES

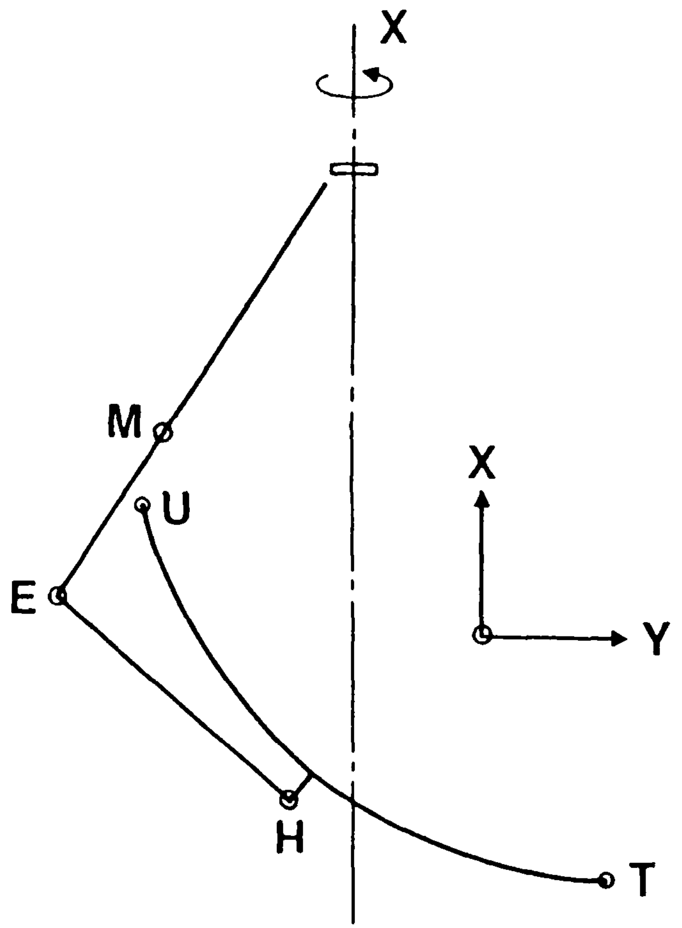

847098 9

Deflections, in.

	I-G	Rotational Force	
	X	X	Y
M	+0.04	−0.007	+0.012
E	−0.05	−0.001	+0.024
H	−0.26	−0.013	+0.017
U	+0.10	−0.290	−0.118
T	−0.93	+0.372	+0.134

AERODYNAMIC EFFECTS

The effects of aerodynamic loading can be compensated for by several methods. The most effective method is to employ a vacuum chamber in which all dynamic balancing of the subsystem would occur. The disadvantages of this method are the cost and the time involved during the multiple pump-downs required during testing. An alternative to dynamically balancing in a vacuum chamber would be to use a rigid aerodynamic enclosure. This method employs a statically and dynamically balanced enclosure of sufficient size to completely isolate the subsystem from aerodynamic loading. This technique has been successfully used on the SSM/I program. Although the enclosure is costly, some of the expense will be offset by the ability to integrate the zero-G tooling into the fixture. The third and least expensive method involves surrounding the subsystem with a helium tent enclosure. It is also the least accurate method, but the known properties of the helium atmosphere can be prorated to space conditions.

AERODYNAMIC EFFECTS

HUGHES

- VACUUM CHAMBER
  - LIMITED LOCATIONS AVAILABLE
  - COSTLY IN OPERATION

- RIGID AERODYNAMIC ENCLOSURE
  - PROVEN TECHNOLOGY (SUCCESS STORY HS-376 20 S/C)
  - EXPENSIVE TOOLING
  - MAY BE USED AS SUPPORT FOR ZERO-G

- HELIUM TENT ENCLOSURE
  - PRORATE RESULTS TO SPACE CONDITIONS
  - MAY HAVE AIR POCKETS - DECREASED ACCURACY
  - RELATIVELY INEXPENSIVE

GROUND BALANCE FEASIBILITY

The ground balancing of the LFMR is feasible. In an attempt to bound the problems involved in dynamically balancing the LFMR, the results of two previous programs at Hughes Aircraft Company are examined. The first is the HS 376 which is spun in an aerodynamic enclosure at 56 RPM. Although this is a much more rigid structure than LFMR, the HS 376 with the enclosure will be on the same order of magnitude in weight as the LFMR (with zero-G fixture) demonstrating the capability of balancing subsystems of this size. The dynamic imbalance of the HS 376 spacecrafts are reduced to less than 4.8 $lb\text{-}in\text{-}s^2$ although much more accurate results could be easily achieved if they were required. The second program examined was SSM/I which was also balanced in an aerodynamic enclosure. Although this subsystem is much smaller in size, the geometry, rotational speed, and some of the deployment techniques are similar to LFMR. In this program, subsystem dynamic imbalance was reduced to 0.03 $lb\text{-}in\text{-}s^2$. The LFMR will require state of the art techniques to adequately dynamically balance the spinning section but the size of the subsystem is within the limits of dynamic balancing equipment presently available.

GROUND BALANCE FEASIBILITY

HUGHES

- HS 376 DESPUN IN ENCLOSURE (AT 56 RPM)
  REQUIREMENT OF 4.8 LB-IN-S^2
- SSM/I IN ENCLOSURE (AT 31 RPM)
  ACHIEVED 0.03 LB-IN-S^2
- LFMR (AT 15 OR 30 RPM)
  WITHIN STATE OF THE ART DYNAMIC BALANCE

HUGHES FLIGHT DYNAMIC BALANCE MECHANISMS (DBM)

The next two charts show the DBM's available and the programs in which they have been used at Hughes Aircraft Company. The most likely candidate and the DBM used for this study is the model used on the HS 350, F6 spacecraft. This device has a ± 9.3 $lb\text{-}in\text{-}s^2$ adjustment capability when mounted at a 72 inch radius about the spin axis. The main bend in the support boom is approximately 72 inches from the spin axis and is the logical location for the DBM.

In conclusion, although the dynamic balance requirements for the LFMR are challenging and will require state of the art techniques in the ground balance tests, the ability to calculate (as the design progresses) the magnitude of the uncertainties to ensure any errors are within the limits of the DBM makes successful completion of this task possible.

HUGHES FLIGHT DYNAMIC BALANCE MECHANISM (DBM)

HUGHES

PROGRAM

PARAMETERS	HS 350 F5	HS 333	GMS II, III	HS 350 FG HS 105, GOES
TOTAL MASS, LB	6	7	2.6	12.2
MOVABLE MASS, LB	3	3	1.7	8.0
TRAVEL, IN	± 4.7	± 4.7	± 6.0	± 6.25

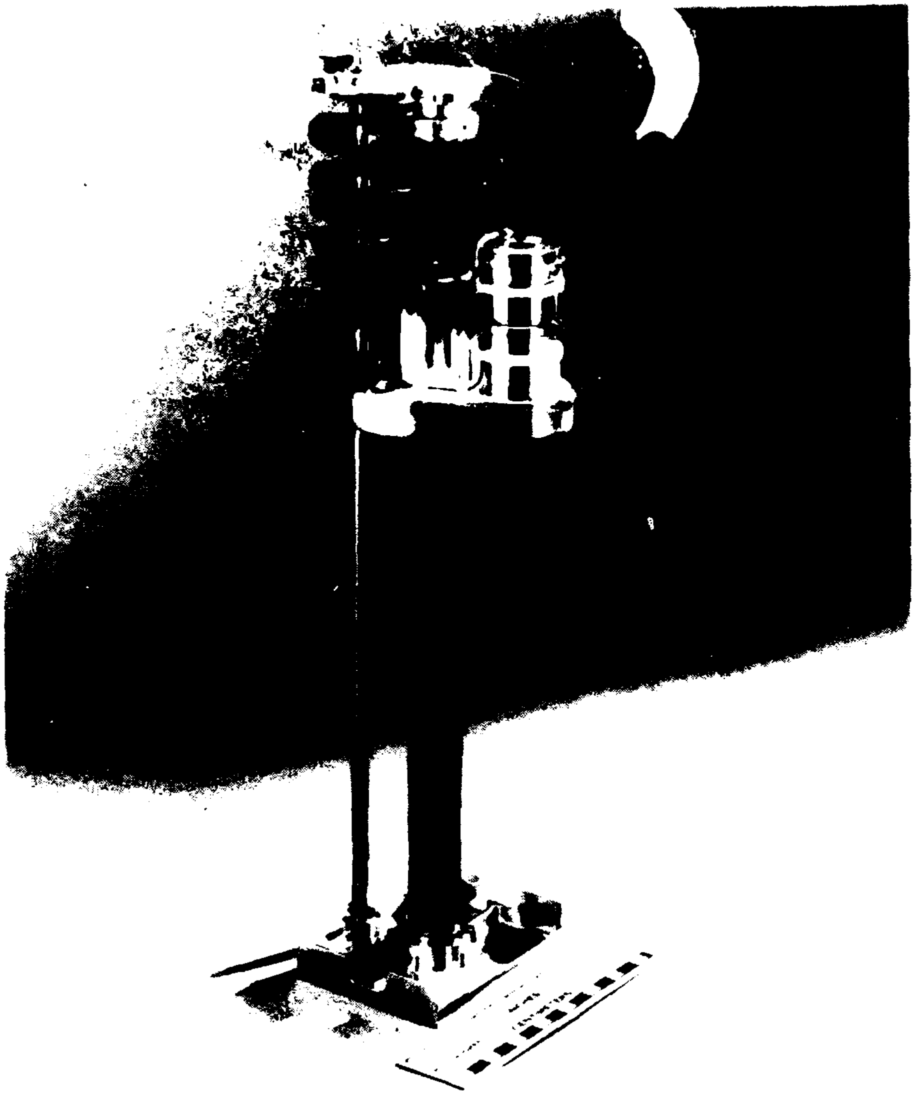

HUGHES

Dynamic Balance
DBM

847098-18

80-87538

OVERALL STUDY CONCLUSIONS

HUGHES

- TWO VENDORS HAVE SIMILAR ENGINEERING MODEL DEPLOYABLE REFLECTORS
- REFLECTOR SURFACE ACCURACY OF .015" MEETS REQUIREMENTS
- ANTENNA PATTERNS MEET REQUIREMENTS (COMPUTER GENERATED)
- MESH PERFORMANCE APPEARS ACCEPTABLE
- TOTAL POWER RADIOMETER WITH EXTERNAL CALIBRATION IS EASILY IMPLEMENTED
- ELECTRONICS
  - ANALOG AND SPIN ELECTRONICS IDENTICAL TO SSM/I
  - RECEIVERS SIMILAR TO HUGHES COMMUNICATION SATELLITE TECHNOLOGY
  - DIGITAL ELECTRONICS NEEDS MODIFIED OUTPUT FORMAT

HUGHES/SSM/I

APPLICABLE INTEGRATION & TEST EXPERIENCE

HUGHES

- ELECTRICAL NOISE ELIMINATION THROUGH ADVANCED INTEGRATION TECHNIQUES
- RADIOMETRIC CALIBRATION TECHNOLOGY
- SPIN BALANCE
- LARGE ANTENNA TESTING

APPLICABLE SSM/I INTEGRATION AND TEST EXPERIENCE

The LFMR can profit from the extensive integration and test experience obtained on the SSM/I program. Noise elimination was achieved through detailed analysis of the grounding during the engineering model testing. Calibration target and test techniques were developed during the SSM/I calibration that are directly applicable to the LFMR.

Hughes routinely balances large S/C to the level necessary for the LFMR. Finally, the Intelsat VI program is testing large reflectors on both near field and far field ranges.

SSM/I APPLICABLE DESIGN - MINIMUM RISK

HUGHES

- MECHANISMS - DEPLOYMENT
- SPIN BEARING
- SLIP RINGS
- DIGITAL ELECTRONICS
- POWER SUPPLIES
- SIGNAL CONDITIONING ELECTRONICS
- COMPOSITE STRUCTURES
- CALIBRATION SUBSYSTEM
- SPIN SERVO ELECTRONICS
- MOMENTUM COMPENSATION SUBSYSTEM

SSM/I APPLICABLE DESIGN

The chart shows the SSM/I hardware that is directly applicable to the LFMR. These items, which are already qualified, will minimize the LFMR schedule risks.

SPIN BALANCE

HUGHES

- LFMR MUST BE BALANCED IN AEROCAN OR VACUUM
- DYNAMIC BALANCE CAN BE ACHIEVED ON GROUND
- ON-ORBIT ADJUSTMENT CAPABILITY MUST BE ADDED TO LFMR TO ELIMINATE UNCERTAINTY OF ERROR MODELING

SPIN BALANCE SUMMARY & CONCLUSIONS

Spin balance of the LFMR can be achieved on the ground, but an on-orbit balance mechanism is recommended for risk reduction. Structural modeling must be used to verify that results obtained during ground testing are valid on-orbit.

SPIN RATE

HUGHES

- STRUCTURAL FREQUENCY CAN BE LOWERED FOR 15 RPM IF LARGE DEFLECTIONS ARE ACCEPTABLE
- MOMENTUM WHEEL WEIGHT AND POWER ARE LOWER FOR 15 RPM
- 15 RPM SPIN RATE REQUIRES TWICE AS MANY FEEDS AND RECEIVERS AS 30 RPM
- POWER MARGIN LARGER AT 15 RPM

SPIN RATE SUMMARY & CONCLUSIONS

The spin rate has the largest effect on the frequency of the structure. The lower (15.6 RPM) spin rate allows a lower structural frequency and thus a lower weight. Spin balance and alignments require small structural deflections to be accomplished easily. Thus the weight savings of the lower spin rate may be negated by ground testing requirements.

The other significant effect is that the lower spin frequency results in lower angular momentum, and thus the weight and power of the compensating momentum wheel are less.

HUGHES

POINTING ACCURACY

- REFLECTOR CONTRIBUTION TO RF BORESIGHT ERROR UNKNOWN
- S/C/LFMR COUPLED MODEL ANALYSIS NEEDED TO DETERMINE LFMR DISTURBANCE INPUT

POINTING ACCURACY SUMMARY & CONCLUSIONS

Two uncertainties remain about the pointing accuracy of the LFMR. The first is the amount of mispointing due to the flexible characteristics of the reflector. The detailed dynamic model of the reflector was not received in time for the study and its contribution, which is expected to be small, remains to be verified. The other uncertainty is the level of disturbance the S/C will input into the LFMR. A coupled model analysis, like the launch analysis, needs to be performed in conjunction with RCA, the S/C contractor.

ELECTRICAL PERFORMANCE

HUGHES

- MESH PERFORMANCE APPEARS ACCEPTABLE
- ALL ANTENNA RF PERFORMANCE PARAMETERS CAN BE MET FOR F/D RATIOS OF .25 TO .36
- EXTERNAL CALIBRATION IS EASILY IMPLEMENTED
- ΔT CAN BE REDUCED BY INCREASING THE NUMBER OF FEEDS AND RECEIVERS

ELECTRICAL PERFORMANCE SUMMARY & CONCLUSIONS

At the start of the study, the use of a mesh for the reflecting surface was questionable. Tests conducted by NRL along with the error analysis presented in this report show the use of the mesh is not a risk factor for the LFMR.

The radiometer RF performance can be met for F/D ratios between .25 and .36 for an offset reflector. The RF parameters satisfied were beam efficiency (90%), cross polarization (1%), beam width (.34°, .68°), and side lobe level (-20 dB).

Finally, the study has shown that external calibration using hot and cold loads can be easily implemented and that the ΔT can be reduced by increasing the number of feeds and receivers.

STUDY SUMMARY

HUGHES

- SUMMARY
- CONCLUSIONS
- RECOMMENDATIONS

OVERALL STUDY CONCLUSIONS (CONT'D)

HUGHES

FLEXIBLE BODY INTERACTION

CONCERN - LFMR MAY INTERACT WITH LFMR CONTROL SUBSYSTEM AND S/C CONTROL SUBSYSTEM

SOLUTION - LFMR MODELING AND COUPLED LFMR/SC MODELING TO IDENTIFY AND SOLVE PROBLEMS

SPIN BALANCE

CONCERN - LFMR UNBALANCE WILL CAUSE S/C MOTION

SOLUTION - GROUND BALANCING IN VACUUM ON-ORBIT BALANCE MECHANISM

ANTENNA POINTING

CONCERN - MISPOINTING WILL CAUSE RESOLUTION AND SEA SURFACE TEMPERATURE RETRIEVAL ERRORS

SOLUTION - GROUND TESTING OF LFMR TO VALIDATE MODELING

HUGHES RECOMMENDATIONS

HUGHES

- SYSTEM POINTING PERFORMANCE ANALYSIS TASK
- REFLECTOR ENVIRONMENTAL DESIGN LIMITS AND PERFORMANCE CHARACTERISTICS MUST BE DEFINED
- DEFLECTION ANALYSIS
- ADOPT 6 FEED, 12 RECEIVERS CONFIGURATION TO PROVIDE SST RETRIEVAL MARGIN

APPENDIX A

OUTPUT FILTER ANALYSIS

FILTERING THE OUTPUT FROM THE RADIOMETER

SUMMARY

Each radiometer on the LFMR includes a square-law detector that produces a voltage output that is proportional to the antenna temperature that needs to be measured. This output voltage $V(t)$ must be either filtered and sampled, or an integrate-and-dump circuit must be used, before the data can be transmitted to the Earth. This appendix compares these two possibilities, and shows that a low-pass filter will perform better than an integrate-and-dump circuit. The filter will have a cutoff frequency corresponding to the spatial frequency cutoff of the antenna, and the sampling rate will be the Nyquist rate for sampling the data in the spatial domain.

ANALYSIS

Let D be the diameter of the antenna aperture; let λ be the wavelength of the radiation. Then the antenna responds to all spatial frequencies $s < s_C$, where $s_C = D / \lambda$ is the cutoff frequency. The Nyquist sample rate is twice the cutoff frequency; $s_N = 2s_C = 2D / \lambda$.

In terms of the output $V(t)$ from the square-law detector, there is a cutoff frequency

$$\nu_C = s_C \omega \sin\beta.$$

Let $v(\nu)$ be the Fourier transform of $V(t)$, and let $b(\nu)$ and $p(\nu)$ be the Fourier transforms of the brightness distribution B and the power pattern P. Using the convolution theorem,

$$v^2(\nu) = b^2(\nu)p^2(\nu) = \sigma^2{}_N;$$

since $p(\nu)$ is zero outside the interval $(-\nu_C, \nu_C)$, the signal contained in $v(\nu)$ is also zero outside this interval.

ANALYSIS (Continued)

First, consider an integrate-and-dump circuit; let τ be the integration time. The output of the integrator is

$$\Psi_i(t) = \frac{1}{\tau} \int_0^\tau V(t + \tau')d\tau';$$

the Fourier transform is

$$\Psi^2{}_i(\nu) = \mathrm{sinc}^2(\nu\tau)[v^2(\nu) + \sigma^2{}_N].$$

The first zero of sinc(x) - sin(πx) / πx is at x - 1; if the integration time is taken to be $\tau_C = 1 / \nu_C$, some of the high-frequency components will be attenuated; if the integration time is one-half of that, some unnecessary noise will be passed.

In the case of the low-pass filter, let ν_O be the cutoff frequency of the filter. Let $h(\nu)$ be the filter modulation transfer function (MTF). The Fourier transform of the filter signal will be

$$\Psi^2{}_f(\nu) = h^2(\nu)[v(\nu) + \sigma^2{}_N].$$

In the case of a perfect low-pass filter with cutoff $\nu_O > \nu_C$, all of the information that is passed by the antenna is preserved, providing that the data are sampled at a frequency $\nu_S > 2\nu_O$, which corresponds to the spatial Nyquist frequency if $\nu_O = \nu_C$.

Figures A-1 to A-6 show some examples where we have plotted the output amplitude against frequency for frequencies between 0 and $2\nu_C$. We have calculated $h(\nu)$ for an integrator ("s" on the figures) and for Chebyschev filters with from one to six poles ("1" to "6" on the figures). Also, we show an assumed signal spectrum ("t"). Figure 1 compares the spectra of 1-, 3-, or 5-pole filters, an integrator with integration time $\tau = \tau_C$, and the signal spectrum. Note that the integrator will attenuate the signal at high frequencies much more than the filter. Figure A-2 shows the same information for 2-, 4-, and 6-pole filters.

In these two figures a 50% ripple has been allowed in $h(\nu)$. In figures A-3 and A-4 this allowable ripple has been reduced to 10%. More importantly, the integration time for the integrater is now $\tau = 0.44\tau_C$.

ANALYSIS (Continued)

This moves the first null out past ν_C, decreasing the signal attenuation at high spatial frequencies at the expense of including more of the noise. It should be clear that any integrate-and-dump circuit is going to require this kind of tradeoff between attenuation of the signal and inclusion of unwanted noise. By way of contrast, the low-pass filter allows an essentially perfect solution to the sampling problem--no attenuation and no noise passed at frequencies $\nu > \nu_C$--provided that we are willing to construct enough poles in the filter and build in low enough ripple.

Another way to look at this problem is to consider the signal-to-noise ratio in the filtered (or integrated) output. If the signal is attenuated by some factor $h(\nu)$, this is exactly equivalent to multiplying the noise by $1 / h(\nu)$. Figure A-5 shows the degree of noise amplification for low-pass filters with 2, 4, or 6 poles, and an integrator with $\tau = \tau_C$. Although the noise performance is the same at low frequencies, the integrator suffers in noise performance at higher frequencies relative to the low-pass filter, because the signal is attenuated. Figure A-6 shows the same thing for an integrator with $\tau = 0.5\tau_C$. Here, the high-frequency noise performance is the same for the integrator and the filter, but the low-frequency noise performance is worse for the integrator since, with the shorter integration time, more noise is included.

These results illustrate an ideal integrate-and-dump circuit affects the information content of $V(t)$, a perfect low-pass filter does not affect it.

IMPLEMENTATION

The low-pass filter *can* be *either* <u>digital</u> or <u>analog</u>. The analog filter, *in* particular, has such serious problems that it should not be considered; this is why to date, all of the satellite radiometers have used integrate-and-dump circuits, even though an ideal filter is known to be superior.

Figures A-1 and A-2 show clearly the ripple in $h(\nu)$. In order to reconstruct the scene seen by the antenna, it is necessary to know $h(\nu)$ very accurately. An analog filter will have an MTF that changes with time and temperature.

On the other hand, a digital filter would have no phase delay uncertainty and the filter MTF would not change. The algorithm for the digital filtering is completely understood and does not require any development.

Twelve digital filters would be required. Each channel also would *need* an *A/D* converter to digitize $V(t)$ as about a 25 kHz rate.

The proper choice for the digital filter would seem to be an LSI customer chip with one 16-bit multiplier. The twelve radiometer outputs would be multiplexed. There is currently no low-power, space-qualified multiplier.

CONCLUSION

Although it is shown that a digital filter would preserve the information content of the signal, the implementation *price may* be *too high for* inclusion *into* the LFMR.

FIGURE 1-A

CHEBYSHEV FILTERS--ODD NUMBER OF POLES

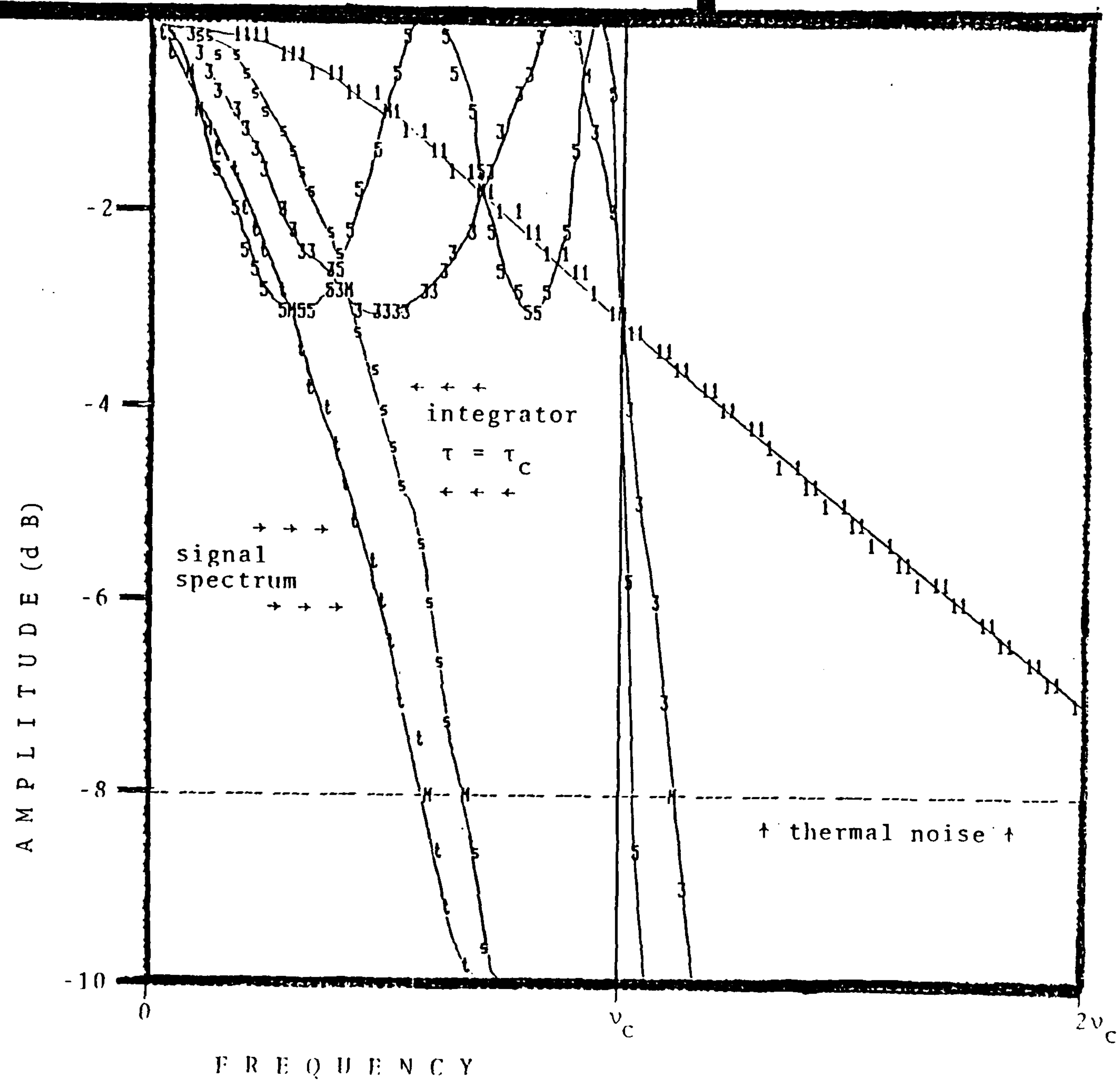

FIGURE A-2

CHEBYSHEV FILTERS--EVEN NUMBER OF POLES

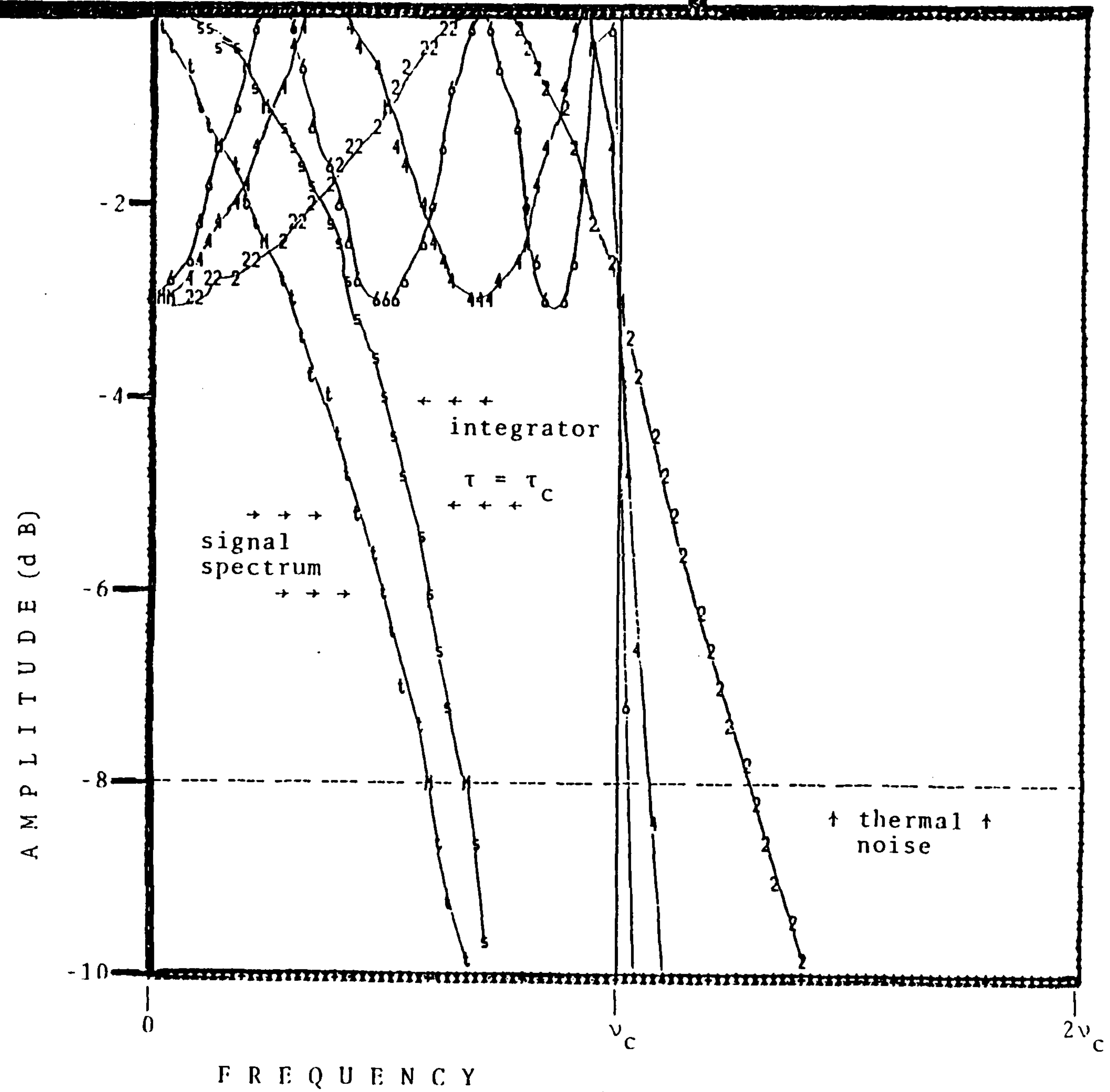

CHEBYSCHEV FILTERS AND AN INTEGRATOR $\tau = \tau_c$

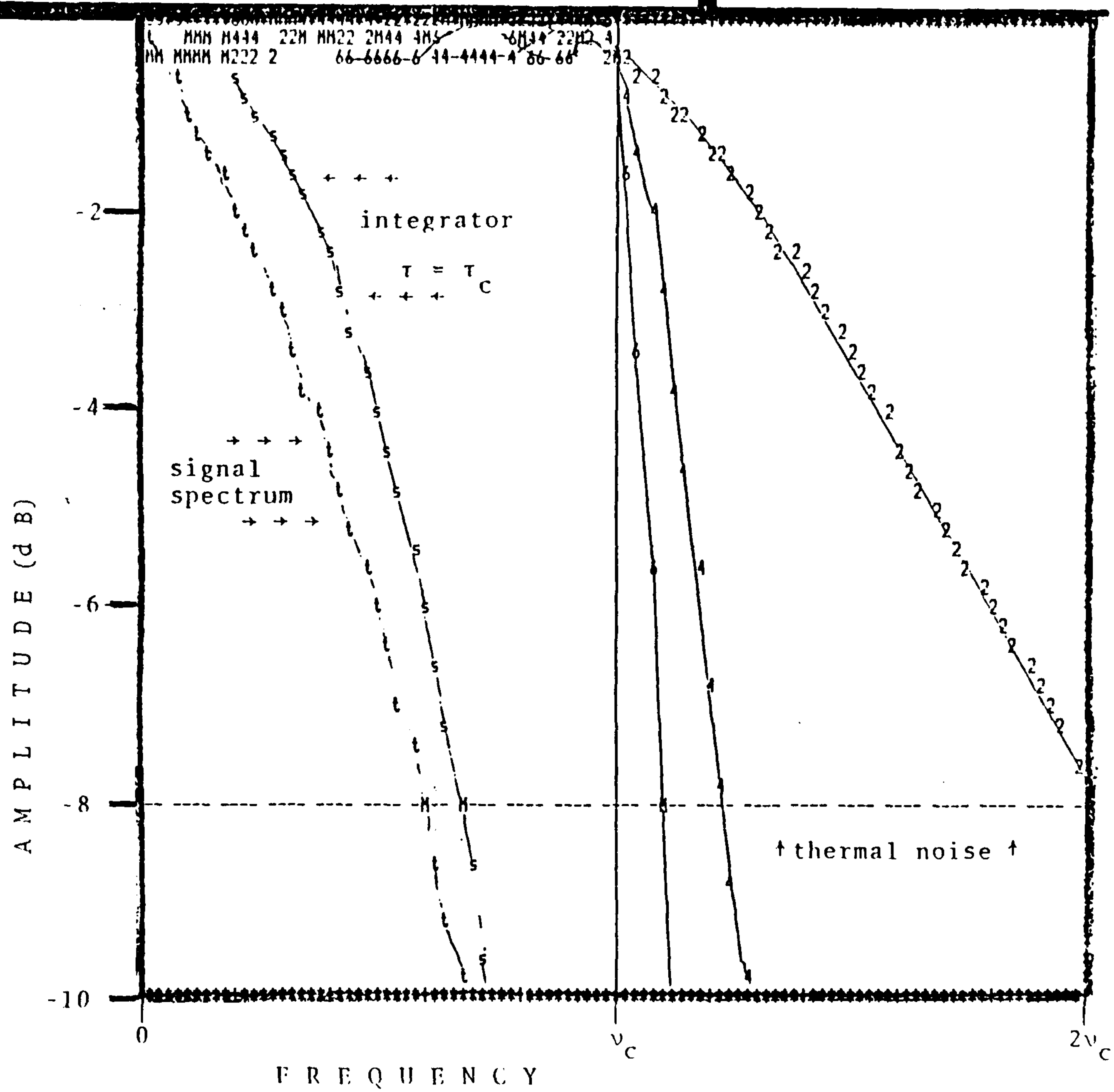

3

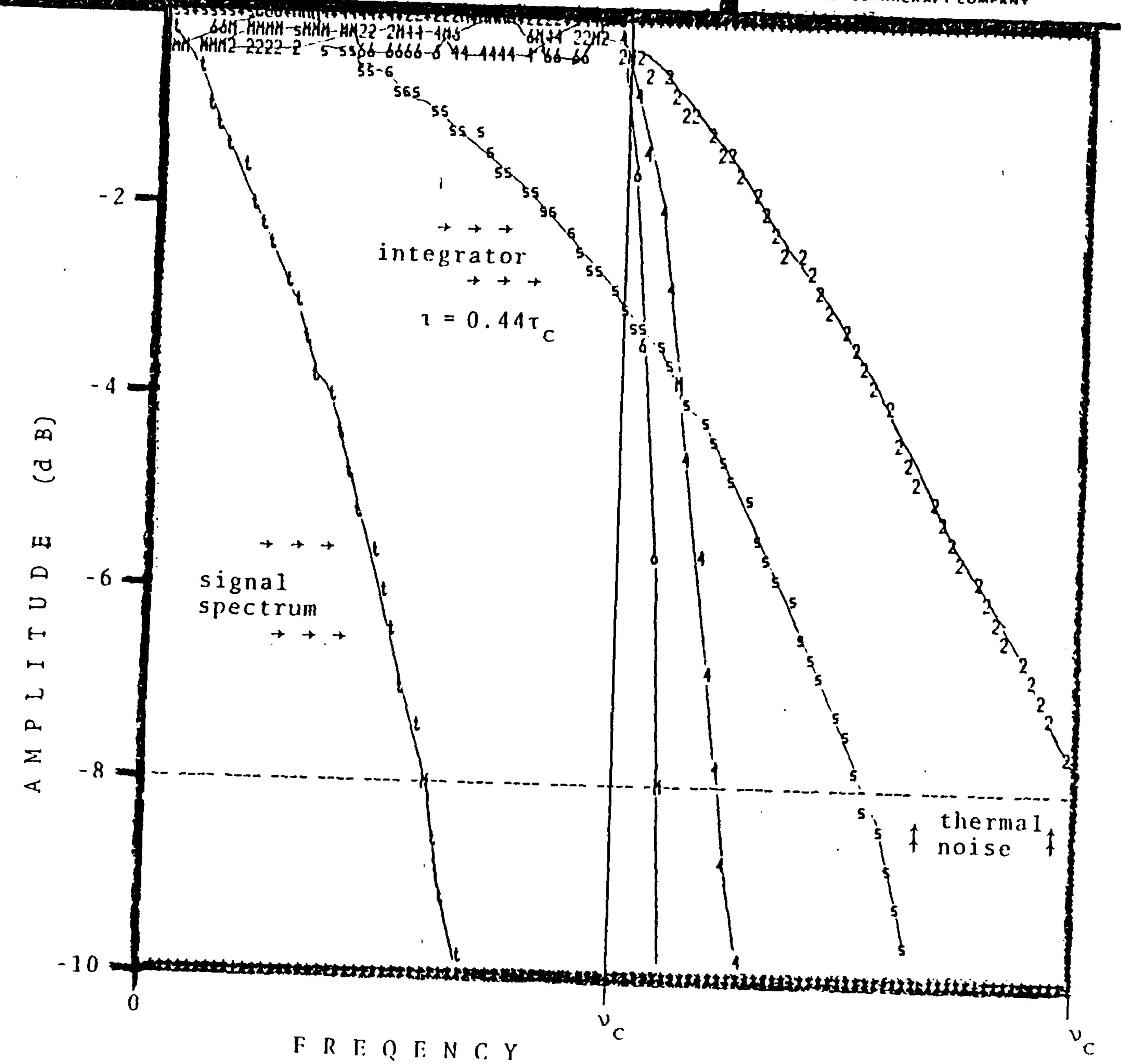
integrator
$\tau = 0.44\tau_c$
signal spectrum
thermal noise
-2
-4
-6
-8
-10
0
ν_c
ν_c
AMPLITUDE (dB)
FREQENCY

FIGURE A-5

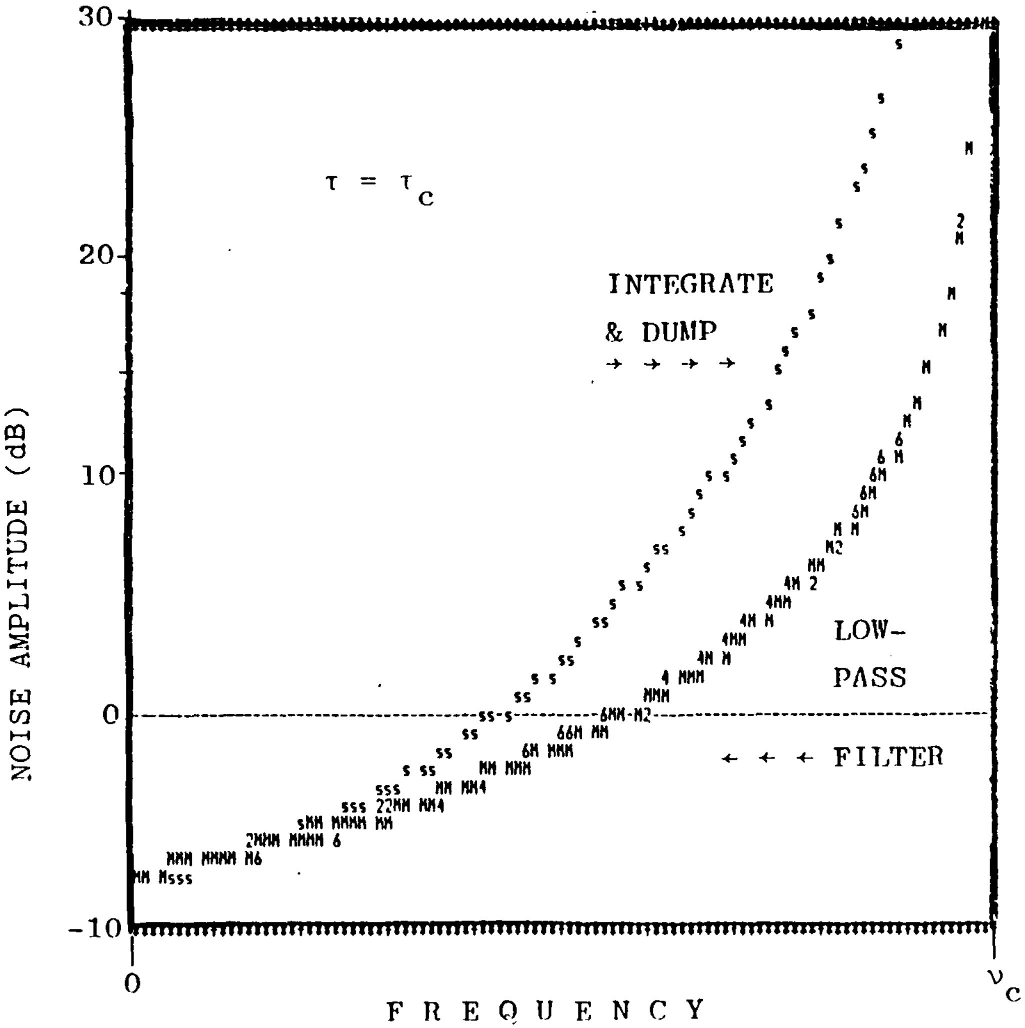

$\tau = \tau_c$
INTEGRATE
& DUMP
LOW-
PASS
FILTER
30
20
10
0
-10
NOISE AMPLITUDE (dB)
0
ν_c
F R E Q U E N C Y

FIGURE A-6

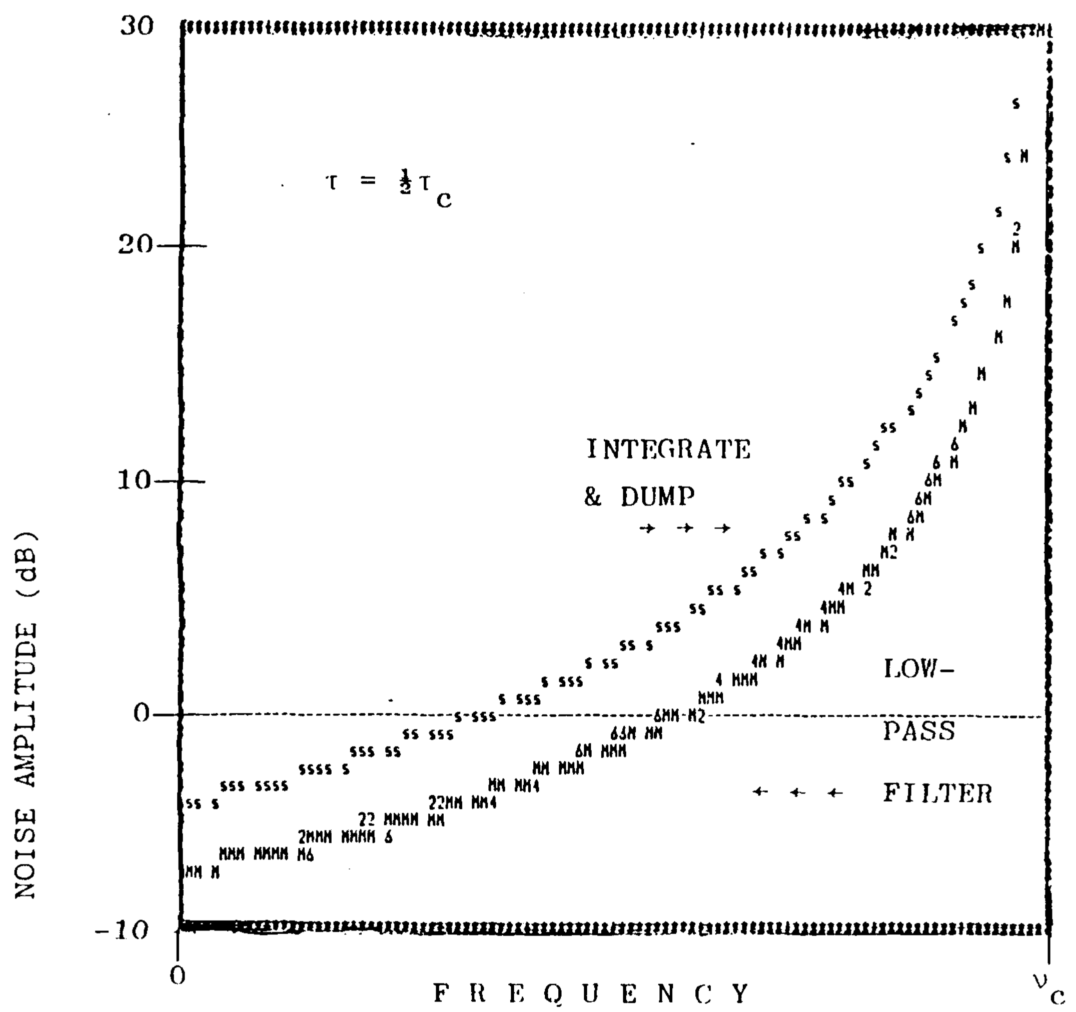

τ = ½τ_c
30
20
10
0
-10
NOISE AMPLITUDE (dB)
0
FREQUENCY
ν_c
INTEGRATE
& DUMP
LOW-
PASS
FILTER

HUGHES

APPENDIX B

PERIODIC ANTENNA DISTORTION ANALYSIS

RESULTS AND SUMMARY

HUGHES

- GEO-TRUSS
  - COMPUTED LOBE POSITION AND AMPLITUDE VERIFIED BY PUBLISHED RESULTS
  - WELL DEFINED GRATING LOBES
  - INCREASED NO. OF FACETS FORCES LOBE AWAY FROM MAIN BEAM: REDUCES AMPLITUDE.
- GORE
  - COMPUTED RESULTS VERIFIED BY PUBLISHED RESULTS.
  - GRATING LOBE BLUR DUE TO AXIAL DEFOCUSING.
  - INCREASED NO. OF GORES FORCES LOBE AWAY FROM MAIN BEAM: REDUCES AMPLITUDE.

RESULTS AND SUMMARY

The results and summary are shown. An increase in either number of facets or number of gores results in improved performance, the upper bound of which being that of a solid reflector.

COMPUTED RADIATION PATTERN OF 20-GORE REFLECTOR

HUGHES

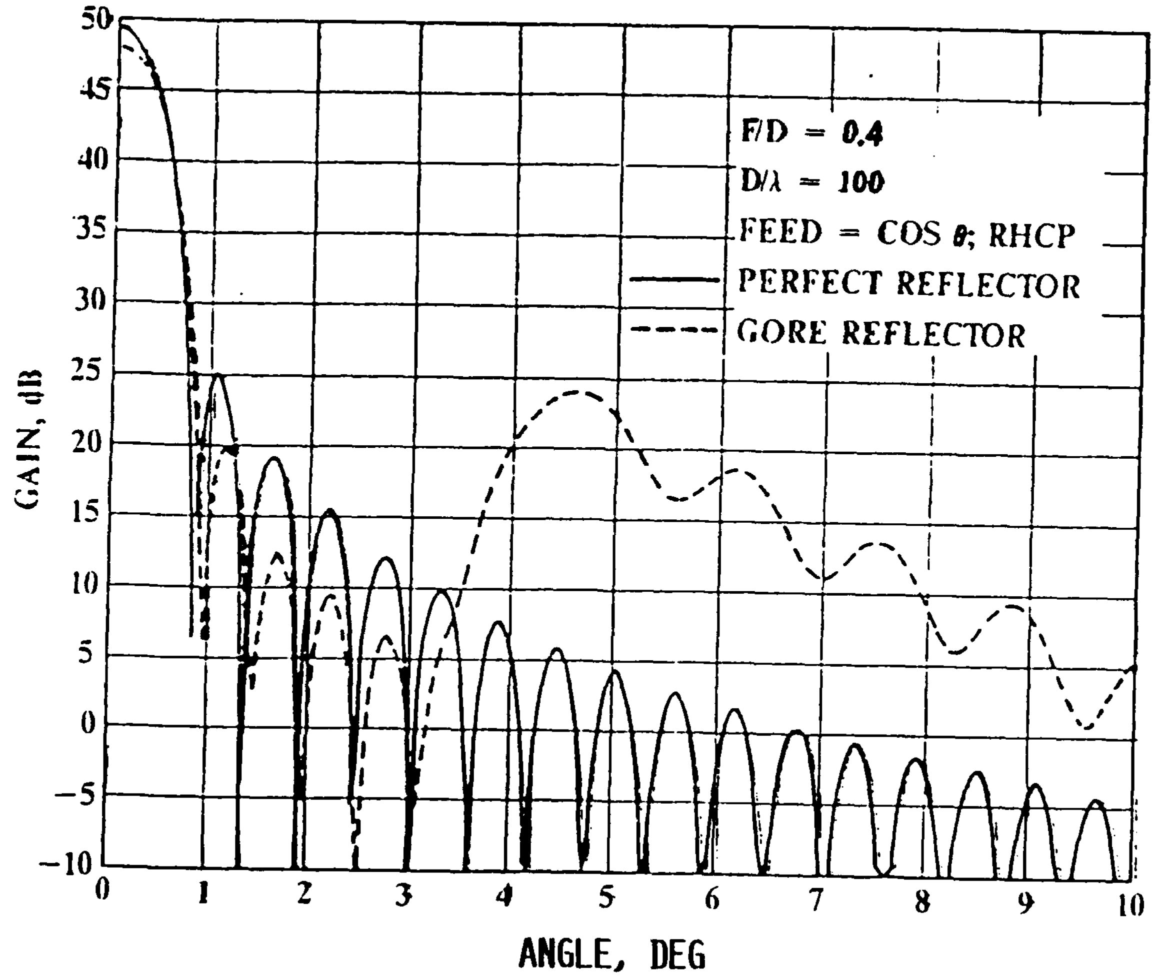

COMPUTED RADIATION PATTERN

The comparison of solid reflector and gore reflector performances is shown. Gain degradation of approximately 2 dB as well as grating lobe formation at $\theta_{gr} = 4.5°$ is depicted. The axial defocusing property is most evident in the grating lobe blur (lack of definition).

MODELING OF GORE TYPE
UNFURLABLE REFLECTOR

HUGHES

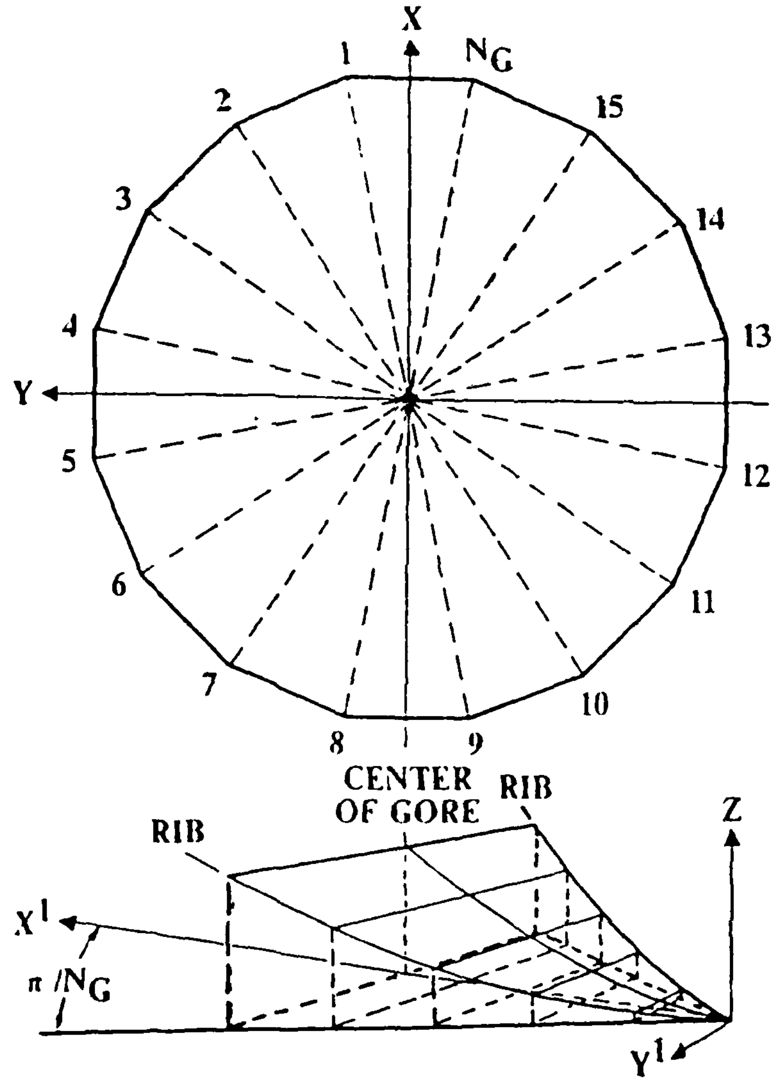

GORE TYPE REFLECTOR MODELING

The projected aperture model used for computation and the gore/rib relationship of the physical structure is depicted.

PERIODIC DISTORTIONS - GORE REFLECTOR

HUGHES

CHARACTERISTICS -

- AZIMUTHAL RIB PERIODICITY
- INHERENT DEFOCUSING (AXIAL)
- GRATING LOBES PRODUCED

LOBE POSITION: $\theta_{gr} = \sin^{-1}\left(\frac{1.2 N_g \lambda}{\pi D}\right)$

"BEST FIT" FOCAL POSITION $F_s = F_r\left(1 - \frac{2}{3}\frac{\pi^2}{N_g^2}\right)$

$N_G \triangleq$ NO. OF GORES

$F_R \triangleq$ PARENT FOCAL LENGTH

PERIODIC DISTORTIONS - GORE REFLECTOR

Gore reflectors exhibit periodicity in the azimuthal direction. Additionally, the structure exhibits an inherent axial defocusing property due to rib nonalignment with an idealized parabolic surface. The periodic nature of the surface gives rise to grating lobes which are rotationally symmetric about the antenna boresight. The spatial position of the grating lobes as well as the "best fit" focal position of the gore reflector is presented by the equations given.

PERIODIC DISTORTIONS

30λ REFLECTOR COMPUTED RADIATION PATTERNS

HUGHES

F/D = 1; ET = 10dB; Potter horn

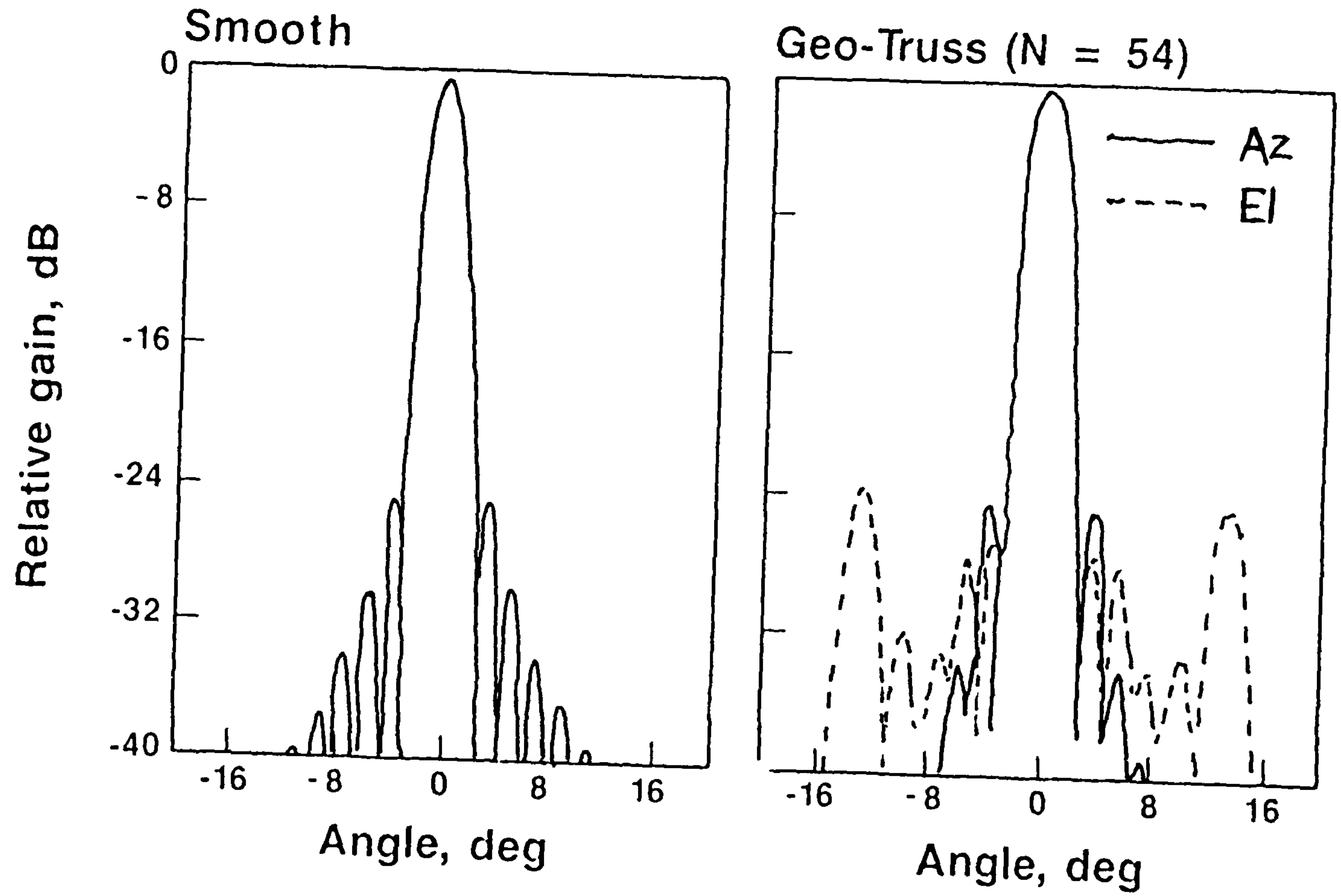

PERIODIC DISTORTIONS

A comparison of solid reflector and geo-truss reflector performances is shown. Not shown is a 2dB degradation in overall gain for the geo-truss reflector when compared to the solid reflector value. In addition, grating lobe formation occurs in the azimuth plane cut for the geo-truss case, well below 40dB at θ = 23.6 deb. This was computed at a frequency of 10.4 GHz.

GEOMETRY OF 54 FACET
GEO-TRUSS UNFURLABLE REFLECTOR

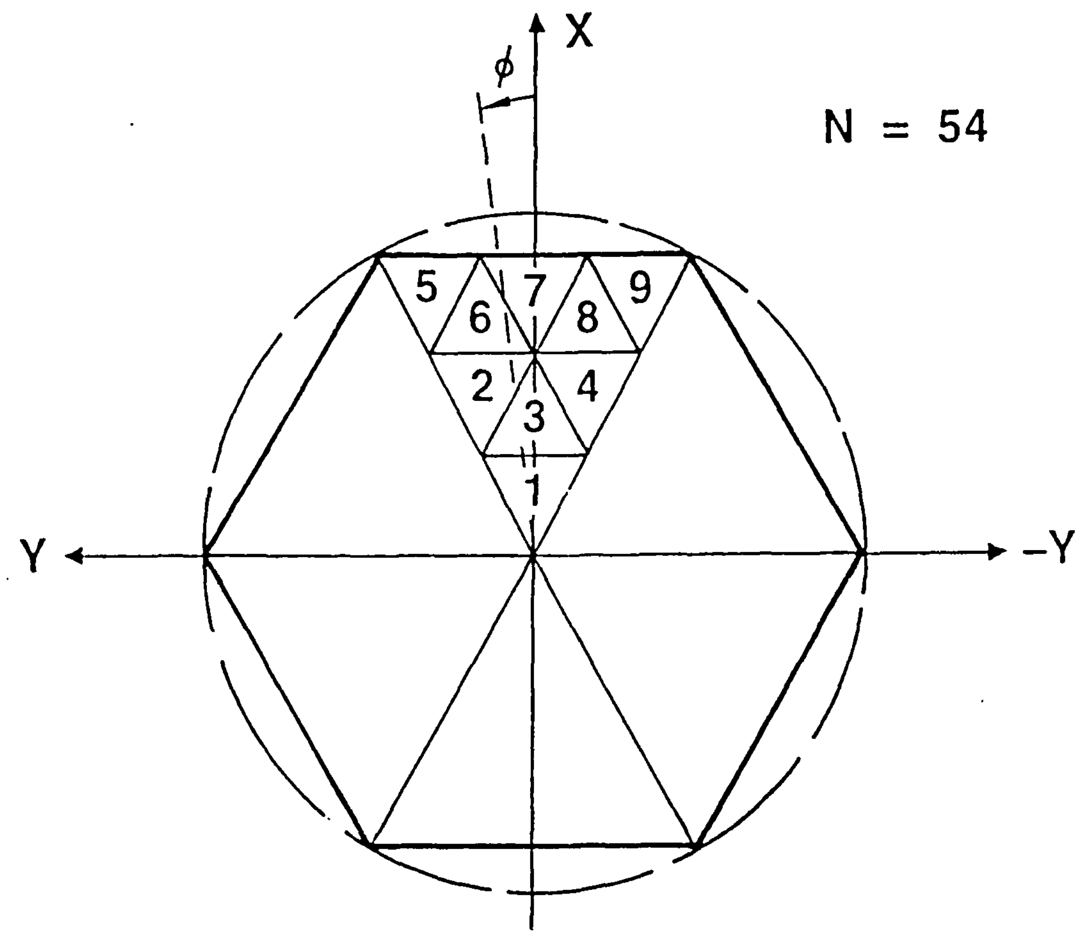

GEO-TRUSS GEOMETRY

Pictoral representation of the projected *aperture computer model* used for geo-truss computations. Depicted is a 3 bay (N=54) structure and its orientation to the focal plane coordinate system.

PERIODIC DISTORTIONS - GEO-TRUSS

HUGHES

CHARACTERISTICS

- RADIAL AND AZIMUTHAL FACET PERIODICITY
- GRATING LOBES PERIODIC W.R.T. GEOMETRY
- PRINCIPAL PLANE LOBE POSITIONS:

AZ: $\theta_{gr} = \sin^{-1}\left(\frac{2\lambda}{S}\right)$

EL: $\theta_{gr} = \sin^{-1}\left(\frac{2\lambda}{\sqrt{3}\,S}\right)$

$S \triangleq$ SIDE OF FACET

PERIODIC DISTORTIONS - GEO-TRUSS

Geo-truss mesh reflectors exhibit periodicity in both radial and azimuthal directions. This periodic nature gives rise to grating lobes found to be periodic with respect to the hexagonal "wedges" which comprise the geo-truss reflector surface. The spatial positions of these lobes are defined by the equations presented for the principal planes of the secondary pattern.

END

FILMED

7-85

DTIC